University of Alberta

A rheological model for composite truck ground behavior

by

Sujith Sundararajan

A thesis submitted to the Faculty of Graduate Studies and Research in partial fulfillment of the requirements for the degree of

Master of Science
in
Mining Engineering

Civil and Environmental Engineering

Spring 2014
Edmonton, Alberta

This thesis is affectionately dedicated to my parents

SUNDARARAJAN

and

PRABHA

for their love, sacrifices, endless support and encouragement that has helped me become what I am today

ABSTRACT

Mining haul trucks are operated on different ground conditions subjected to adverse shock loading, creating the need to give more attention to the truck components like suspension, tire, and the operating ground. Extensive experimental research has been done on these components at scale.

In order to understand the deformation behavior and the overall relationship between truck components and the operating ground for a full sized truck, mathematical equations have been derived for truck operation on both rigid and oil sand ground surfaces.

A rheological model is also proposed here that has the ability to predict the total and individual strain of the components. A model consisting of suspension, tire, and ground is created using MATLAB (Simulink). Finally, using the data obtained from the three methods, graphs are plotted and comparisons made with previous laboratory and field test results to validate the models and their equations.

ACKNOWLEDGEMENT

I would like to thank my supervisor Dr. Tim Joseph for his guidance and support throughout my time as a Master's student in Mining Engineering. He was more than a supervisor for me. Without his persistent support this research would have not been possible. The discussions with him helped me to understand the real picture. I would like to extend my thanks to Dr.Jozef Syzmanski for his valuable inputs and feedback.

I am thankful for my great friends, who supported, encouraged, helped me in editing the thesis, and provided valuable feedback throughout my graduate studies, especially Sridhar Dasani, Swetha Parvathaneni, Santhanakrishnan Ragupathy, Selvakumar Raju, Dineash Raju, Karthik Vaidhyanathan, Sumi, and Yao Tang.

I would also like to thank Sanjith and Priya, my brother and sister-in-law, for their continuous encouragement and support.

Special thanks to my office mates Zhihan Lin, Enjia Shi, Magreth, Niousha Rahmani, Choushi Hu, and Ibrahim for their help. The support provided by them in every aspect they could really helped me. The friendship with them will never be forgotten.

I acknowledge the financial support provided by NSERC and the University of Alberta. I offer my thanks to the Department of Civil and Environment Engineering (UofA) for employing me at research/teaching assistant positions during my graduate studies.

Finally, I thank all my family members for their support and encouragement.

Sujith

TABLE OF CONTENTS

LIST OF TABLES

LIST OF FIGURES

LIST OF SYMBOLS

"	Inch
ε	Strain
$\dot{\varepsilon}$	Strain rate
σ	Stress
γ	Isentropic gas constant
$\dot{\gamma}$	Shear rate
λ	Relaxation time
δ_{tr}	Deformation of tire on rigid surface
δ_{ts}	Deformation of tire on oil sand
δ_{os}	Deformation of oil sand
ϕ_t	Diameter of tire
$	Dollars
#	Number
%	Percentage
μ	Constant of proportionality
τ	Shear stress
θ	Bulk stress
η	Viscosity
ω	Angular frequency
°	Degree
ξ	Damping ratio

LIST OF ABBREVIATIONS

A_C	Area of suspension cylinder
A_{tr}	Footprint area of tire for rigid surface
A_{os}	Total area of oil sand
c	Damping coefficient
c_C	Critical damping coefficient
C	Celcius
CAT	Caterpillar
D	Depth of influence
d	Ground deformation
E_{ps}	Post peak modulus of oil sand
E	Young's modulus
F_S	Force on suspension
F_g	Force on the ground
F_t	Force on the tire
$F_{OEM,F}$	Damping force for full size OEM strut
$F_{OEM,S}$	Damping force for scale OEM strut
F	Load or Force
F_{ft}	Force on the front tire
F_{rt}	Force on the rear tire
f	Function
G	Rigidity modulus
g	Load level
Hz	Hertz
k_r	Radial stiffness of tire
k_s	Stiffness of spring

k_t	Stiffness of tire
$K_{OEM,F}$	Full size OEM strut stiffness
$K_{OEM,S}$	Scale OEM strut stiffness
kN	Kilo Newton
kPa	Kilo Pascal
k_p	Oil sand pressure stiffness
LR	Left rear
LF	Left front
m	Metres
Mpa	Mega Pascal
mm	Millimetres
min	Minutes
m_s	Mass of the spring
NC	Number of cycles
OEM	Original equipment manufacturer
P_s	Suspension pressure indicated by VIMS for every second
P_u	Suspension pressure at unloaded condition
p_i	Inflation pressure of tire
Psi	Pounds per square inch
Pas	Pascal second
P	Pressure
RR	Right rear
RF	Right front
R	Gas constant
S_a	Available stroke length
S_u	Stroke length at unloaded condition
SAE	Society of Automotive Engineers
sec	Seconds
t	Time

T	Absolute temperature
U/L	Unloaded condition
VIMS	Vital information management system
V	Volume
w_t	Width of the tire

CHAPTER 1
INTRODUCTION

1.1 Overview

The truck is one of the most important components in the surface mining industry. Repeated occurrence of high shock loading will result in premature failure of truck components like suspension and the tire and could pose a danger to an operator's health and safety. The efficiency and utilization of the truck are also decreased because of this resulting increased downtime. Production requirement and global competition have driven global surface mining operations to move to bigger equipment. Trucks have moved into the ultra-class category based on this criteria. The two most commonly used trucks are CAT 797B and CAT 797F, which have payloads of 380 tons and 400 tons. There has been an increase in payload with years and this could increase further in the future resulting in a huge load acting on the ground. Therefore, it is necessary to develop an understanding of suspension-tire-ground interactions which can be used for the performance prediction of various trucks operated on hard and soft surfaces.

The knowledge of deformation behavior and the relationship between the components is still not evident. Until now researchers have focussed on performance of suspension, tire and the ground separately and under small scale, which do not provide any relationship between these components. This motivated the research further to understand the overall behavior of the truck from the suspension to the ground under full scale.

The performance of each of the components are interrelated and depend on the conditions of each other. Even a small change in the performance of any one of the components would make the truck deviate from its normal behavior. Ground conditions are a critical factor behind this and especially oil sand deforms providing an undulated surface for the truck to be operated on. Hence understanding of the composite behavior of the truck over varying load conditions is essential to rid a solution for the problems faced by truck operators.

1.2. Purpose of research

Nowadays, most of the trucks in the mining industry are equipped with the VIMS payload system. In a sample field study conducted by Sarma (2009) on CAT 797B truck, it was found that when the truck started its hauling cycle, the available stroke length was only 0.032m (1.27”). Also after 500 operating hours, the available stroke length of the suspension dropped from 0.152m (6”) to 0.124m (4.9”) [61]. This difference in available stroke length is high and the loading effects on components of a truck will be very large, resulting in premature failure of truck components. Hence, the study on suspension cylinder to predict performance is vital for the truck to eliminate the detrimental effect of varying ground conditions.

Tires, on the other hand are subjected to high g-level, causing unexpected failures due to sidewall bulge and impacts [13]. The cost of a single tire is over $130,000 and companies experience shortage of tires [14]. Over time the rim and the tires experience cyclic loading at high g loads resulting in crack and premature failure. So understanding the performance of the tire for varying load conditions helps in ensuring that they are operated with minimum damage for a longer period of time and in turn maximizing the tire life.

The in-pit ground, especially oil sand, deteriorates within a few cycles resulting in uneven surfaces. Oil sand exhibits two main charateristics, deformation and rutting. The behavior of oil sand under these two categories are relatively well unknown and correlating these effects to the action of the hauler will help the operators to operate the truck with less downtime. Also the strength of oil sand is very poor to bear a huge amount of load from the truck. Due to these, the driving becomes very difficult causing a huge force to be transferred to the truck components, which leads to major fatigue, equipment instability, and improper payload distribution [11] [40] [41].

All these factors highlight the need for evaluating the suspension, tire and the ground together and finding an effective solution for understanding the behavior and relationship between the respective components. It is necessary to provide a better way for prediction and understanding of the complexity of composite truck-ground behavior. The mathematical equations and rheological models proposed in this research will help the individuals concerned with truck and road maintenance to monitor and improve either the ground condition or the components on the truck.

1.3 Research approach

Dynamic behavior of truck components is a subject of on-going interest to the mining industries and so are the practical models to interpret, characterize, predict, and interrelate the various phenomena such as available stroke, deformation, damping, and load impact.

This research work begins with the derivation of mathematical equations using various fundamentals of physics related to materials. Basic thermodynamics of gases, general stiffness equations of tires involving parameters like inflation pressure, overall diameter and width were used to find equations relating the stroke length of the suspension and the deformation of the tire. The work on the interaction of tires on oil sand by Sharma (2009) is also included when truck is considered to be operated on oil sand.

Finally with all the derived equations, comparisons have been made with previous data obtained for the following on rigid and oil sand surfaces

- Field data for a CAT 797B with 3.84m diameter tires (55/80R63) [60]
- Experimental data for a 0.368m diameter labscale tire [60]
- Experimental data for a 2.85m diameter tire (30 00R51) [13]

Next, a rheological model is proposed here that predicts the total deformation and the deformation of individual truck components and the ground. Basic mechanical models like Burgers, Kelvin-Voigt, and Maxwell have been used. The normal stress-strain Hooke equation and the Newtons fluid equation are used to derive an expression for individual component models. Data measured up by Sharma (2009) for oil sand parameter of Burgers model are used and extended here by including suspension and tires in the picture. Finally, comparisons were made to the mathematical equations derived earlier.

Finally a model consisting of suspension, tire, and ground was modelled using MATLAB (SIMULINK) in order to understand the behavior and deformation characteristics of each component. Plots were produced to better understand the response of the Simulink model for various conditions. With the results obtained from the Simulink model, comparisons were then made with the results of the mathematical and rheological methods.

The mathematical and rheological methods used here to analyze the behavior of components provides good information to understand the relationship between the components of the truck and also on the increasing problems of shock loading due to bad road conditions. Using the models in this paper, graphical analyses were conducted to easily correlate the functionality of each component for various loading conditions.

This work enables engineers and operators concerned with truck performance to better understand the impact of high loads and the behavior of the truck components to the ground. This will also help operations teams in industry to perform on-time maintenance of the equipment, and maintain the quality of haul roads for a safe work environment, cost reductions and improvement in reliability.

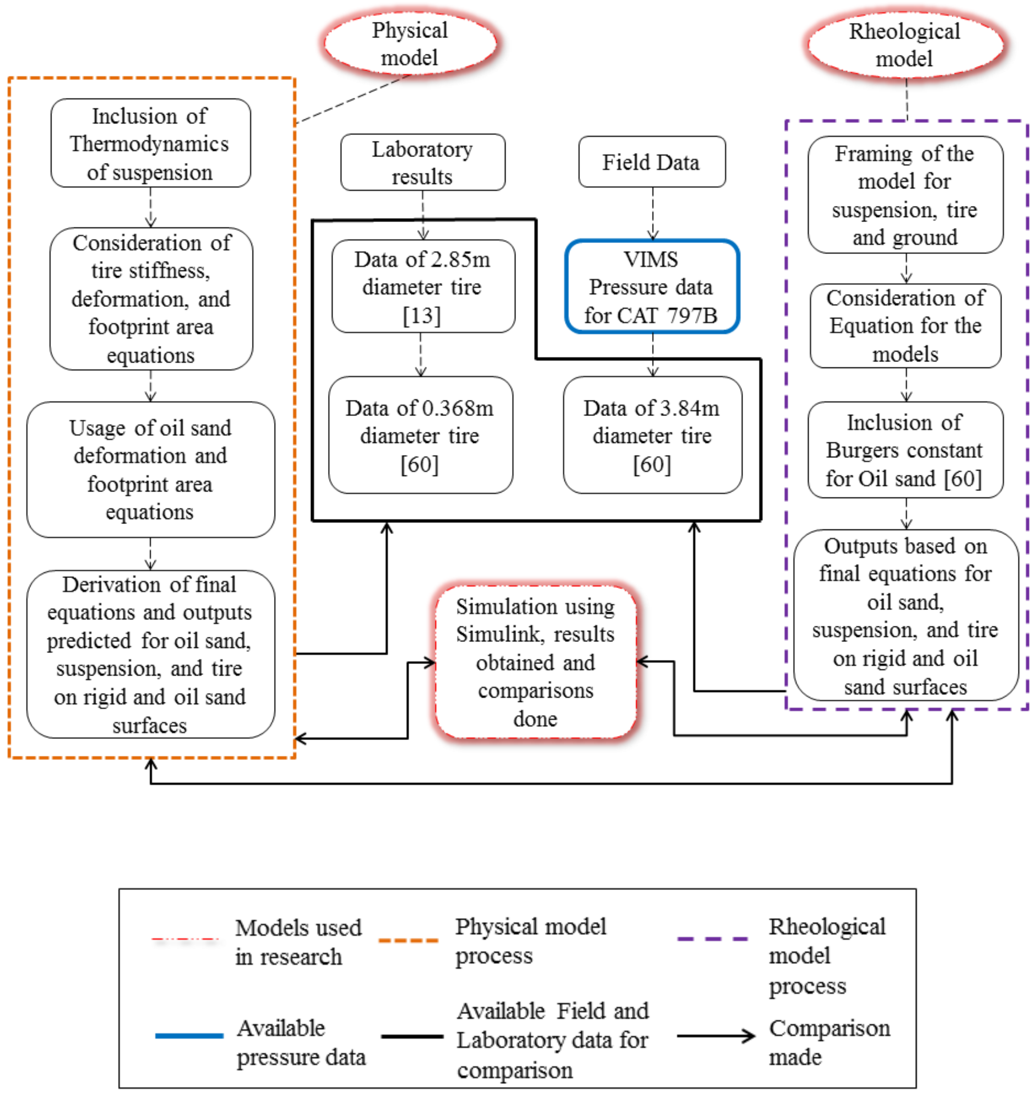

Figure. 1.1. Flowchart showing the methodology and research approach to predict the composite truck ground behavior

CHAPTER 2
LITERATURE REVIEW

2.1. Introduction

This chapter provides an understanding of previous work to better understand the scope of the research. A truck has a complex behavior while loaded and in motion and which depends on the performance of components like suspension and tires. The effects of these components are further related to the ground conditions. Firstly, a rheological method for predicting the deformation of both the truck components and ground has been examined. Field studies had been conducted by researchers in an attempt to realize and improve the performance of components like suspension, tires and ground involved in truck – ground behavior. Also, experimental results were obtained under large and small scale. Finally, these are reviewed and where applicable, incorporated into this study.

2.2. Fundamentals and stride towards the branch of rheology

"Rheology is the study of materials deformation and flow properties" [10]. In general, for a beginner, it is a discipline known as a mixture of more than one branch. The formal explanation of rheology was accepted in the year 1929. Since it is quite a new science, its prominence came only during the latter half of the 20th century. It is now recognized worldwide and many countries now have national societies of rheology [10].

The most important aspect of rheology is the time dependent behavior of materials. Rheology is essentially concerned with materials that show a combination of elastic, viscous and plastic behavior. Two well-known British scientists, Isaac Newton and Robert Hooke, set the borders of the present knowledge of rheology. Their work set the frontiers of "classical elasticity" and "fluid dynamics" [65].

Weber (1835) performed an experiment on silk threads and it showed a non – perfect elastic behavior. He noted that during application of load, it showed an instantaneous elongation followed by an additional extension with time. Conversely it showed an instantaneous reduction in length followed by an additional steady decrease in length till it reached its original length. This response matched with the behavior of a viscoelastic solid [71]. Thus, materials having a solid-like behavior which cannot be defined by Hooke's law alone and similarity to flow like a liquid were termed as "viscoelasticity" [65].

Scientists then realized that there are also materials which do not come under the category of pure solid or pure liquid. Thus "Rheology" is focussed on the study of the behavior of materials that fall under the two parameters termed as, "viscoelasticity" and "non-Newtonian fluid mechanics" [70]. Also, the terms "elasticity" and "viscosity" are very important in rheology because materials display either of the property or mixture of both at once.

2.3. Important parameters in rheology, viscoelastic models and their studies

The most influential period in rheology was the introduction of mechanical models. Viscoelastic materials are basically modelled using two elements, the spring and the dashpot (Figure.2.1).

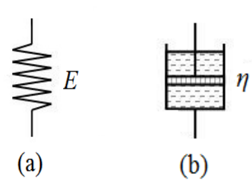

Figure.2.1. Mechanical elements (a) Hooke Spring and (b) Newtonian Dashpot (after [25])

There are basically four main mechanical models (Figure.2.2) and each of these is made up of spring and dashpot elements in parallel or series combination. The constitutive equations for these models are usually derived based on the force, extension, stress, strain and time dependancy of materials [71].

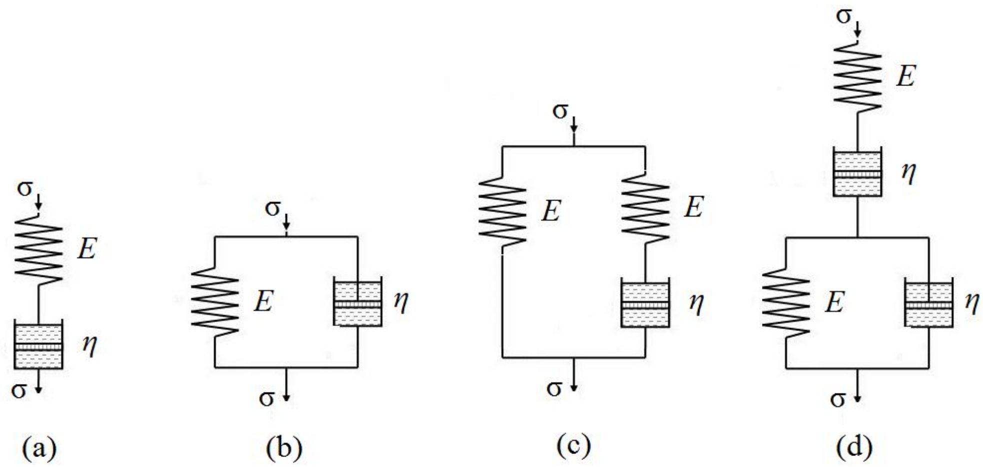

Figure.2.2. Mechanical models (a) Maxwell (b) Kelvin-Voigt (c) Standard linear solid or Poynting - Thompson (d) Burgers (after [25])

Whatever the type of model used in rheology, it is mainly interested with four main sub-areas [10]

i) *Rheometry: Measurement of rheological properties*

ii) *Constitutive equations*

iii) *Measurement of flow behavior in complex geometries*

iv) *Calculation of behavior in complex flows*

In terms of springs in mechanical models, it is purely an elastic component with the rheological property such as Young's Modulus. Hooke (1678) presented a one-dimensional law that relates stress over two material factors: the modulus of elasticity (E) and axial strain (ε) [1] [2], which can be generalized that stress is proportional to strain and is given by,

$$\sigma = E\varepsilon \qquad [2.1]$$

Barnes (1999) indicated the difference between a pure elastic material (Hooke model) and Kelvin model (Figure.2.3). He noted that when a sudden stress is applied, the final strain value of the elastic material reached immediately whereas the strain took a time curve since it also has a viscous element [10].

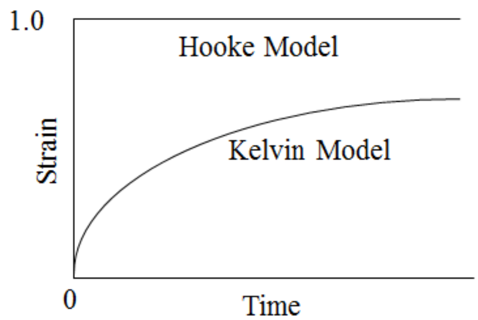

Figure.2.3. Strain response of Hooke and Kelvin model (after [10])

In terms of a damper in mechanical models, viscosity is the main parameter and is a "*property of liquid, which can be stated as the resistance to fluid flow*" [62]. The viscosity of a viscoelastic material does not remain constant and varies according to the parameters affecting it. Barnes (1999) noted that the following is the main cause for a change in viscosity.

i) *Change in Shear rate and time of shearing*

ii) *Change in Pressure*

iii) *Change in Temperature*

The effect of shear rate on viscosity for a particular temperature was found to reduce for a low-density polyethylene melt [48]. He also gave the sketch which shows the variation (Figure.2.4).

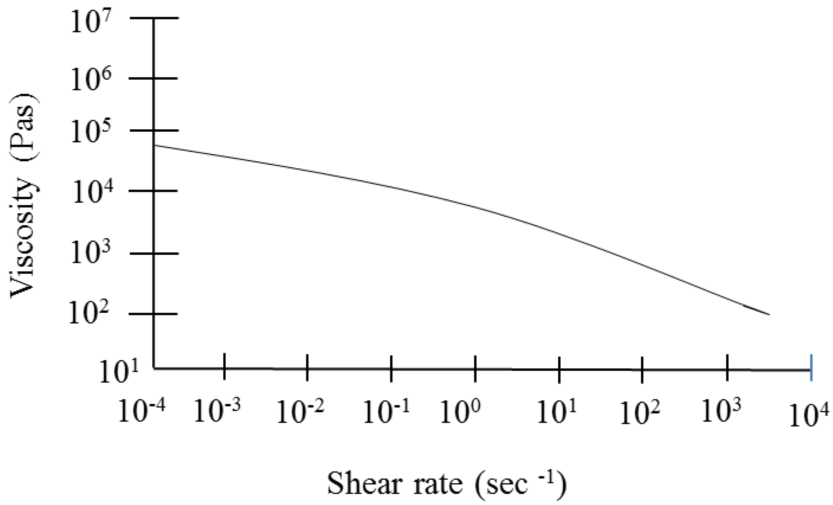

Figure.2.4. Shear rate vs Viscosity for low-density polyethylene melt (after, [48])

Similarly Lewis (1987) noted that the magnitude of change in viscosity is 2% per degree C change in temperature. An experiment was conducted on liquids to verify the effect of temperature on viscosity [62] and it was found that the relationship followed the "*Arrhenius equation*" (Equation. 2.2)

$$\mu = \mu_{\infty} \exp\left(\frac{Ea}{RT}\right) \qquad [2.2]$$

Where, μ is the viscosity (Pas), μ_{∞} is a constant (Pas), E_a is the activation energy (Kcal g-mole), R is the gas constant (kcal/g-mole °K), and T is the absolute temperature (°K).

The important difference between "Non-Newtonian fluids" and "Viscoelasticity" that forms the scope of rheology was described by Barnes (1999). He stated that "*All Viscoelastic liquids are non-Newtonian but not all non-Newtonian liquids are Viscoelastic*" [10]. Nguyen (2012) studied the flow behavior of various Non-Newtonian fluids. The flow characteristics of these fluids vary in different ways from Newtonian fluids. He studied the characteristics of different Non-Newtonian fluids and presented a graph (Figure.2.5) to represent the variation [52].

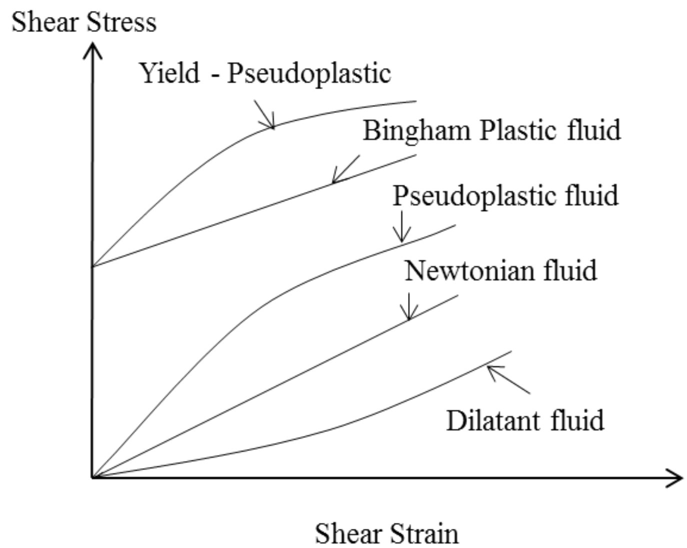

Figure.2.5. Shear strain vs shear stress for Newtonian and Non-Newtonian fluids (after [52])

Further, Non-Newtonian fluids are classified into time – dependent and time-independent. The materials described as per figure. 2.5 are time-independent fluids. For a “Newtonian fluid”, the viscosity is a constant. Viscosity decreases with increase in shear rate for a “Pseudoplastic fluid” and it increases for a “Dilatant fluid”. “Bingham plastic” has a yield stress and the for the materials to start flowing, the applied stress should be more than the yield stress. “Yield – Pseudoplastic” has both yield stress and non-linear flow. Time-dependent fluids are thixotropic and rheopectic fluids. The vast majority of fluids are time-independent [52].

The linearity of many materials under rheology that show characteristics in-between that of a pure solid and pure liquid are not known until now since it can provide either a linear or non-linear behavior [48]. A solid which shows a viscoelastic behavior is known as “viscoelastic solid” and a liquid which shows a viscoelastic behavior is known as "viscoelastic liquid". Regarding linear models, Kelvin (1865) came with a linear rheological equation for a "viscoelastic solid" (equation. 2.3) and Maxwell for a "viscoelastic liquid" (equation 2.4) [71].

$$\sigma = G\varepsilon + \eta \frac{\mathrm{d}\varepsilon}{\mathrm{d}t} \qquad [2.3]$$

where, G is a material constant

$$\sigma + \lambda \frac{\mathrm{d}\sigma}{\mathrm{d}t} = \eta \frac{\mathrm{d}\varepsilon}{dt} \qquad [2.4]$$

where, λ is the time constant, η is the viscosity (Pas), ε is the strain

Later on, Jeffrey (1929) extended the Maxwell equation and came up with a constitutive equation in one dimension that could relate to modern science (equation 2.5) [39].

$$\lambda \frac{\partial \tau}{\partial t} + \tau = \eta \frac{\partial u}{\partial x} + \lambda\mu \frac{\partial^2 u}{\partial x \partial t} \qquad [2.5]$$

where, η is the elastic viscosity (Pas), λ is the relaxation time (sec), τ is the shear stress, μ is the Newtonian viscosity (Pas).

He used the one-dimensional equation to solve some of the problems related to earth's crust [2]. Boltzmann (1874) provided an integral constitutive equation (equation 2.6) which can describe both solid like and liquid like behavior [53].

$$\sigma(t) = \int_0^t E(t-\tau) \frac{\mathrm{d}\varepsilon(\tau)}{d\tau} \mathrm{d}\tau \qquad [2.6]$$

Where, σ is the stress, ε is the strain, E is the relaxation function, τ is the variable of integration

Provenzano et al (2002) stated that for relaxation function is not dependant on stress and strain as per Boltzmann's equation. So he used two non-linear viscoelastic theories known as "Schapery's single integral non-linear theory" and "Modified superposition principle" to study and identify the best theory to predict the behavior of ligaments. He found the later to provide better results in predicting the elastic and viscous non-linearity [53].

Various research has been done on the applicability, merits and demerits of viscoelastic models. Roylance (2001), stated that there are three commonly used "*Viscoelastic tensile test*". They are *creep, relaxation, and dynamic (sinusoidal) loading.* These three tests exhibit a time – dependant behavior [55]. Apart from *creep* and *relaxation*, viscoelastic materials also exhibit "hysteresis" [29].

Hackley and Ferraris (2001) discussed about various rheological terminologies and even gave the equation for the sinusoidal loading (equation.2.7 and 2.8) of stress and strain, which is a property of linear viscoelasticity. Both creep and relaxation can be considered as Time-Dependant behavior [35].

i) *Creep: Materials response of strain with time to a constant stress loading*

ii) *Relaxation: Materials response of stress with time to a constant strain*

$$\varepsilon = \varepsilon_0 \cos \omega t \qquad [2.7]$$

$$\sigma = \sigma_0 \cos(\omega t + \delta) \qquad [2.8]$$

where, ω is the angular frequency, δ is the phase angle, t is the time

Roylance (2001) found the use of the sinusoidal loading method in polymers, which provides a suitable value for its "short time" response. He studied the linear viscoelastic and creep compliance response of polymers and polymer – matrix composites and noted that upon loading, initial strain occurs similar to elastic deformation (glassy compliance - C_g) and later on it reaches the equilibrium position (rubbery compliance - C_r). He also stated that the accuracy of both creep and relaxation of time equal to seconds or less is very low and is appropriate only for studying material reaction from minutes to days [55].

Both de Haan and Sluimer (2001) and Robert et al (2012) say that both Kelvin – Voigt and Maxwell models are not good in predicting the time – dependant behavior (i.e. creep and relaxation). Dey and Basudhar (2010) noted that when analyzed the creep and relaxation behavior for a viscoelastic soil, the Maxwell model and Kelvin-Voigt model were not able to predict the time-dependant behavior properly.

To overcome the demerits of these two models, De Haan and Sluimer (2001) studied the time – dependant behavior of building materials using a standard linear solid model. They found that this model was able to handle damping situations for building materials very well and a direct relation could be set for time-dependant behavior like creep and relaxation [23].

Attila et al (2004) used another three parameter model, the Poynting-Thomson model to define the stresses and the displacement that arise in a foil tube with time for a temperature range of -20°C and 45°C. They identified the Poynting-Thomson model as the best model in describing creep and relaxation characteristics. They used separate models and equations for both creep (equation 2.9) and relaxation (equation 2.10) by changing the location of the mechanical element, and derived the rheological parameters using a least square and finite element method [6].

$$\sigma + \frac{\eta}{E_1 + E_2}\dot{\sigma} = \frac{E_1 \cdot E_2}{E_1 + E_2}\varepsilon + \frac{E_1 \cdot \eta}{E_1 + E_2}\dot{\varepsilon} \qquad [2.9]$$

$$\sigma + \frac{\eta}{E_2}\dot{\sigma} = E_1\varepsilon + \eta\left(1 + \frac{E_1}{E_2}\right)\dot{\varepsilon} \qquad [2.10]$$

Where, η is the viscosity, $\dot{\sigma}$ and $\dot{\varepsilon}$ are the stress and strain rates, E_1 and E_2 are the Young's modulus of springs 1 and 2, σ and ε are the stress and strain

Dey and Basudhar (2010) did a study of viscoelastic soils and showed how the "Burgers model" is more effective than the other mechanical models (Maxwell, Kelvin-Voigt, and Poynting-Thompson) in predicting the time-dependant behavior of "saturated viscoelastic soil" and described the "Burgers model" as the most effective model [25].

Later, Sharma (2009) used the "Burgers model" to find a stiffness value for oil sand through interpretation of the deformation – time curve. The strain time curve for oil sand at 536 kPa was plotted (Figure.2.6) and the slope of the straight line drawn asymptotic to the strain-time curve at constant load to determine the value of the viscosity of the second damper. Similarly the values of the other parameters were found using the model [60].

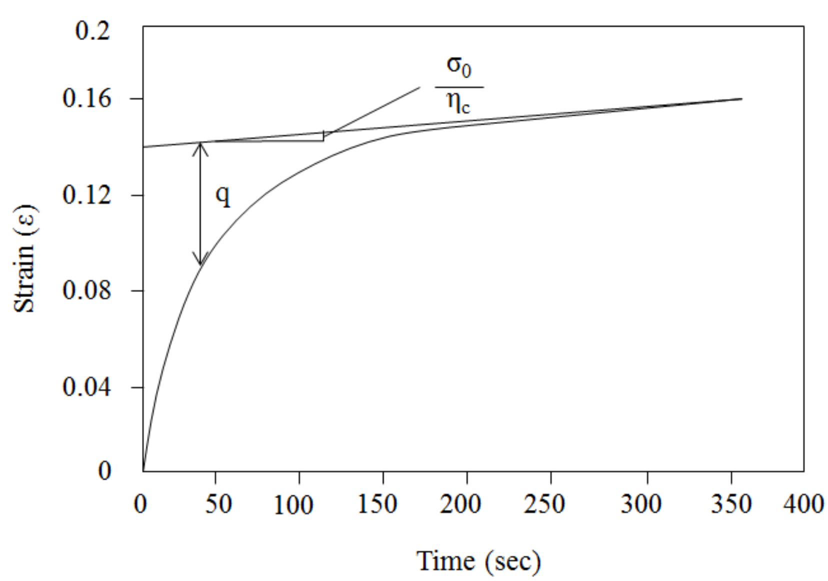

Figure.2.6. Oil sand Strain – time curve for 536kPa stress (after [60])

2.4. Complex fluid models and application of rheology in various fields

Larson (1999) noted that materials with both properties of elasticity and viscosity can also be regarded as "complex fluids", which comes under the category of rheology. Some examples of complex fluids are suspensions, foods, shampoo, fresh cement and concrete, agricultural products, toothpaste etc [48]. Most of the fluids discovered are non-Newtonian with only a few being Newtonian like water and some oils. Hence non-linearity is important in describing the complex fluids which are the complex fluid models [63]. Various types of model and their use were explained by Hackley and Ferraris (2001). They noted that the models can be regarded as two, three or four parameter models based on a number of unknown parameters [35].

i) "Power – law model" - Shear-thinning and Shear – thickening fluids

ii) "Herschel-Beckley", "Bingham Plastic" and "Casson" – Viscoplastic fluids exhibiting a yield response

iii) "Cross" and "Carreau-Yasuda" – Pseudoplastic flow

iv) "Ellis" and "Meter" – Pseudoplastic material exhibiting a power law relationship

The simplest of all the models is the "Power – law" model [63]. Balhoff (2005) studied various models and modelled the non-Newtonian flow of packed beds at pore scale and described the Power law relationship (equation. 2.11) [7].

$$\tau = \mu_0 \dot{\gamma}^n \qquad [2.11]$$

Where, τ is the shear stress (Pa), μ_0 is the viscosity (Pas), $\dot{\gamma}$ is the shear rate (1/sec), n is the power law index

"If the value of n is less than unity it is a Shear – thinning fluid and if it greater than unity it is a Shear – thickening fluid" [7]. Hou et al (2007) studied the shear

– thinning effect on a fluid viscous damper. He tested the effect on Silicone oil and found that the shear rate of the oil was high enough to cause a shear thinning effect. He found the shear rate value to be 24000sec^{-1} and concluded that this value of Silicone oil is very high and it confirms that it is a non-Newtonian liquid [38].

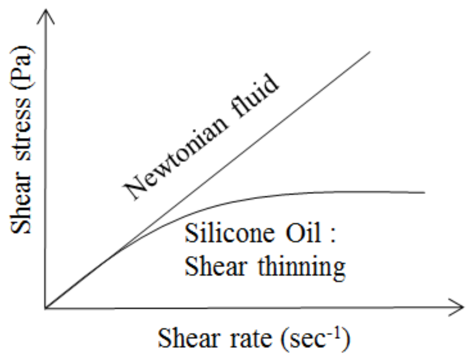

Figure.2.7. Newtonian vs Shear thinning fluid (after [38])

A comparison of different models was done on toothpaste [63]. It was found that for the behavior of toothpaste, the “Herschel-Beckley” model was found to be the best fit. Larson (1999) studied the rheological properties of a glassy liquid like zinc alkali and found that the property is dominated by the modulus and a very long relaxation time [48].

Banfill (2006) studied the rheology of fresh cement and concrete to understand the performance with practical situations. He found the behavior very close with Bingham model and was able to understand the link between rheology and technology [8].

After the formal naming of rheology in 1929, a lot of new things were developed in rheology and the application of it improved vastly. Differential integral equations related to experimental advances were made, different advance fluids like memory fluids were found out, and finally computational rheology came into the picture with the ability to perform various simulations. Today the scope of rheology is wider and has applications in various fields like polymers, suspension, synthetic-fiber, plastic-processing industries, pharmaceutical and food industries, biotechnology, chemical processing industries [26].

2.5. Mathematical Parameters and suspension studies

In the mining industry, there has been a rise in unplanned downtime due to increase in equipment capacity and production requirements [27]. Components like suspension, tire, and ground conditions are the main reason behind this and research has been done for each component separately. Suspension systems can improve the characteristics of a vehicle like safety and ride comfort. A lot of research has been carried out to meet the requirement of better ride quality and safety of the operator [5] [17] [72]. The important parameters of the suspension are that it provides better handling by making the contact between the tire and road stable, and also reacting to load variations resulting in ride comfort [74].

El-Sayed (2003), in his research, discussed the history, types and characteristics of suspension systems. His main focus was investigating the suspension system for a large ultra-class truck such as the Caterpillar 797B. He recorded suspension data from the field and found that “topping-Up” seemed as the main reason for failure of the system. There was only a clearance of 3.18 cm at the rear strut location when a trip cycle started. Due to this, the main concerns were truck reliability and spinal injury to the operator [28]. The majority of the weight during truck hauling was distributed at the rear suspension [18].

El-Sayed (2003) conducted a thermodynamic and fluid flow analysis and studied some parameters on the current shock absorber, known as a “simple shock absorber” or “oleo-pneumatic suspension”. He was the first to make an attempt to understand the effect of a variable orifice in suspension design [28]. “Oleo-pneumatic suspensions” are the most effectively designed suspensions for aircraft and its characteristics are affected even with a small deviation from the normal operating parameters [36].

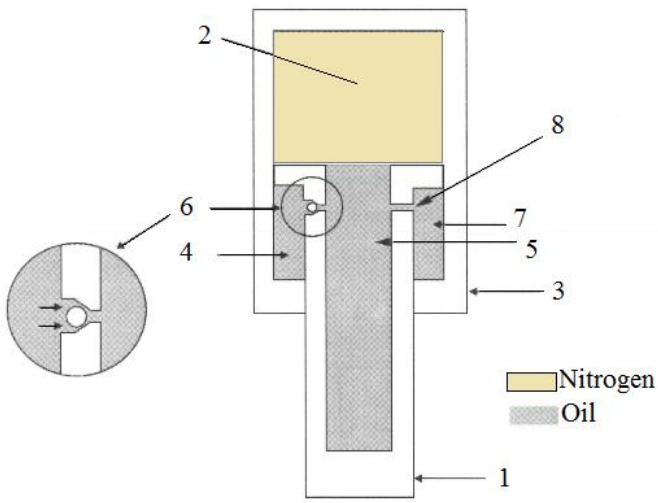

Figure.2.8: Oleo-pneumatic suspension

1. Piston rod, 2. Nitrogen chamber, 3. Cylinder, 4 and 7. Opening, 5. Oil chamber, 6. Ball check valve, 8. Fixed Orifice (after [61])

Comparisons were made between these two types of suspension using the modeling software “MATLAB (Simulink)”. He found that the variable orifice suspension showed a better performance than the fixed orifice suspension by varying the damping force with load conditions [28].

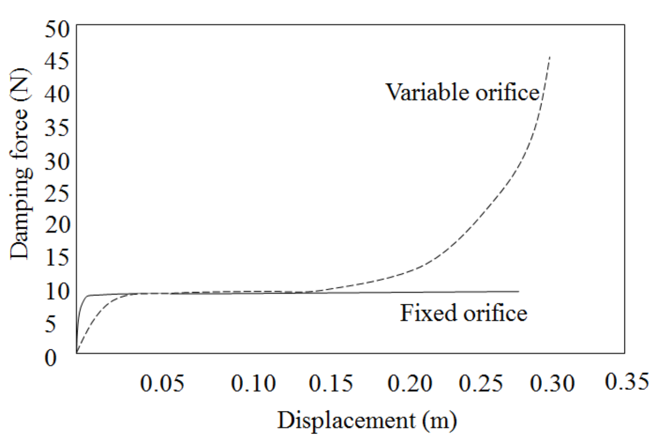

Figure.2.9: Fixed and variable orifice (after [28])

Later on, Santos (2007) focussed on reducing the shock loading effect caused due to "topping-up" by introducing a modified suspension model. He performed laboratory tests on a scaled version of the OEM and modified struts. The test was carried out for compression stroke and with hydraulic oil only. To collect the signals from sensors, a data acquisition system was used. Processed via a LabView system [57].

Even though Santos (2007) showed the effectiveness of a modified strut, there were certain exceptions. The velocity had to be greater than 45mm/s to significantly affect the damping force. The modified damper showed improved performance only at 75mm of stroke. The computer model was valid only at higher frequencies [57]. Finally the most important thing is that the test was done with only hydraulic oil, which is not the case in an actual mining truck suspension, where both oil and gas are used.

Finally, Soni (2009) continued the work ignored by El-Sayed (2003) and Santos (2007). He performed the test by including Nitrogen gas in the suspension and found the effects due to it. A scaling approach was carried out to predict the performance of the full size suspension. Four parameters were obtained such as stroke, displacement, internal pressures, and damping force with respect to loading frequency and initial charging pressure [61].

$$\left(\frac{K_{OEM,F}}{K_{OEM,S}}\right)_{Closure} = \frac{F_{OEM,F}}{F_{OEM,S}} \qquad [2.12]$$

Where, $K_{OEM,F}$ and $K_{OEM,S}$ are the stiffness of full size and scaled original equipment manufacturers strut, $F_{OEM,F}$ and $F_{OEM,S}$ are the force on the full size and scaled original equipment manufacturers strut

2.6. Ultra-class truck tires

The development of pneumatic tires began in 1845 [68]. The construction work and details of its parts appeared only in 1950 [51]. They also stated that study of a tires individual component's fatigue behavior is very expensive and sometimes requires the destruction of the entire tire. 73% of the tires produced usually are for passenger cars. These are classified basically into two types: bias and radial. The latter is mostly used in industries [69]. The characteristics of a pneumatic tire is still not fully understood and studies are going on to predict the exact behavior [47].

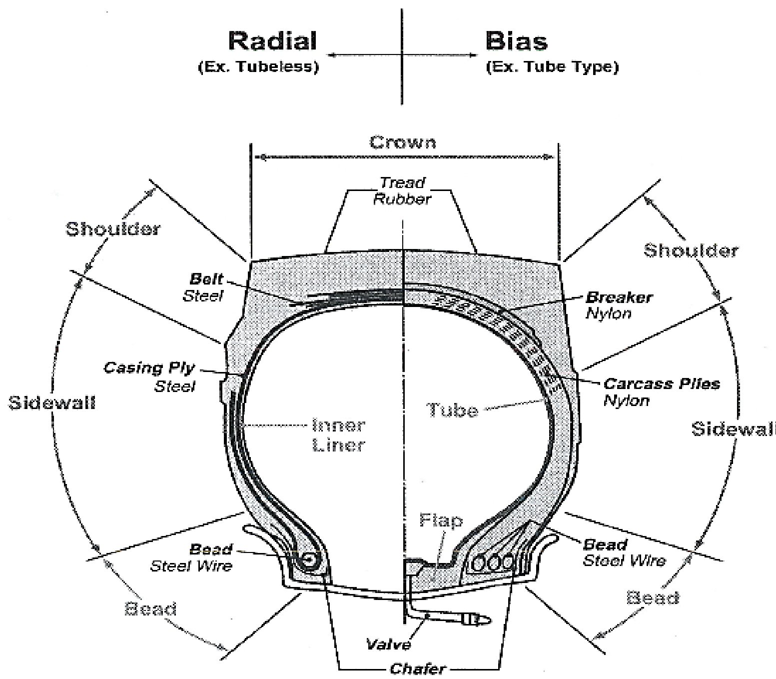

Figure.2.10: Components of a radial and bias tires (after [19])

Literatures only exists for passenger and highway tires. But, these do not provide sufficient information to model or predict the performance of ultra-class "off-road" tires used by the mining industry [22] [66] [67]. Various large scale experiments and analysis are performed by tire manufacturers, but they are very reluctant to provide that information to the public because of competition.

However, Bolster (2007), obtained information from the 'Society of Automotive Engineers (SAE)' about tires and rims. Several site visits in BC and Fort McMurray were made and even manufacturers, service providers, and end users of rims and tires were approached [13].

He obtained the material properties of a tire sidewall and tread from Goodyear (Table.2.1). Even though the purpose of these components of the tire are the same, the properties varied. Mainly the Young's modulus value which is the parameter that is used to find out the deformation for various loads also varied [13].

Material Property	Tire Tread	Tire Sidewall
Elastic modulus (N/ m^2)	3.75×10^6	2.9×10^6
Poissons ratio	0.49	0.49
Shear modulus (N/m^2)	2.9×10^6	2.9×10^6
Thermal expansion coefficient	6.7×10^{-4}	6.7×10^{-4}
Density (kg/m^3)	979	979
Thermal Conductivity (W/mk)	0.14	0.14
Tensile strength (N/m^2)	1.4×10^7	1.4×10^7
Yield strength (N/m^2)	9.2×10^6	9.2×10^6

Table.2.1. Material properties of Tire tread and sidewall (From [13])

Bolster (2007) performed tests on 30.00R51 series rims and tire at the I.F. Morrison Laboratory, University of Alberta. A 170 ton hauler model was used for this test. Stress and strain data were collected for various rim and tire positions and at various g-loads. It showed that the value of load is concentrated more at the base contact (180 Deg). Predictions were made for load values higher than 1.4g due to laboratory loading restrictions [13].

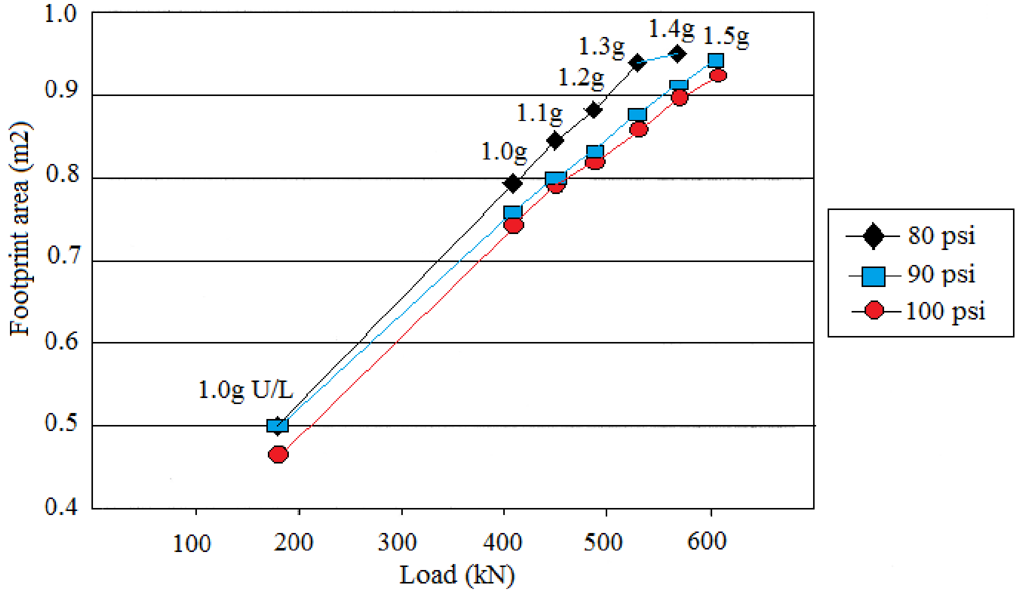

Figure.2.11: Load vs Footprint Area of tire for various inflation pressures (after [13])

Lin (2007) studied the strengths of all tire parts and discussed how the modulus varies for different tire manufacturers. He also stated the importance of inflation pressure. With the measurement of pressure changes in many large size tires, he came up with a formula known as “Ryne’s regression formula”, which has a great influence for pneumatic tire design [51].

Kasprzak et al (2006) described that the shape, size, and contact footprint of the tire is influenced by the inflation pressure and it should be considered as a parameter of the tire rather than as an operating condition [45].

Sharma (2010) conducted a tire flexure test on a rigid surface, sand, and oil sand. He used a 0.368m diameter tire and made comparisons with the field and experimental values of 2.85m, 3.84m, and 0.368m tire sizes at 1g – 1.4g load. Both static and cyclic tests were conducted for different inflation pressures [60].

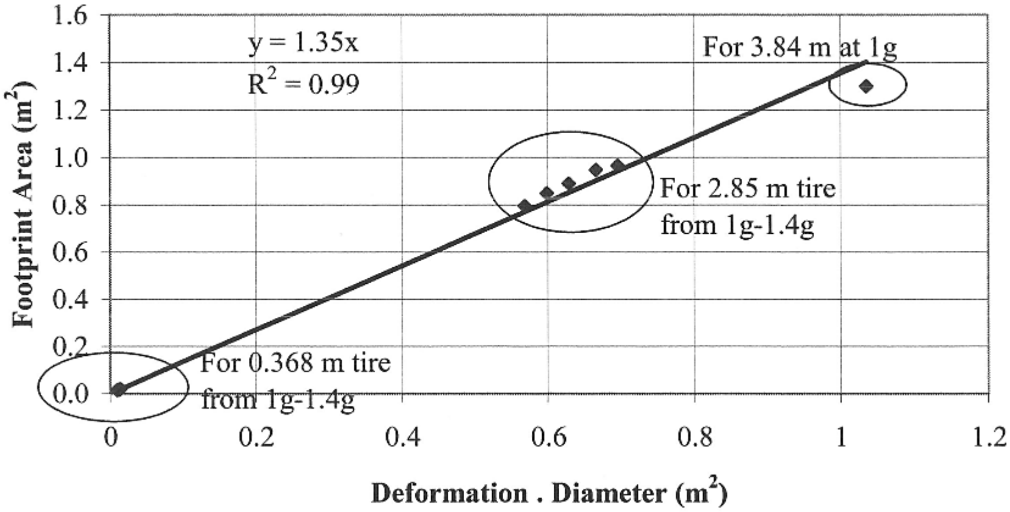

Figure.2.12: (Deformation. Diameter) vs Footprint area (after [60])

Figure.2.12 shows that the result is a common linear line connecting the lines of all the tire sizes. He obtained an empirical equation (Equation 2.13) for the tire footprint area of a rigid surface and proved that the equation could be valid for when compared to the field value.

$$A = 1.35\delta\phi \quad [2.13]$$

Where, δ, ϕ, and A are the deformation, diameter, and footprint area of the tire

Sharma (2010) also noted that the value of 1.35 in equation 2.13 changes for oil sand with 11% bitumen content. He described that variability as C, which has a value between 1.66 to 1.11 based on the number of cycles. Finally, he obtained a relationship for deformation of a tire on oil sand (Equation.2.14) [60].

$$\delta_{ts} = \frac{1}{2}\left[\left(\delta_{os}^2 + \frac{4F_t}{CE}\right)^{\frac{1}{2}} - \delta_{os}\right] \quad [2.14]$$

Where, δ_{os} and δ_{ts} are the deformation of oil sand and tire on oil sand, E and F_t are the Young's modulus and force on the tire, C is the oil sand model constant

2.7. Ultra – class truck haul road

Haul roads are built basically with three materials. Sand for the sub-base, pit run for the base, and crushed gravel for the surface layer [73]. There has been an improved application of crushed limestone for the surface layer, which has shown better stiffness and rolling resistance than the crushed gravel [37].

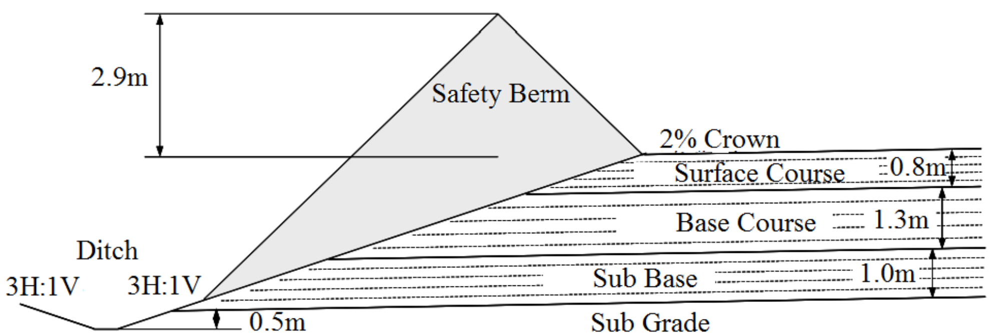

Figure. 2.13. Layout of Haul road for a 340ton truck (after [64])

Haul roads also play a vital role in mining operations similar to trucks and shovels. Tannant and Regensburg (2001) predicted the deflections at the surface for various truck sizes (170ton – 340ton) and found that for a 340ton truck the deflections was around 8mm [64].

Most mine haul roads have problems like Potholes, rutting, and settlement. These generate impact forces, which are then transferred to the frame and suspension of the truck through the tires. Impact forces due to poorly maintained haul roads reduces the life of the tire, causes metal to metal contact in suspension, shortens truck life, increases maintenance costs and safety issues. Hence for today's mining industries operating trucks with higher truck loads and speeds, it is very important to maintain the road surface condition in perfect condition to avoid all the consequences [64].

Concrete and Asphalt are the materials that can offer better traction and rolling resistance than crushed gravel, but it is more costly and mining companies are not ready to invest so much. The largest trucks are used in the oil sand fields, which handles a large amount of materials every year. The worlds largest deposit of oil sand is in Alberta, Canada. Nowadays in the oil sand fields, for permanent and temporary roads, oil sand is used as a construction material. [4].

Mining, construction, and manufacturing companies are mainly concerned with bituminous oil sand since it creates mobility problems for large haul trucks and shovels. The main reason for this difficulty is the presence of the bitumen content ranging between 8% to 15% by volume. Usually the deterioration rate is higher during summer than winter [3]. Joseph et al (2003) found that the stability of the truck and shovel worsens with just few cycles of operation on a soft-ground [41]. Grozic (1999) stated that as the number of cycles increases, the stiffness of almost all the Geotechnical materials becomes less and this is truly applicable for oil sands [33]. Joseph (2002) showed that as the number of loading cycle on the truck increases, the oil sand softens and in turn decreases the stiffness [40].

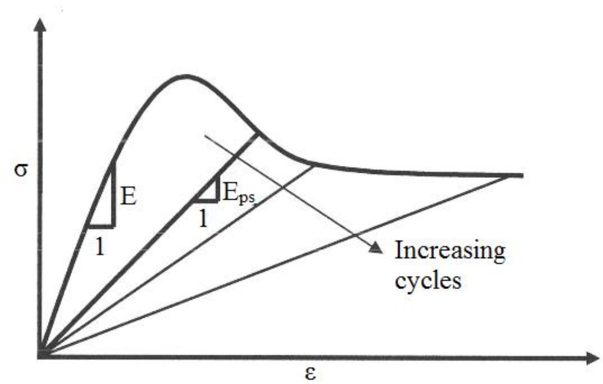

Figure.2.14: Variation of oil sand stiffness under cyclic loading (after [41])

Joseph (2002) also stated that the oil sand stiffness is a function of deformation regardless of temperature, grade, and Geotechnical properties. He proposed an empirical equation (2.15) to predict the stiffness and the relationship between other parameters [43].

$$\left(\frac{kD}{F}\right)\left(\frac{1-\nu}{\nu}\right)=C\left(\frac{d}{D}\right)^{-B} \qquad [2.15]$$

Where, k is the ground stiffness, F is the load, D is the depth of influence, d is the ground deformation, B and C are empirical constants.

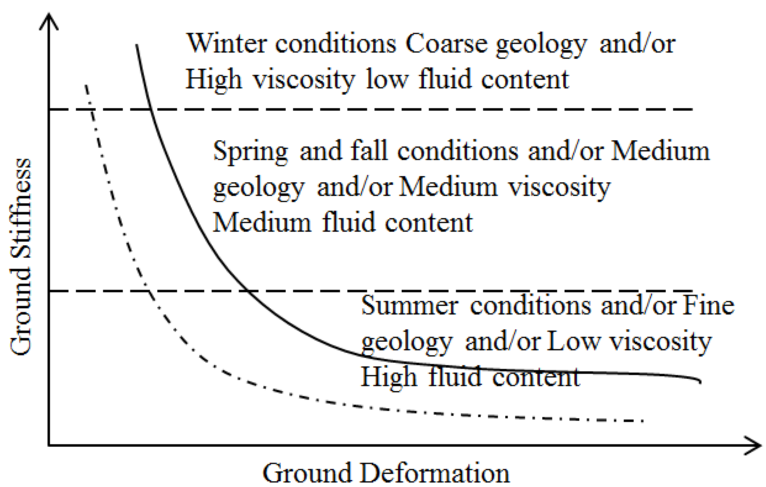

Figure.2.15: Oil sand stiffness with season (after [44])

Sharif – Abadi (2006) conducted an experiment on oil sand and came up with an empirical equation to predict the total deformation (equation. 2.16) [59].

$$\delta_t=\left(\frac{\sigma}{At^B}\right)+\left(\frac{\sigma}{106.7\left(NC\right)^{0.3}}\right) \qquad [2.16]$$

With $A=0.0317\sigma+7.318$, $B=-0.0002\sigma-0.036$

Where, δ_t is the total deformation of the ground, σ is the stress, t is the time, NC is the number of cycles, A and B are empirical constants

Sharif – Abadi (2006) performed a plate load test in the laboratory and to eliminate the effects of varying footprint, he used pressure instead of force, which is the pressure per unit deformation, known as "Pressure stiffness". He also found out that for oil sand, regardless of the number of cycles, loading frequency, relaxation interval between cycles, the "Pressure stiffness" converged to a constant value of 8KPa/mm (Figure. 2.16) [59].

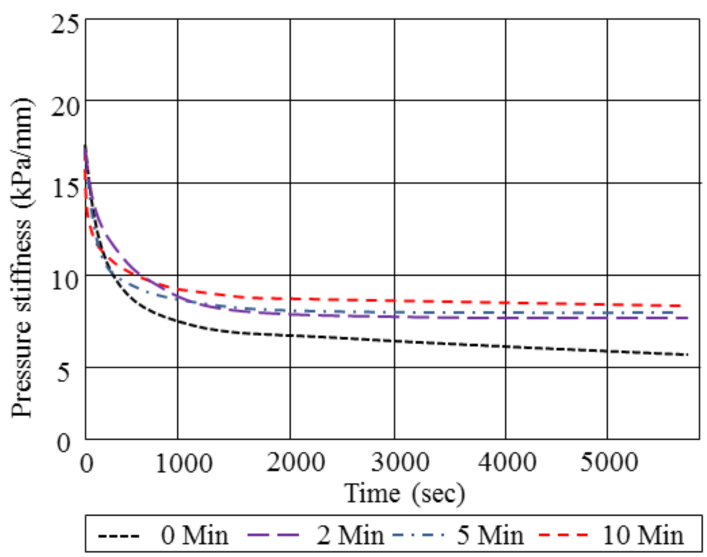

Figure.2.16: Pressure stiffness with time for Oil sand (after [59])

Anochie - Boateng et al (2010) conducted experiments on three oil sands with bitumen content of 8.5%, 13.3% and 14.5% by volume and found from the results that the behavior of oil sand and its modulus is affected by bitumen content, temperature, and applied stress. He found the dynamic modulus as the best parameter that can take into account of all the characteristic that affect the behavior of oil sand. Comparing with various model outputs and the accuracy of it, he proposed an adjustable model for practical use in the field [4].

$$E^{*} = 204\theta^{1.712} w_b^{-1.882} T^{-1.930} \qquad [2.17]$$

Where, E^{*} is the dynamic modulus, θ is the bulk stress ($\sigma_d + 3\sigma_3$), T is the temperature, w_b is the bitumen content, σ_d is the cyclic stress, and σ_3 is the constant confining stress

On the other hand, regarding permanent deformation of soils, Barksdale (1972), and Lekarp et al (2000) found moisture content and loading parameters as the most important parameters [9] [49]. Anochie - Boateng (2007) believed that this permanent deformation may be due to two main parameters known as "Sinkage" and "Rutting" [3]. Sinkage is measured when the truck is being loaded and rutting is measured at a point when the truck makes a number of passes [56].

Joseph (2005) described "*oil sand as elastic-plastic material and proposed a constitutive model (equation. 2.18)"*[42]. But this model is applicable only for static loading condition. He also stated that oil sand shows viscous behavior also along with elastic and plastic properties [42].

$$E_{ps} = 1.37\sigma_3 \varepsilon_1^{-1.43} \qquad [2.18]$$

Where, E_{ps} is the Elastic modulus, σ_3 is the confining pressure, and ε_1 is the axial strain

Li and Chalaturnyk (2005) proposed few empirical models to describe the behavior of oil sand (equation. 2.19 and equation. 2.20) [50].

$$E = 950 P_a \left(\frac{\sigma_3}{P_a} \right)^{0.5} \qquad [2.19]$$

$$E = 343\sigma_3^{0.875} \qquad [2.20]$$

Where, E is the Elastic modulus, σ_3 is the confining pressure, and P_a is the atmospheric pressure

The depth of influence (stress level) beneath the ground surface was studied by Joseph (2002) and he described that the depth upto which the stress influence depends on the footprint area of the tire (equation. 2.21) [40].

$$D = 3\sqrt{A} \qquad [2.21]$$

Where, D is the depth of influence, and A is the footprint area of the tire

Further, the parameters of the stress bulb; including size, shape, and magnitude in the layers of a haul road depends on the inflation pressure and size of the tire [64]. It was also found that pore pressure are not a major concern beneath the surface since it is dissolved mostly on the surface of the ground and do not pose any influence while calculating the effective stress [59].

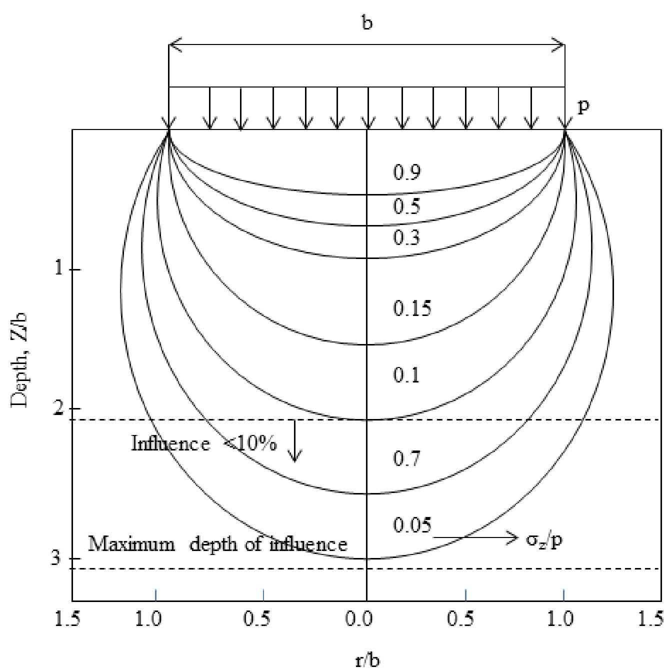

Figure.2.17: Stress bulb beneath the ground surface (after [60])

CHAPTER 3

MATHEMATICAL MODEL FOR THE PERFORMANCE PREDICTION OF TRUCK SUSPENSION AND TIRE ON A RIGID SURFACE

3.1. Introduction and Objective

The main aim of the mathematical model is to provide a means of understanding the performance and characteristics of truck components like suspension, tire and the ground without complicated mathematics. This chapter consists of the mathematical model for the truck components on a rigid surface. Mathematical equations are the fundamentals for finding the required parameters without any simulation or analysis. These equations are simple and can be derived based on basic mathematics, which most of the people concerned with truck operation and maintenance can understand.

The important truck components like suspension and the tire are considered here and each component has their applicable mathematical equation based on the properties of the respective component. These parts work together and the overall performance of each part depends on the condition of the other parts. This means they are interrelated and dependant on each other for the overall success and failure. Obtaining the performance relationship between them is interesting since each part has a separate functions and characteristics.

3.2. Basic assumptions

Some assumptions have been made such that they do not affect the parameters and accuracy of the model and their outputs.

i) The force throughout the system is the same (i.e. Force on the suspension = Force on the tire = Force on the ground)

ii) The Nitrogen gas inside the suspension cylinder behaves isentropically (i.e. there is no change in Temperature) such that PV^{γ} = a constant

iii) The deflection of a rigid surface is very small when compared to the deflection of the tire and suspension, hence it can be neglected and the performance of the rigid surface due to load conditions are ignored

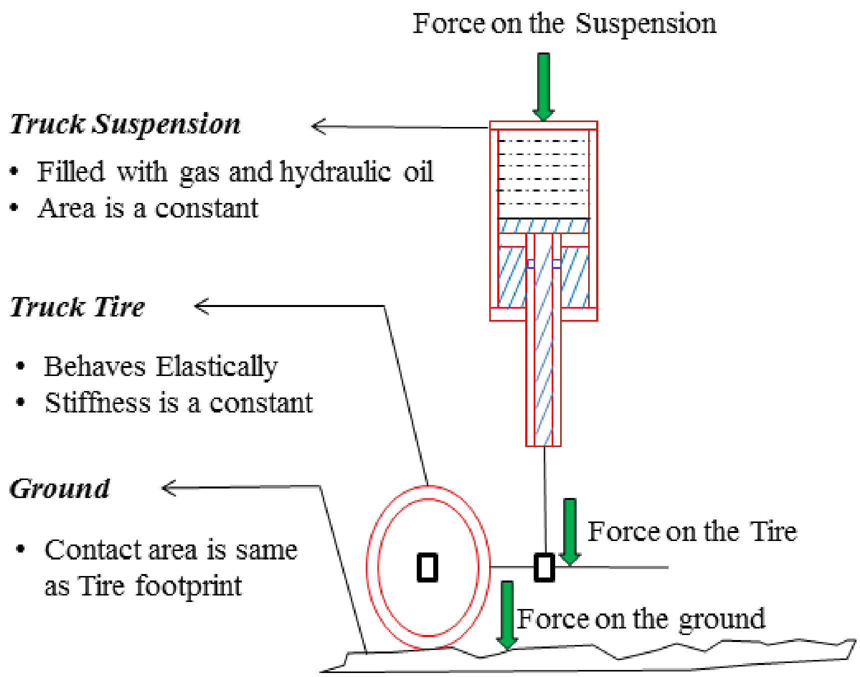

Figure.3.1. General Layout of components considered for the model

3.3. Suspension model parameters and its equations

Most mining trucks are equipped with electronic devices that can display field data directly on the dashboard, which the operator can easily view for reference and safety. Vital information management system (VIMS) is one system used in mining trucks and which provides suspension pressure data at 1Hz. This data was used as the reference point for this research; and all equations and parameters were derived and calculated with the help of this data.

The force passing throughout the system is constant from suspension to ground (Equation.3.1) and any variation per second depends on the pressure response of the suspension. The area of the cylinder is constant and hence only the available length of the suspension (the stroke) varies per second.

$$F_s = F_t = F_g = P_s \cdot A_C \qquad [3.1]$$

Where, F_s , F_t , and F_g are the Force on the suspension, tire, and the ground (kN), A_C is the area of suspension cylinder (m^2), P_s is the suspension pressure indicated by VIMS per second (kPa).

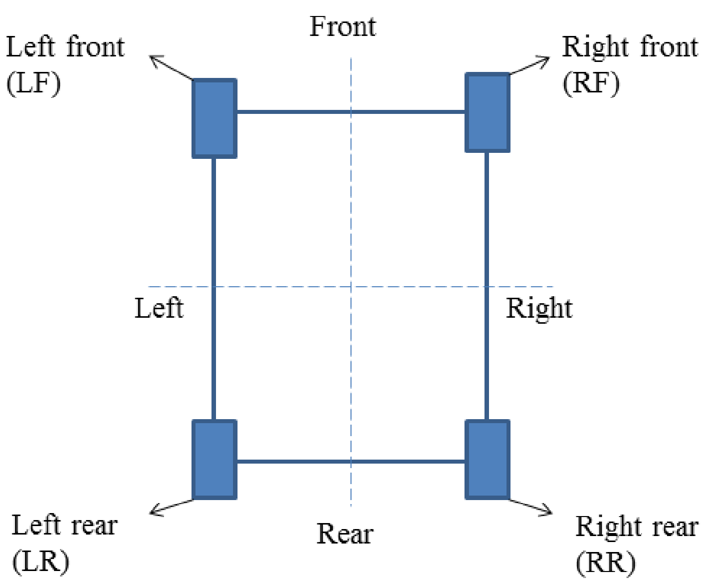

Figure.3.2. Haul truck positions and nomenclature

Different nomenclatures have been considered for each position of the truck and used in this research (Figure.3.2). Both the left front (LF) and right front (RF) position has a single tire and suspension respectively, but the left rear (LR) and right rear (RR) positions have two tires and a suspension. The force on the LF and RF tires match the force acting on the LF and RF suspension respectively. But the truck rear has four tires connected to two suspensions and hence the total force acting on the LR and RR tires is always split into half from the total force acting on the LR and RR suspensions respectively.

$$F_{rt} = \frac{F_s}{2} \qquad [3.2]$$

Where, F_{rt} is the force on a rear tire (kN)

An example of suspension pressure variation derived from the VIMS system for CAT 797B haul truck during field operation is given in Figure.3.3 for one cycle; that includes truck loading, travel, and dumping. The data provides some sense that the load was not equally distributed throughout the body of the truck. LR strut had the highest suspension pressure at all times. This shows that the truck was loaded more on one side, i.e. the left. This variation results in damage to the truck components through load precession, which could cause operator injury, suspension damage, tire failure, and frame breakage. Any of the above impacts constitutes a reduction in life of the truck, which in turn affects the reliability, increases downtime and decreases the production.

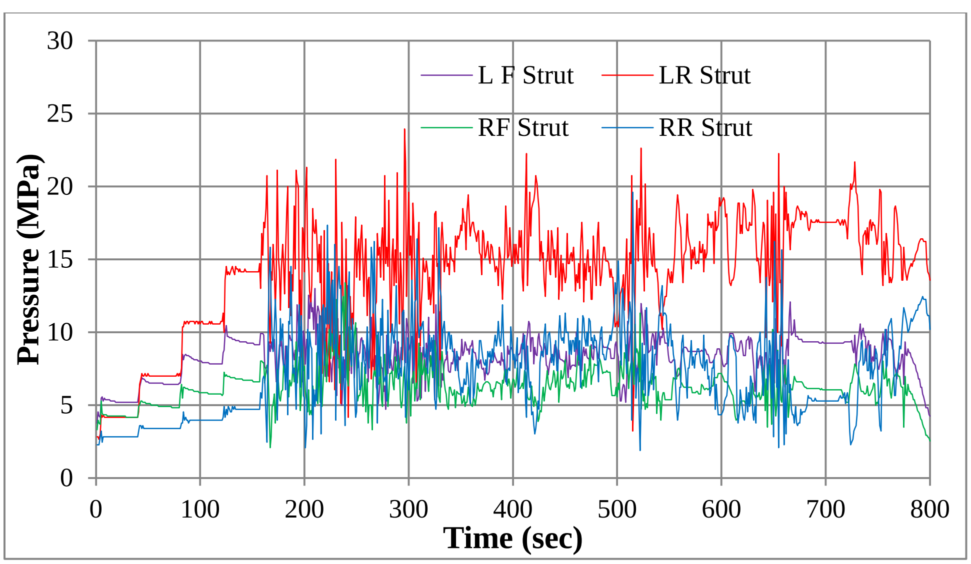

Figure.3.3. Pressure variation at Front and Rear struts for one cycle of CAT 797B

It is important to understand that the pressure of the cylinder is proportional to the g-level impacts on the truck. Road conditions and improper load on the truck causes the suspension try and operate outside the total available stroke length. This phenomenon is known as "*Bottoming out and topping - up"* as described by El-Sayed (2003) and Santos (2007).

Frequent "*Bottoming out"* damages the inner parts of suspension due to metal to metal contact. Also the impact force on the tire and the ground is magnified. As such, it is necessary to verify the variation in available stroke length of the suspension. Equation [3.3] is the isentropic equation which relates pressure and the available stroke length [61].

$$S_a = \left(\frac{P_u}{P_s}\right)^{\frac{1}{\gamma}} \cdot S_u \qquad [3.3]$$

Where, S_a is the available stroke length (m), S_u is the stroke length at the unloaded condition (m), P_u is the suspension pressure at the unloaded condition (kPa), P_s is the suspension pressure per second (kPa), γ is the Isentropic gas constant which is 1.39 for Nitrogen

The performance and the force deformation curve for the suspension depends on degree of inflation, area of the cylinder and the initial available stroke length. These parameters were included into this model. Any suspension is based on the design requirements. The gas inside the suspension acts as a spring and the hydraulic oil provides the damping force. The ratio of liquid and gas should be maintained for appropriate performance of both the suspension and overall the truck. The available stroke length of the suspension provides the fundamental for the prediction of the varying suspension parameters, bad road conditions, and improper load distribution.

A full analysis completed for the unloaded and loaded conditions showed that the load on the truck was not distributed in balance and varied from the actual load distribution data recommended by the truck supplier (Figure.3.4).

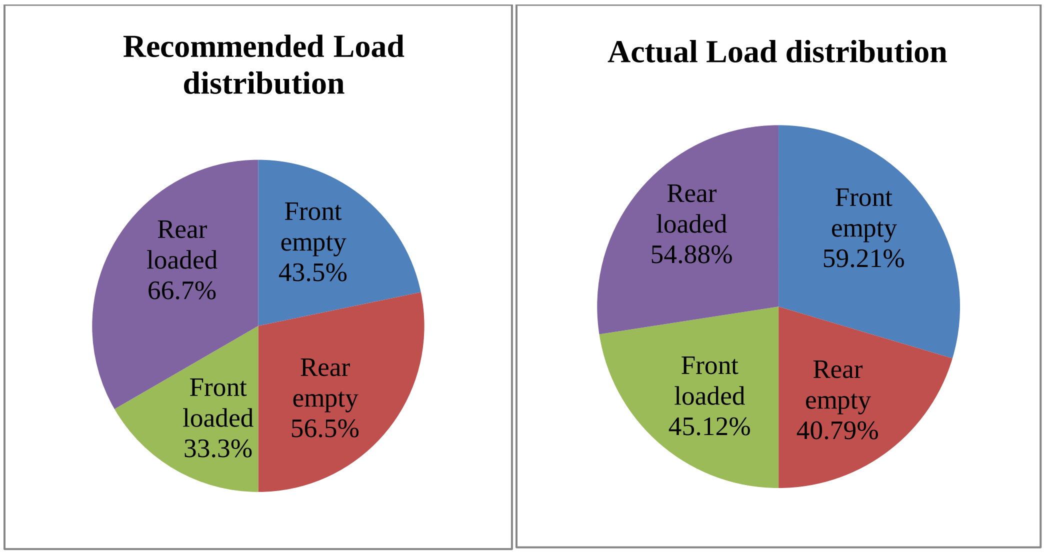

Figure.3.4. Recommended vs actual load distribution for CAT 797B

From this analysis it was found that the rear end of the truck was loaded less than the recommended value. But when the truck was in motion, the pressure at the rear end increased due to motion fluctuations (See Figure.3.3). The available stroke length at the rear suspension was only 0.152m when compared to the front suspension which had an available stroke length of 0.343m. From the data, the maximum pressure experienced by the front strut was 13200 kPa which developed an available stroke length of 0.088m. Compared to rear struts where the minimum available stroke length was 0.026m. Given the common status it was decided to perform the analysis only on the rear suspension and its tires.

A sample field data set from a CAT 797B hauler was analyzed using equation [3.3] with the corresponding stroke lengths determined. Figure 3.5 provides the calculated values for the available stroke lengths with time.

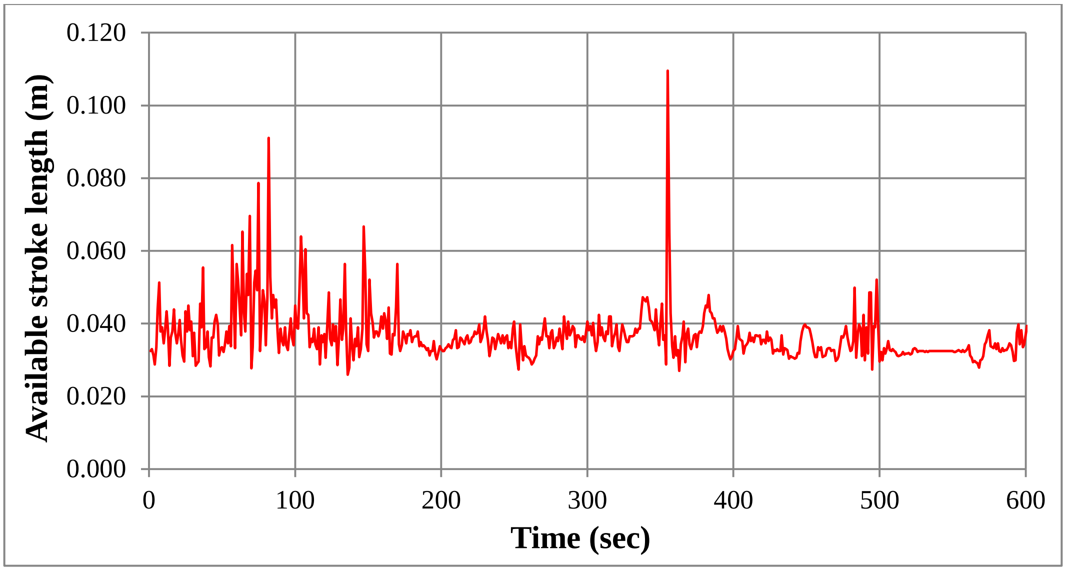

Figure.3.5. Available stroke length data for moving cycle of LR Strut

Figure 3.6 provides a variation of stroke length with the pressure of LR Strut during moving cycle under load condition. The stroke length varied throughout the truck moving cycle and the minimum value reached was 0.028m. The change in the stroke length by pressure for a CAT 797B truck essentially follows an exponential function.

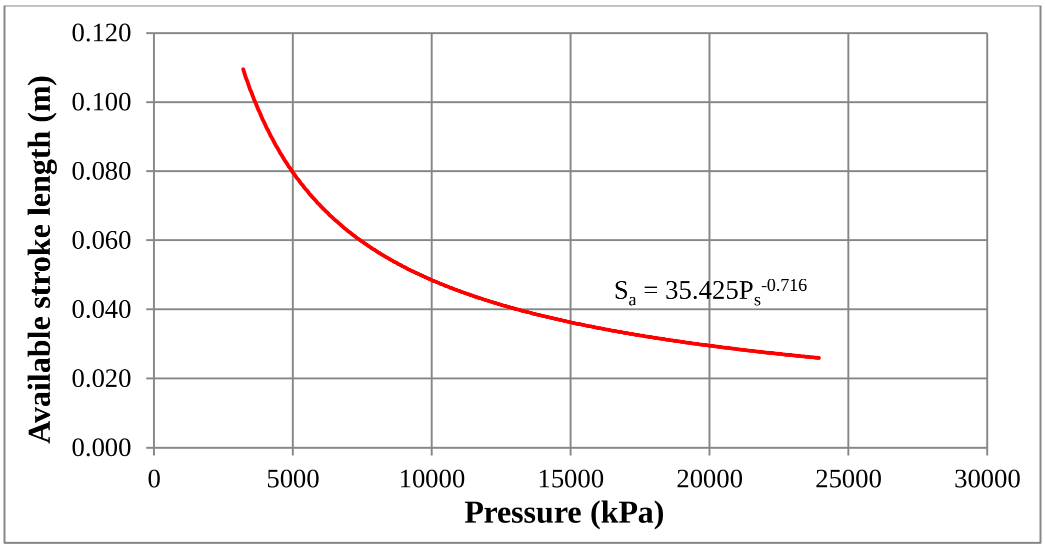

Figure.3.6. Variation of available stroke length with pressure during movie cycle for LR Strut

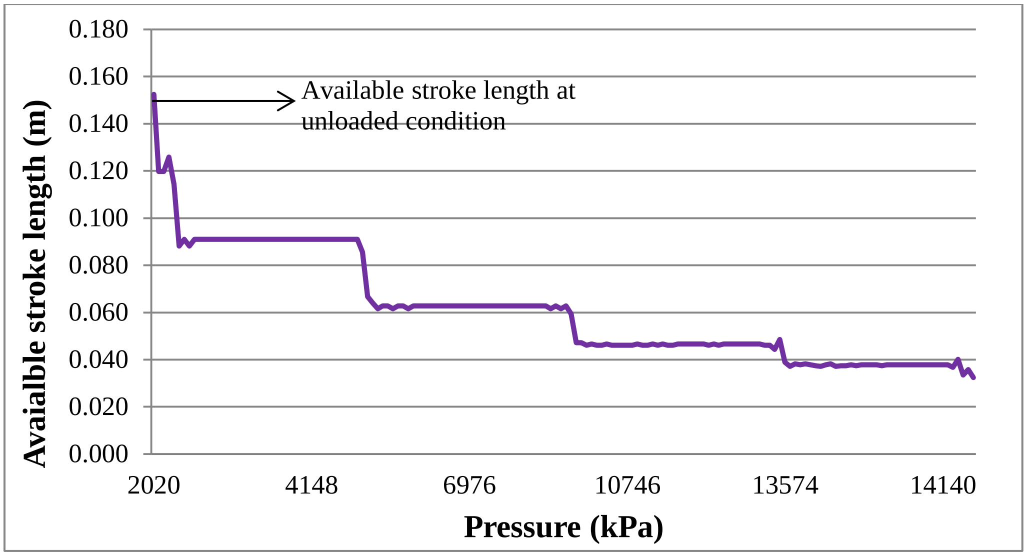

Figure.3.7. Variation in available stroke length with pressure during loading cycle for LR Strut

Figure.3.7 shows that as per the field data, the initial pressure and available stroke length of the truck at unloaded condition were 2020kPa and 0.152m, where the pressure and stroke length varied based on the load acting. The truck after being loaded had an available stroke of only 0.033m before motion. This clearly indicated an opportunity for *bottoming out* to occur. Similarly Soni (2009) did a comparison and found that a truck had only 0.032m to start with. It seems that the degree of remaining closure for most trucks operated in the field after being loaded is low, which makes the suspensions susceptible to serious damage. This does not look good with regard to the overall truck structural performance with even a small change in the condition of the road affecting the suspension and other components of the truck.

3.4. Truck tire model parameters and its equations

Given a procedure to evaluate the performance of the suspension, it is necessary to consider the tire parameters. Truck tire performance is dependent on the loads applied. Both the suspension and the ground conditions are very important in defining the performance of a tire. If the truck tire is exposed to high g-level, it will fail sooner resulting in lower availability and utilization of the truck.

Most tires used in the mining industry are radial tires. From the literature review the following points were noted for pneumatic tires highlighting several important parameters to be considered in any tire evaluation for input into a model.

i) It is clear from the tires literature that only a few researchers have considered incorporating pressure into models [45] [47] [51]. It is important that the shape of the tire should be always maintained through appropriate inflation pressure. Poor inflation pressure results in improper load distribution and causes high impact forces on the tire as well as other components of the truck. Regular checking of inflation pressure is a must since deflection of the tire varies according to this.

ii) A pneumatic tire contains several components. The tread and sidewall are made up of different rubber. Young's modulus is the property which defines the strength of these components and this is also different for both the tread and the sidewall even though they perform the same function. It is difficult to obtain the Young's modulus value for different tires and hence to avoid any difficulty in obtaining the appropriate deflection value for a given loads, stiffness was considered instead of Young's modulus. Young's modulus is more related to the elastic limit of a material but stiffness is related to the interionic distance of the material. Overall stiffness value gives an indication of the overall tire performance.

Lin (2007) provided a stiffness equation for a pneumatic tire, which is known as "*Ryne's regression equation (equation. 3.4)*". This equation was considered in the model to predict the change in deformation due to inflation pressure [51].

$$k_r = 2.68 p_i \sqrt{w_t \cdot \phi_t} + 33.1 \qquad [3.4]$$

Where, k_r, p_i, w_t, and ϕ_t are the radial stiffness (kN/m), inflation pressure (kPa), width (m), and diameter of the tire (m)

Rubber acts as an elastic component similar to an elastic spring and the general stiffness equation for any spring type material depends on the force applied and the experienced deformation (Equation.3.5 and 3.6) [24].

$$k_r = \frac{F_t}{\delta_{tr}} \qquad [3.5]$$

$$\delta_{tr} = \frac{F_t}{k_r} \qquad [3.6]$$

Where, δ_{tr} is the deformation of the tire on a rigid surface (m), F_t is the force on the tire (kN), k_r is the radial stiffness of the tire (kN/m)

3.5. Mathematical model equations

To predict the overall relationship between the suspension and the tire, equations from sections.3.3 and 3.4 were used to derive the final equations. Using equation (3.1) and (3.4) in equation (3.6) provides the deformation of the tire with respect to pressure of the suspension and inflation pressure of the tire (Equation.3.7)

$$\delta_{tr} = \frac{P_s \cdot A_C}{2 \cdot 68 p_i \sqrt{w_t \cdot \phi_t} + 33.1} \qquad [3.7]$$

Where, P_s is the suspension pressure (kPa), A_C is the area of suspension cylinder (m^2), p_i, w_t, and ϕ_t are the inflation pressure (kPa), width (m), and diameter of the tire (m), δ_{tr} is the deformation of tire on a rigid surface (m)

The objective here is to understand the relationship between the available stroke length and deformation of the tire for variable inflation pressure on a rigid surface. Hence the final equation providing such a relationship was derived considering equation (3.3) and equation (3.7).

$$\delta_{tr,f} = \frac{P_u \cdot A_C}{\left(\frac{S_a}{S_u}\right)^{\gamma} \cdot \left(2.68 p_i \sqrt{w_t \cdot \phi_t} + 33 \cdot 1\right)} \qquad [3.8]$$

$$\delta_{tr,r} = \frac{P_u \cdot A_C}{2\left(\frac{S_a}{S_u}\right)^{\gamma} \cdot \left(2.68 p_i \sqrt{w_t \cdot \phi_t} + 33 \cdot 1\right)} \qquad [3.9]$$

Where, S_a is the available stroke length (m), S_u is the stroke length at unloaded condition (m), $\delta_{tr,f}$ and $\delta_{tr,r}$ are the deformation of a front and rear tire on rigid surface (m), P_u is the suspension pressure at unloaded condition (kPa)

It should be noted that the equation (3.8) is applicable for the front tires and equation (3.9) for rear tires on a rigid surface. The denominator for the rear end equation is multiplied by 2 since there are two tires for one suspension and the pressure acting on the rear suspension is equally divided and transferred to the two tires.

The deformation of a tire as per the derived equation (Equation.3.8 and 3.9) depend only on one variable, i.e. the available stroke length. All other parameters are constant and this relationship gives the performance of the tire with respect to the suspension performance. Conversely, the deformation of the tire is inversely proportional to the available stroke length since as the available stroke length decreases, the deformation of the tire increases. In this scenario, under field conditions, the deformation of the tire and available stroke length react opposite to each other.

As the tire deforms as per the loading condition, it creates a footprint on the ground. The footprint area of the tire is an important factor that should be considered in any model since the contact between the tire and the ground gives an idea of the tire load withstanding capability and inflation pressure accuracy. It also allows for the prediction of the total surface of the ground exposed to the applied force, which helps in calculating the stresses experienced by the ground.

As seen in the literature review, Sharma (2009) compared various tire sizes to obtain an equation for the footprint area of the tire (equation. 3.10), which is used in the model. It basically depends on the deformation of the tire and its diameter [60].

$$A_{tr} = 1.35\delta_{tr}\phi_t \qquad [3.10]$$

Where, A_{tr} is the footprint area of tire on rigid surface (m^2), δ_{tr} is the deformation of tire on a rigid surface (m), ϕ_t is the diameter of tire (m)

3.6. Mathematical model equation validation with field and laboratory results

It is always better to compare the derived equations with field and laboratory results since it can prove the accuracy of the equations determined for various scenarios. Sharma (2009) performed laboratory test on 0.368m diameter tire and obtained the field tire deformation and footprint area for 1g load (1040kN) of a full size truck (CAT 797B). Bolster (2007) performed laboratory tests on 2.85m diameter truck tire and obtained deformation characteristics for various loads and inflation pressures. To check the validity, accuracy and applicability of the derived equation under full scale loading for different truck sizes, comparisons were made with these field and laboratory results obtained by the previous researchers.

3.6.1. Comparison with laboratory results

Initial comparisons were made with tires used by Sharma (2009) and Bolster (2007). They performed laboratory tests and obtained results for various loads and inflation pressures. The dimension of the 0.368m diameter tire was obtained from a data sheet given by Sharma (2009). Bolster (2007) provided the dimensions of the tires used as 30R0051 with an external diameter of 2.85m and width of 0.762m (Bolster, 2007). The first parameter (30) in the designation of the tire model gives the width of the tire in inches. So, converting that to the required unit gives the exact width of the tire.

Both Sharma and Bolster used a ram for the application of force to the tires tested. As such, it was difficult to find out the exact parameters like the isentropic constant of gas used (a constant value = 1.39), the initial and final pressure, and the initial and final available stroke length. Hence in this study the force value was used instead of pressure, stroke length and area of the cylinder from tire deformation equation (3.8). Equation (3.9) was used for loads applied to two tires and equation (3.8) was used here since both researchers performed laboratory tests on a single tire and the force applied is then directly transferred to that tire.

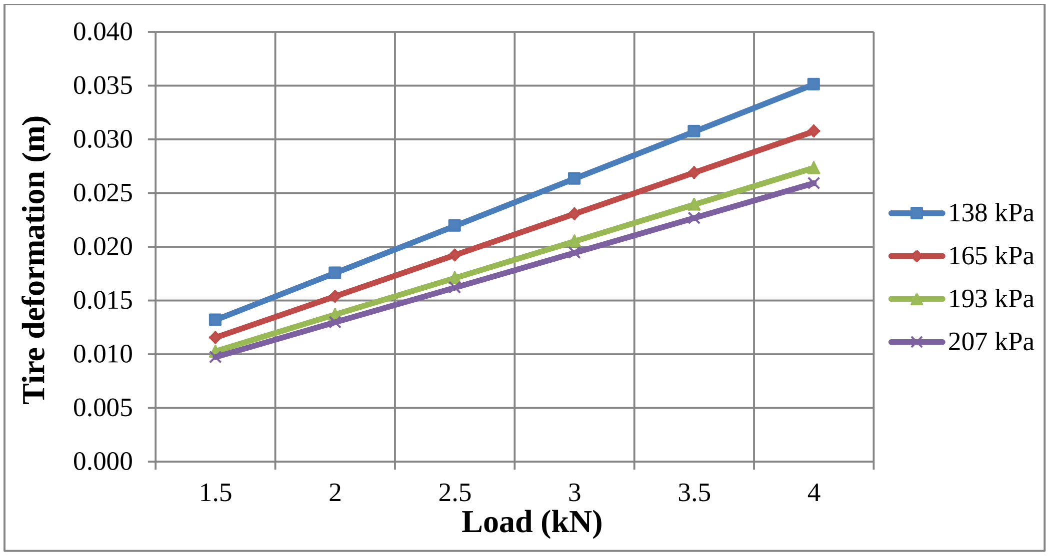

Figure 3.8.Load vs Deformation for 0.368m diameter tire

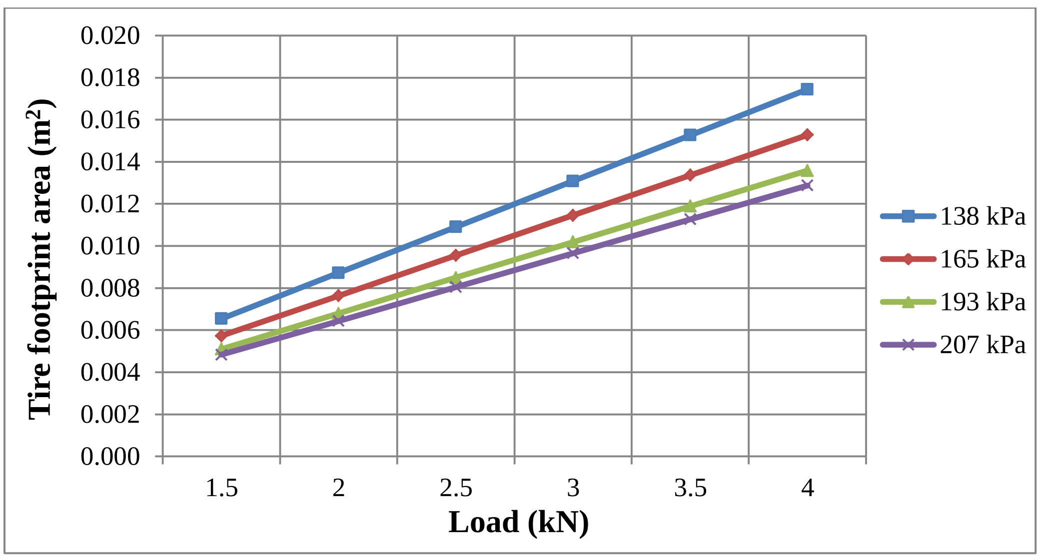

Figure 3.9.Load vs Footprint area for 0.368m diameter tire

Figure 3.8 and 3.9 provides the data for the variation of deformation and footprint area with load for a 0.368m diameter tire. The increase in both parameters is linear since the only variation when using equation (3.7) is the force and the stiffness is a constant for a given pressure. The comparisons between the model and laboratory values are provided in Table.3.1.

Inflation pressure (kPa)	Load (kN)	Tire deformation (m)		Tire footprint area (m^2)	
		Model	Laboratory results	Model	Laboratory results
138 (20psi)	2.0	0.018	0.019	0.009	0.012
	2.5	0.022	0.023	0.011	0.014
	3.0	0.026	0.028	0.013	0.016
	3.5	0.031	0.033	0.015	0.018
165 (24psi)	2.0	0.015	0.017	0.008	0.010
	2.5	0.019	0.021	0.010	0.013
	3.0	0.023	0.025	0.011	0.014
	3.5	0.027	0.029	0.013	0.016

Table.3.1. Model output and laboratory value comparison for 0.368m diameter tire

There are deviations in tire deformation and footprint area comparison. This deviation is due to the values compared are low in magnitude, which resulted in some measurement error. A better understanding could have been made if the initial available stroke length of the suspension was known.

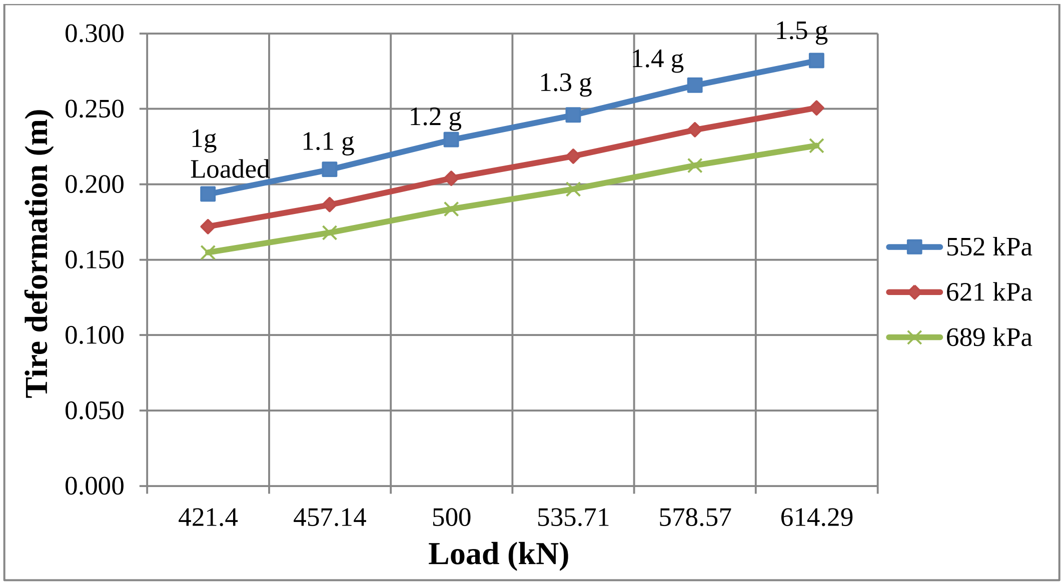

Figure 3.10.Load vs Deformation for 2.85m diameter tire

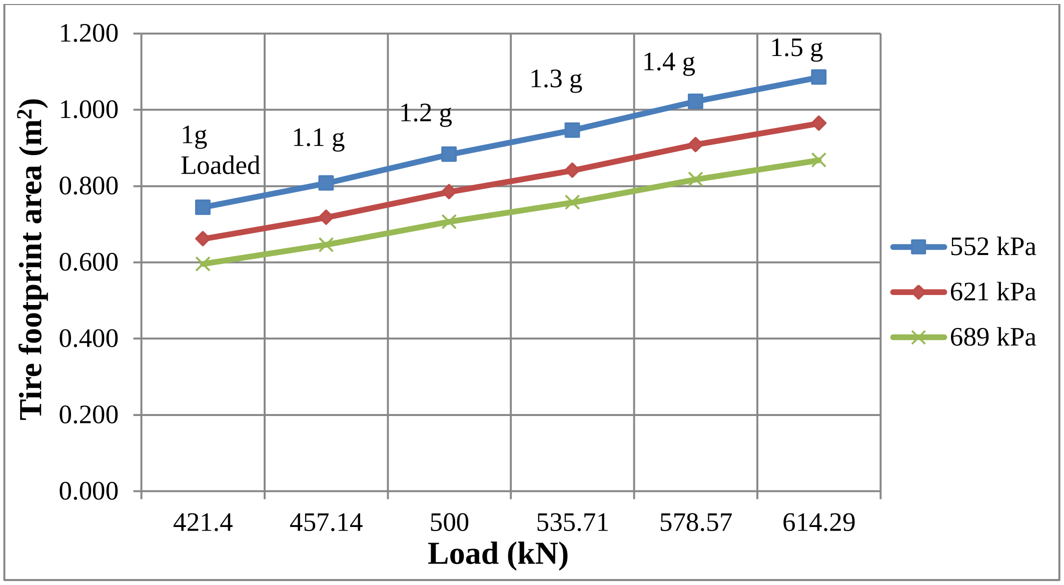

Figure 3.11.Load vs Footprint area for 2.85m diameter tire

Figures 3.10 and 3.11 provide data for the variation of deformation and footprint area with load for the 2.85m diameter tire. The increase in both parameters is effectively linear since the only variation when using equation (3.7) is the force, and the stiffness is constant for a given pressure. The comparisons between the model and laboratory values are provided in Table.3.2.

<table>
<tr><th rowspan="2">Inflation pressure (kPa)</th><th rowspan="2">Load (kN)</th><th colspan="2">Tire deformation (m)</th><th colspan="2">Tire footprint area (m^2)</th></tr>
<tr><th>Model</th><th>Laboratory results</th><th>Model</th><th>Laboratory results</th></tr>
<tr><td rowspan="6">552 (80psi)</td><td>182.14</td><td>0.084</td><td>0.111</td><td>0.322</td><td>0.502</td></tr>
<tr><td>421.43</td><td>0.193</td><td>0.200</td><td>0.744</td><td>0.796</td></tr>
<tr><td>457.14</td><td>0.210</td><td>0.211</td><td>0.807</td><td>0.849</td></tr>
<tr><td>500</td><td>0.230</td><td>0.221</td><td>0.883</td><td>0.889</td></tr>
<tr><td>535.71</td><td>0.246</td><td>0.234</td><td>0.946</td><td>0.947</td></tr>
<tr><td>578.57</td><td>0.266</td><td>0.245</td><td>1.022</td><td>0.964</td></tr>
</table>

Table.3.2. Model output and laboratory value comparison for 2.85m diameter tire

Again there is a minor deviation between the results of the mathematical model and laboratory values. The deviation in comparison to tire deformation might be due to measurement error due to the low measured value. In the case of the tire footprint area, the deviation is also low. But when the standard footprint area equation (3.10) is used for the laboratory values, the footprint area does not match with the corresponding deformation values. This may explain the deviation in footprint area between laboratory and model results.

3.6.2. Comparison with Field value (CAT 797B)

Sharma (2009) performed a field test and found the values for the deformation of the CAT 797B truck with 55/80R63 truck tire size. He found that the deformation of the rear tire at 1g load (1040kN) and 600 kPa inflation pressure was 0.27m resulting in 1.29m^2 of the contact footprint area (Sharma, 2009).

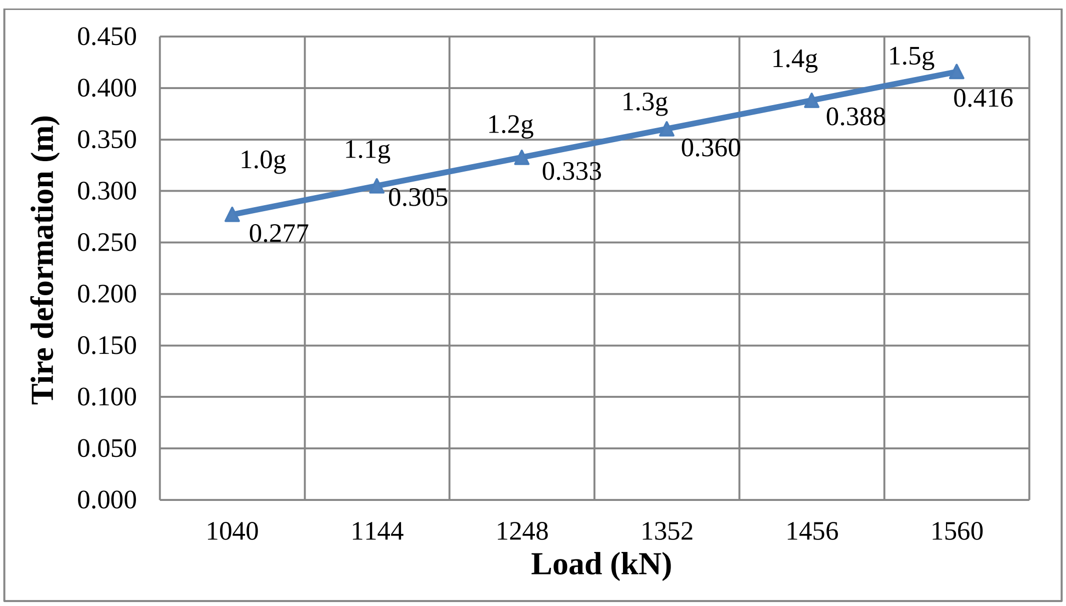

Figure 3.12. Load vs Tire deformation for 55/80R63 tire at 600 kPa

Comparison with laboratory results showed that the mathematical model equation is valid (Equation.3.7 to 3.10). Further validation by comparison with field values would enhance their accuracy. Equations (3.9) and (3.10) were used for this comparison. Equation (3.9) was used since the comparison is made for a rear tire, where the pressure from the suspension is divided equally between the two tires.

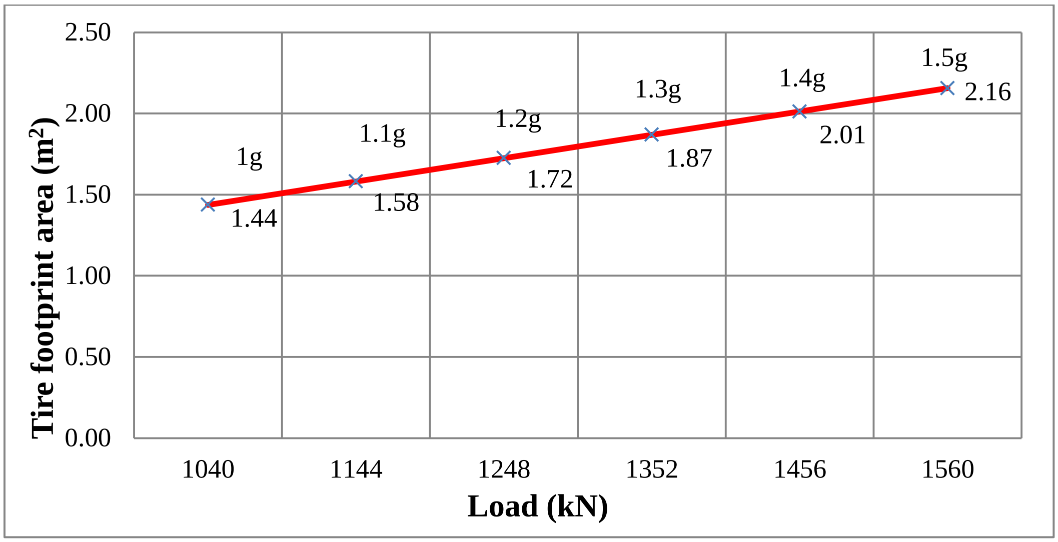

Figure 3.13. Load vs Tire footprint area for 55/80R63 tire at 600 kPa

Both deformation and the footprint area for the tire were obtained. Table.3.4 provides a comparison of values obtained from the field; the predicted value by Sharma (2009), and the model output for 1-g load (1040kN).

Description	Tire diameter (m) and designation	Inflation pressure (kPa)	Tire deformation (m)	Tire footprint area (m^2)
Field value	3.84 (55/80R63)	600	0.270	1.30
Predicted value (Sharma, 2009)	3.84 (55/80R63)	600	0.270	1.40
Model output	3.84 (55/80R63)	600	0.277	1.44

Table.3.3. Model output and field value comparison for 1-g load of CAT 797B

It can be seen that the values from the mathematical model equations matches with the field values. It was not possible to do a comparison for the values above 1g due to lack of data. Further validation is required for the derived equations above this load. Hence from the comparison of both the field and laboratory results it can be said that the mathematical model equations appear valid and may be used to predict results close to actual field data, extended to full scale truck size. Also it is clear that the mathematical equations model can predict deformation and footprint for any size tire, for small to larger loads.

3.7. Understanding the relationship between stroke length of suspension and deformation of tire for full size truck

All the above comparisons were made considering the action of force on a tire without considering the pressure and available stroke length of the suspension. The results obtained in all the comparisons provided a linear relationship. But in order to have a better understanding, the available stroke length of the suspension was also included here for the comparison (i.e. using equation. 3.9).

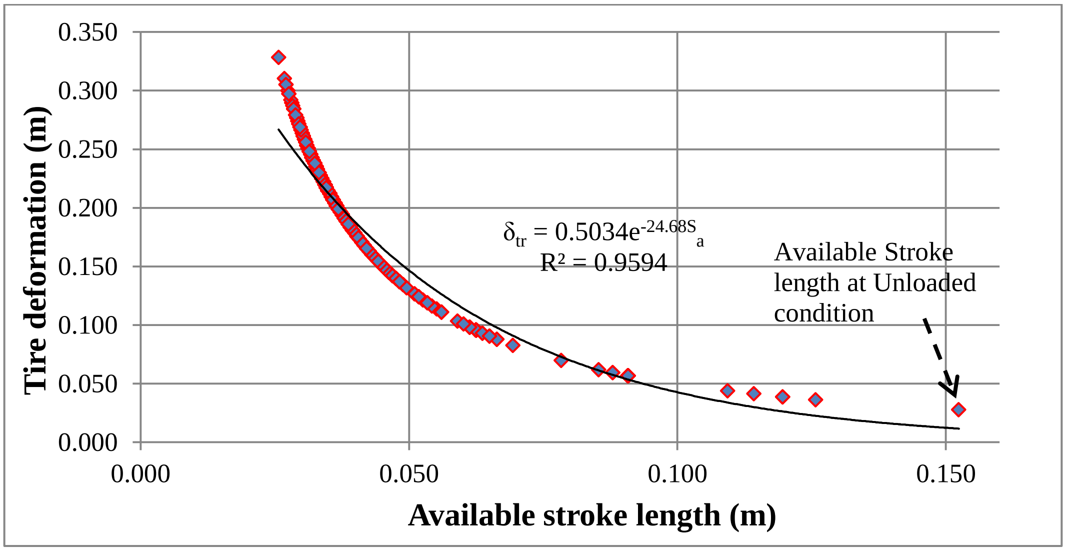

Figure 3.14.Available stroke length vs tire deformation for CAT 797B at 600 kPa

There are no field or laboratory results for the comparison between suspension and tire performance for a full sized ultra-class truck. Hence it was decided to study the relationship for a CAT 797B truck since the suspension pressure data and characteristics of both the suspension and the tire were known. Equation (3.9) was used for this comparison. The stroke length variation and tire deformation follows an exponential form (Figure.3.14).

This shows that as the available stroke length increases or decreases, the deformation does not increase or decrease linearly, since more than one parameter is involved to affect the relationship. There are many parameters and each parameter is important to provide the overall relationship between the available stroke length and the deformation of the tire. Those parameters are the ones given in equations (3.8) and (3.9). Similarly, these equations can be used for different types of trucks used in the mining industry, where some of the parameters of the suspension and the tire are known.

CHAPTER 4

MATHEMATICAL MODEL FOR PERFORMANCE PREDICTION OF TRUCK SUSPENSION, TIRE, AND THE OIL SAND

4.1. Introduction and objective

Oil sand exhibits a total different behavior from a rigid surface. From the literature review it is clear that sinkage and rutting are the main characteristics that occur in oil sand during truck loading and movement. By amount of bitumen content present in the oil sand, the truck tire will sink into the ground proportionally. Also the oil sand due to its poor load withstanding capability deflects under the action of truck loads. A method to discern the sinkage of oil sand with 11% bitumen content and the corresponding deformation of a tire on oil sand under varying load conditions has been addressed in this chapter.

In chapter 3 the mathematical model equations and results for truck component's performance on rigid surface were provided. This chapter deals with the model equations and their results for the performance prediction relative to oil sand and the truck component's on oil sand. Since laboratory tests are already done by Sharma (2009) on oil sand as deformation for various loads, it was decided not to perform the tests again as the same results would be obtained.

The main focus of this chapter was to provide a method to discern the relationship and behavior of a composite truck - ground model including the truck suspension, tire and the oil sand. Also prediction using the mathematical model without the influence of laboratory test results is a main goal of this research. The equations obtained by Sharma (2009) and pressure stiffness predicted by Sharif-Abadi (2006) for 11% bitumen oil sand are considered in this model and modified as per the objective of this research.

4.2. Suspension model equations

The suspension parameter accounting for the ground condition is dependent only on reaction force due to the ground. Characteristics are not dependant on the bitumen content, moisture content of oil sand or atmospheric pressure and temperature. Hence the equation for the change in stroke length of the suspension is the same as used in chapter 3.

4.3. Tire model equations

Since the tire comes into contact with the oil sand which has lower stiffness than a rigid surface, the equations related to the tire will change from that on the rigid surface.

Most of the tests performed to predict the deformation of oil sand was conducted with a plate. But in field, only tire comes into contact and there is a difference between the reaction caused on oil sand due to tire and normal cylindrical plate. Sharma (2009) performed cyclic tests with a 0.368m diameter tire on oil sand of 11% bitumen and room temperature. After comparing with several data from the laboratory results he found out the relationship for the deformation of the tire on oil sand (Equation.4.1) (Sharma, 2009). He was the first to perform the test with a tire on oil sand and hence it was decided to use equation (4.1) and modify it to obtain the relationship exactly as per the field operation.

$$\delta_{ts} = \frac{1}{2}\left[\left(\delta_{os}^2 + \frac{4F_t}{CE}\right)^{\frac{1}{2}} - \delta_{os}\right] \qquad [4.1]$$

Where, δ_{ts} is the deformation of tire on oil sand (m), δ_{os} is the deformation of oil sand (m), F_t is the force on the tire (MPa), E is the Young's Modulus of the tire (MPa), C is the oil sand constant

As discussed previously since Young's modulus of tires varies for different components, it was decided to use the equations in chapter 3 to predict it. As Young's modulus is a constant value, it does not vary with load. Also since Sharma (2009) obtained the deformation and footprint area for a 1g load for 55/80R63 tires from the field, it was possible for him to evaluate a stiffness equivalent for Young's modulus. In the mathematical model here that problem is eliminated, as measurement of a field value is not necessary.

The procedure for determining Young's modulus for a tire is as follows. First the deformation and footprint area of a tire on a rigid surface is calculated for a 1g load using equation (3.2) and equation (3.3). Finally the obtained values are used in equation (4.4) to predict a Young's modulus value for the tire. Since the tire effectively acts as an elastic spring, the Hooke equation is applicable and is used here (Sharma, 2009). A similar method can be used in predicting the Young's modulus value for different tires with the condition that the inflation pressure and dimensions of the tire are known.

$$E = \frac{\sigma}{\varepsilon} \qquad [4.2]$$

$$E = \frac{\left(\dfrac{F_t}{A_{tr}}\right)}{\left(\dfrac{\delta_{tr}}{\phi_t}\right)} \qquad [4.3]$$

$$E = \frac{F_t \cdot \phi_t}{\delta_{tr} \cdot A_{tr}} \qquad [4.4]$$

Where, σ and ε are the stress (MPa) and the strain, F_t and ϕ_t are the force on the tire (kN) and diameter of the tire (m), δ_{tr} and A_{tr} are the deformation (m) and footprint area of tire on rigid surface (m^2)

Replacing equation (4.4) in equation (4.1) provides a modified equation for prediction of deformation of a tire on oil sand.

$$\delta_{ts} = \frac{1}{2}\left[\left(\delta_{os}^2 + \frac{4F_t}{CE_{g_1}}\right)^{1/2} - \delta_{os}\right] \qquad [4.5]$$

Where, E_{g_1} is the Young's modulus of the tire predicted at 1g load (MPa)

4.4. Oil sand model equations

An array of models predicts the dynamic modulus and resilient modulus of oil sand. But none of the models from the literature prove to predict field values when a tire acts on oil sand, and each model is applicable only for a particular condition, with each model having their own constants that could be determined only with the help of performing experiments in the laboratory.

Hence with all these difficulties, to be able to predict the deformation value of oil sand with just the mathematical equations, it was resolved to use the pressure stiffness developed by Sharif – Abadi (2006) and the equations given by Sharma (2009) modified it as per the research objective here. Sharif – Abadi (2006) performed instantaneous loading cyclic tests on oil sand at 200, 400, 600, and 800 kPa.

From the test results he predicted that regardless of the duration of loading and relaxation, the pressure stiffness value converged to 5.5kPa/mm. Using the pressure stiffness, the problem of varying footprint area of the tire with cyclic loading is eliminated. Also the deformation of the oil sand depends on the total area of oil sand exposed to the load, which cannot be predicted with the current available mathematical equations. Hence pressure stiffness is a parameter that can used to effectively ignore the effects of varying footprint area and in turn predicting the deformation of oil sand.

The number of loading cycles ranged from 15 – 20 cycles for every full load. With just few loading cycles, the oil sand does not reach a maximum stiffness value, hence the pressure stiffness of 5.5kPa/mm is considered as the standard value in this analysis. Pressure stiffness is the ratio of total pressure to the total deformation (Equation.4.6) (Sharif – Abadi, 2006).

$$k_p = \frac{P_{os}}{\delta_{os}} \qquad [4.6]$$

$$k_p = \frac{\left(\dfrac{F_g}{A_{os}}\right)}{\delta_{os}} = \frac{F_g}{A_{os} \cdot \delta_{os}} \qquad [4.7]$$

Where, k_p is the oil sand pressure stiffness (kPa/m), F_g is the force on the oil sand ground (kN), A_{os} and δ_{os} are the footprint area (m^2) and deformation of oil sand (m)

It should be noted that since the tire sinks into the oil sand, the total area of oil sand under load depends on both the deformation of oil sand and deformation of the tire which inherently changes the contact footprint area. Equation (4.8) has an oil sand deformation term and a constant C. This constant clearly gives the differentiation between the deformation and footprint area of the rigid and oil sand grounds. The value of C after performing tests on oil sand for 80 cycles was obtained by Sharma (2009) and it varies from 1.66 to 1.11 from the first cycle to the 80th cycle (Sharma, 2009).

$$A_{os} = C\left(\delta_{os} + \delta_{ts}\right) \cdot \phi_t \qquad [4.8]$$

Where, A_{os} is the area of oil sand (m^2), δ_{os} is the deformation of oil sand (m), δ_{ts} is the deformation of the tire on oil sand (m), ϕ_t is the diameter of the tire (m)

The modified equation is obtained by substituting equations (4.5) and (4.8) in equation (4.7). Since the force on the ground is equal to the force on the tire, the term F_g is replaced by F_t in the final equation.

$$k_p = \frac{F_t}{C \cdot \left(\delta_{os} + \delta_{ts}\right) \cdot \phi_t \cdot \delta_{os}} \qquad [4.9]$$

Now bringing the deformation parameter on one side, the equation (4.9) becomes,

$$\left(\delta_{os} + \delta_{ts}\right) \cdot \delta_{os} = \frac{F_t}{k_p \cdot C \cdot \phi_t} \qquad [4.10]$$

Substituting equation (4.1) in equation (4.10)

$$\left[\delta_{os} + \left[\frac{1}{2}\left(\left(\delta_{os}^2 + \frac{4F_t}{CE}\right)^{\frac{1}{2}} - \delta_{os}\right)\right]\right] \cdot \delta_{os} = \frac{F_t}{k_p \cdot C \cdot \phi_t} \qquad [4.11]$$

Expanding equation (4.11),

$$\delta_{os} = \sqrt{\frac{F_t \cdot E}{\left(k_p^2 \cdot C \cdot \phi_t^2\right) + \left(k_p \cdot C \cdot E \cdot \phi_t\right)}} \qquad [4.12]$$

Where, δ_{os} is the deformation of oil sand (m), k_p is the pressure stiffness of oil sand (kPa/m), F_t is the force on the tire (kN), E is the Young's modulus of the tire (kPa), ϕ_t is the diameter of the tire (m), C is the oil sand model constant

The pressure stiffness of oil sand, and Young's modulus and diameter of the tire are a constant. The variables related to the deformation of oil sand are the force on the tire and the oil sand model constant. Hence equation (4.12) is the modified equation that can predict the deformation of oil sand with bitumen content of 11% under cyclic loading activity of the truck.

4.5. Oil sand mathematical model equations output

The process in obtaining the mathematical model equations for the oil sand is totally different from the process used for the rigid surface. In the same way the procedure in obtaining the output for oil sand and the truck components on oil sand using the model equations are also different.

i) Calculate the Young's modulus of the tire on a rigid surface for 1g load (Equation.4.4)
ii) Substitute the Young's modulus value in equation (4.12) and find out the deformation of oil sand for every loading cycles
iii) Substitute the obtained value from step 1 and step 2 into equation (4.5) and calculate the deformation of tire on oil sand for every loading cycle

4.5.1. Performance Output for CAT797B truck on oil sand

CAT 797B pressure data, the tire parameters, and the pressure stiffness value were used in the derived equations to obtain the deformation output for the suspension, tire, and the oil sand. Three different loading cycle methods were considered for the analysis to predict the response of the derived equations for various load conditions.

A first loading cycle consists of applying a constant 1g load. The second loading cycles consist of applying a constant increasing load of 52kN. Finally the last loading cycle consists of applying a load as per the field data where the load varies with time.

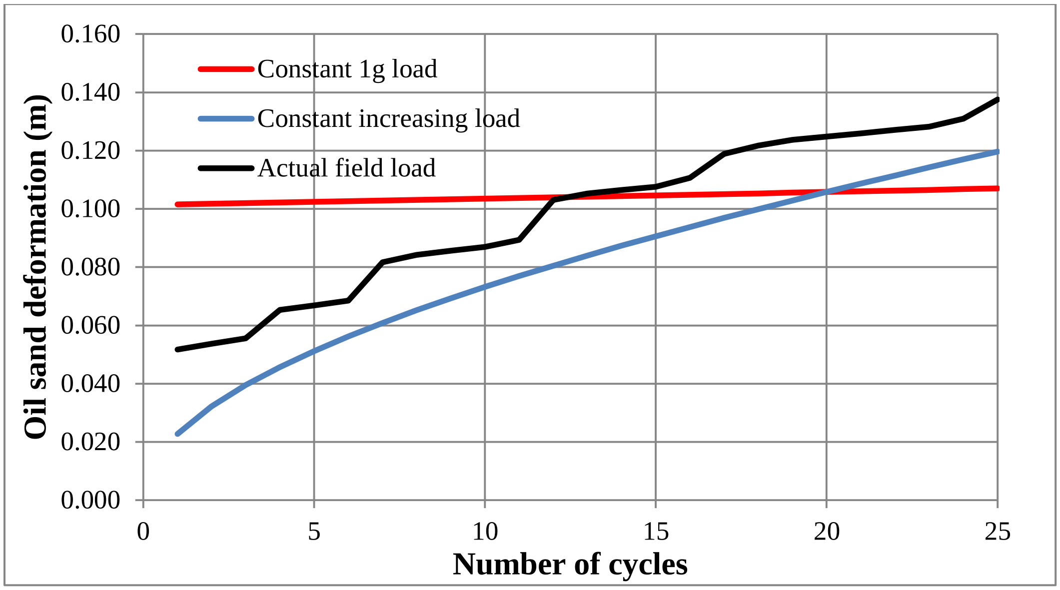

Figure.4.1. Oil sand deformation with different loading cycle

It can be seen that the oil sand cyclically deformed differently for each of the methods (Figure.4.1). For a constant 1g applied load, the oil sand deformed gradually and for an increasing load (52kN) the oil sand deformed rapidly. But the third cyclic loading method allowed the oil sand to deform at a faster pace than the other two methods. As the load increase was higher by number of cycles, this allowed the oil sand to compact further with fewer numbers of cycles.

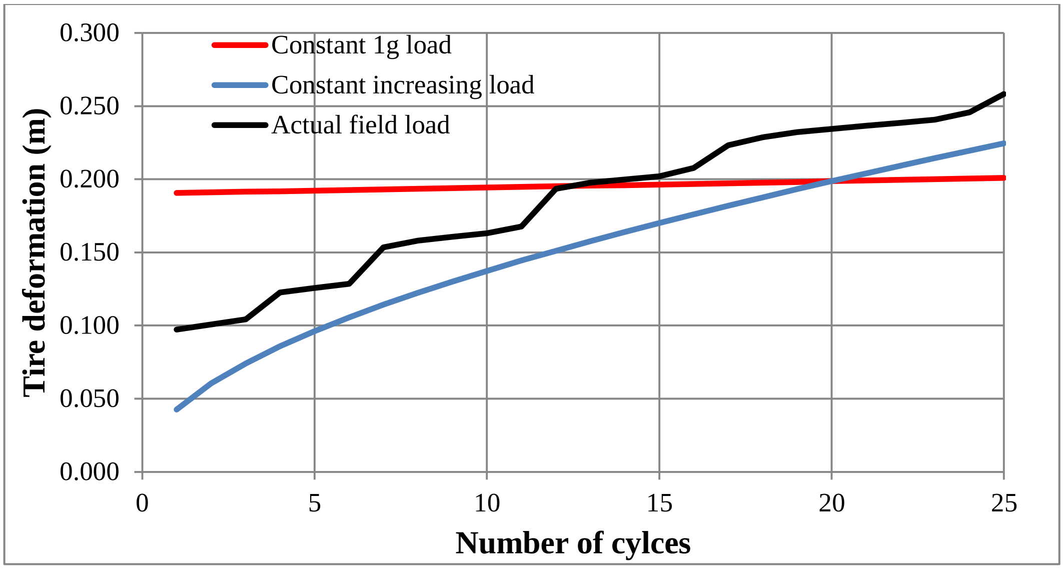

Figure.4.2. Tire deformation with different loading cycle

Tire also deformed in the same manner as oil sand (Figure.4.2). The rate of deformation of both oil sand and tire decreased gradually with increasing number of cycles. This would follow for any truck acting on oil sand as the ground would become stiffer and increase its ability to withstand load with gradually decreasing deformation.

4.5.2. Performance Output for CAT797B truck on oil sand as per field condition

As such, from chapter 3 it was evident that the tire rear was loaded more than the front (figure.3.4). To understand the effect due to this high loading at the rear, comparisons were done between the LR and RR position of the same truck to evaluate numerous parameters like total deformation (tire and oil sand), tire deformation, oil sand deformation, footprint area, and the available stroke length (for suspension). Figure.4.3 compares tire deformation for the LR vs RR tire sets during a loading cycle.

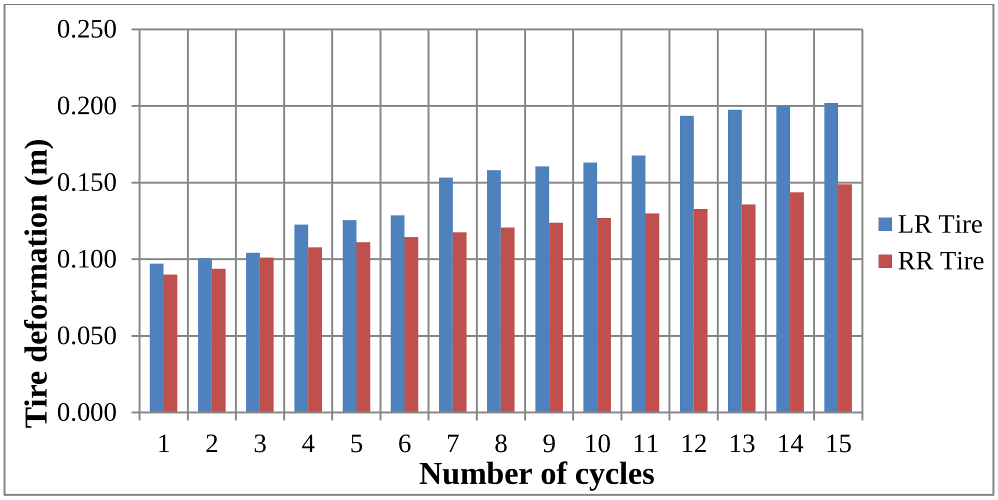

Figure.4.3. Tire Deformation on oil sand with number of cycles for LR and RR Tire

The deviation in the total deformation (oil sand + tire) with cyclic loading was also studied. Figure.4.3 clearly shows that the total deformation at the LR position is higher than the RR position. The deformation of oil sand and the tire at LR position was higher than at RR position because of varying load conditions and ground pressure, and this made the total deformation also to be more on LR position.

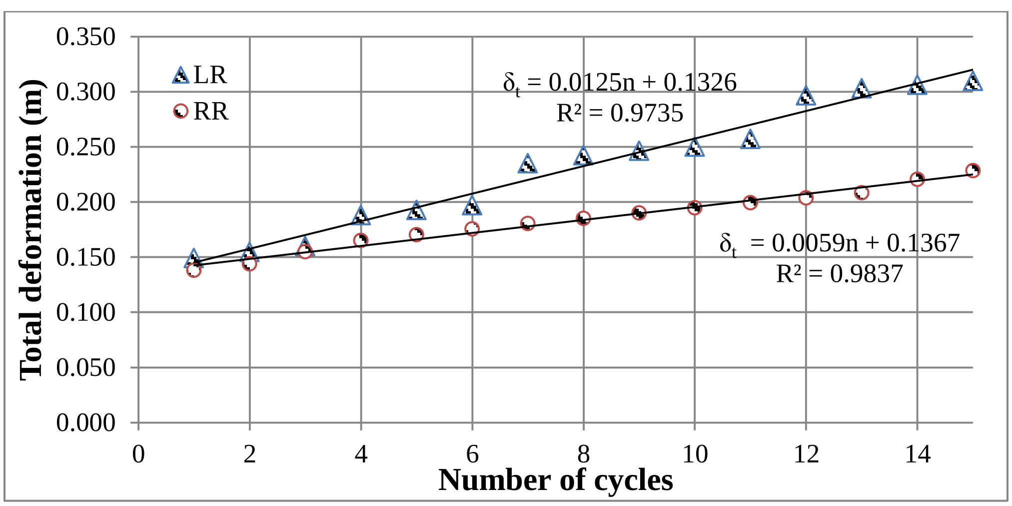

Figure.4.4. Comparison of total (tire and oil sand) deformation with increasing number of cycles

Clearly the LR strut had larger forces acting due to a higher payload and this caused the difference in the total deformation for both sides. In an ideal scenario this should not be the case, since the load should be equally distributed. This shows that the truck was not loaded properly and while travelling it created an unequal deformed running surface. The problem generated here is for the same truck and also for the next truck. Even if the next truck has a balanced payload distribution, because of the evenness that follows along the same road in the running surface causes the balanced truck to move reflecting the ground deformation.

4.5.3. Understanding the relationship between stroke length of suspension and deformation of tire and oil sand for full size truck

A study was made to find the relationship between the available stroke length and the deformation of the tire, oil sand and the overall total deformation (tire and oil sand) (Figure.4.5 and Figure.4.6) using the mathematical model equations.

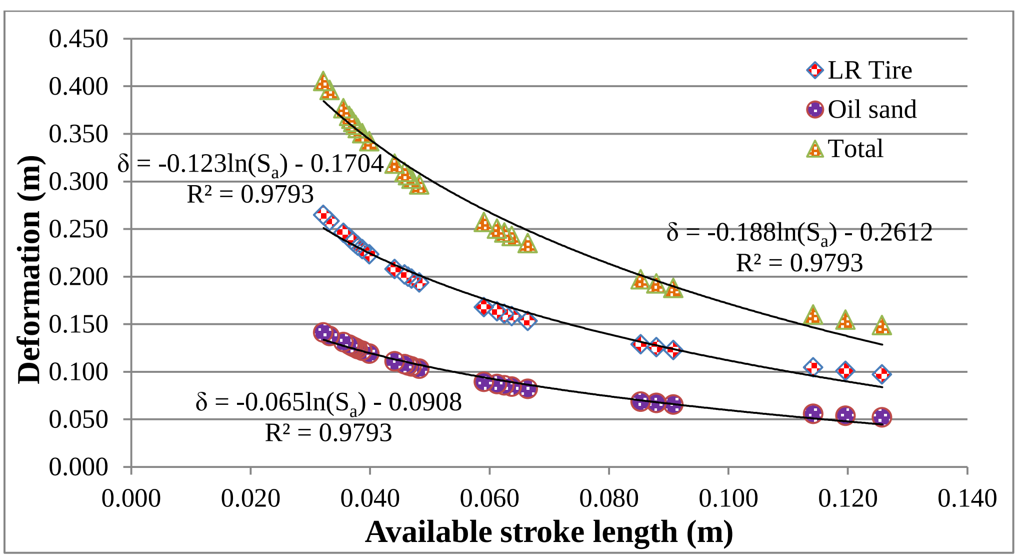

Figure.4.5. Comparison between available stroke length and deformation of tire, oil sand and total deformation at LR position

Since the LR strut had the highest pressure, the total available stroke length at the end of the loading cycle was only 0.032m when compared to RR value of 0.062m as seen in figures (4.5) and (4.6). This could also lead to metal to metal contact in the suspension resulting in suspension failure, LR tire damage and were an indicator of unbalanced load. At the end of the loading cycle, the oil sand under RR position deformed to 0.087m. But under LR position it deformed to 0.141m, which is 1.62 times the deformation under RR position. This would create an undulated ground condition causing the truck to sink more towards the LR. The final deformation of the LR tire (0.265m) is 1.61 times the deformation of the RR tire (0.164m) and this difference is very high.

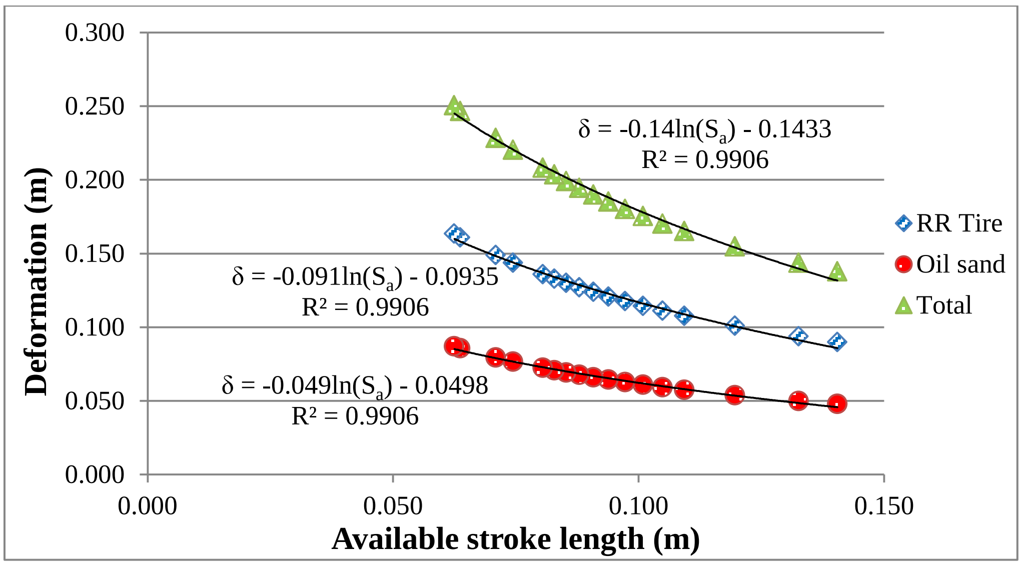

Figure.4.6. Comparison between available stroke length and deformation of tire, oil sand and total deformation at RR position

4.5.4. Tire footprint area and ground stress comparison for CAT 797B truck

Footprint area of a tire and the ground stress variation for various loading conditions of LR and RR positions were compared here (Figure.4.7 and 4.8). The stress followed close to a linear pattern. As the number of cycles increased, the stress on the ground also increased. The stress at the LR was more than that at RR because of higher load. The footprint area of oil sand at the LR is also more than at the RR.

At the end of the loading cycle, the LR tire has footprint area of 2.31m^2 when compared to the RR, which has only footprint area of 1.49m^2. The higher load factor is the reason for more stress and contact area at the LR.

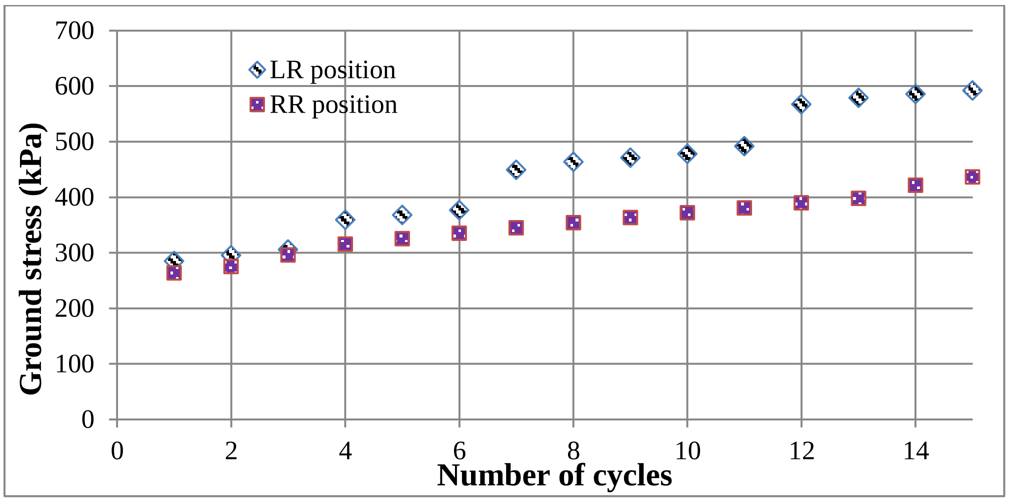

Figure.4.7. Ground stress distribution at the rear position of the loading area

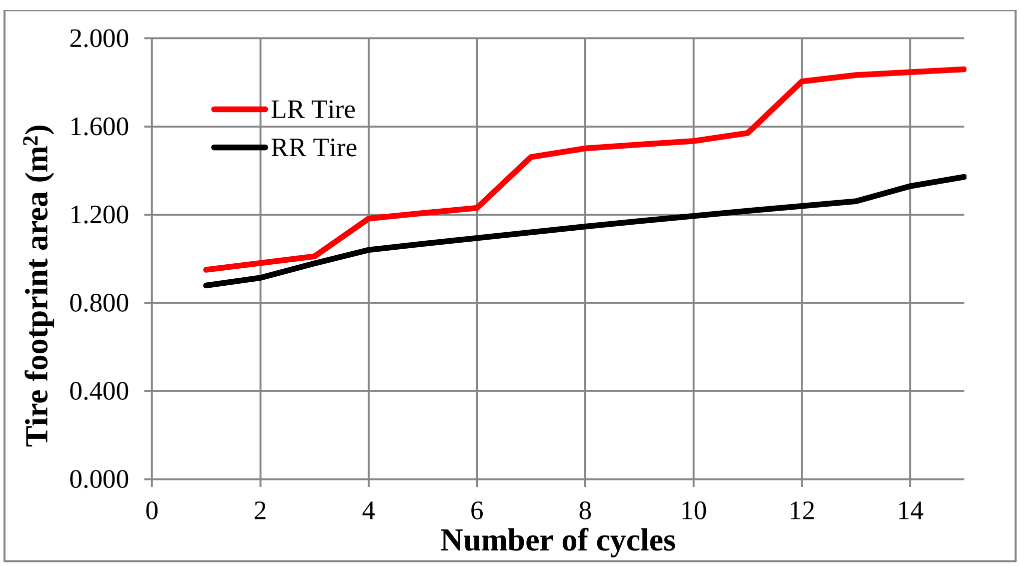

Figure.4.8. Tire footprint area with increasing number of cycles

It could be seen that parameters such as deformation of tire and oil sand, footprint area of oil sand, and ground stress distribution can be found out using the derived equations but the most important parameter is the sinkage (deformation of oil sand under loading cycle) of the truck on oil sand deformable ground. This is very important because as the truck is loaded, it gives an idea of how the oil sand deforms and in turn how it affects the stability of the truck. No comparison could be made for the final output because there are no field values available, but further comparisons using the model equations for various trucks and for lower and higher g loads are required.

4.5.5 Performance prediction for 2.85m and 0.368m diameter tires

Tire and oil sand deformation was evaluated for the tires used by Bolster (2007) and Sharma (2009), but without including an available stroke length for comparison, since the pressure data and suspension parameter were not known. The values of load and inflation pressure were considered similar for the tests performed by Bolster (2007) and Sharma (2009). Since the tires were different in size for each researcher, the load and the inflation pressures varied.

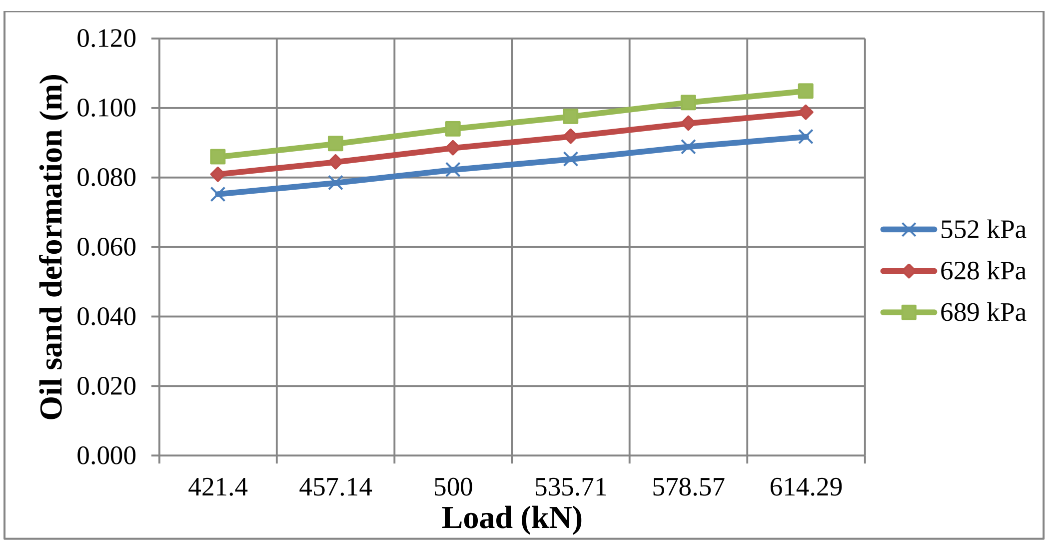

Figure.4.9. Oil sand deformation with load for 2.85m diameter tire

Figures (4.9) and (4.10) provide the oil sand and tire deformation for a 2.85m diameter tire. Analysis was done for three tire inflation pressures (552, 628, and 689kPa). As expected the oil sand deformation was higher for tire with higher inflation pressure. This is because a stiffer tire creates a smaller footprint area and resulting in a higher stress on the ground in turn yielding a higher oil sand deformation. The opposite applies for tires of lower stiffness which create a larger footprint area and lower stress on the ground a lower oil sand deformation. Tire deformation is higher for softer tires and lower for stiffer tires. This is true as a tire with higher stiffness can better withstand load.

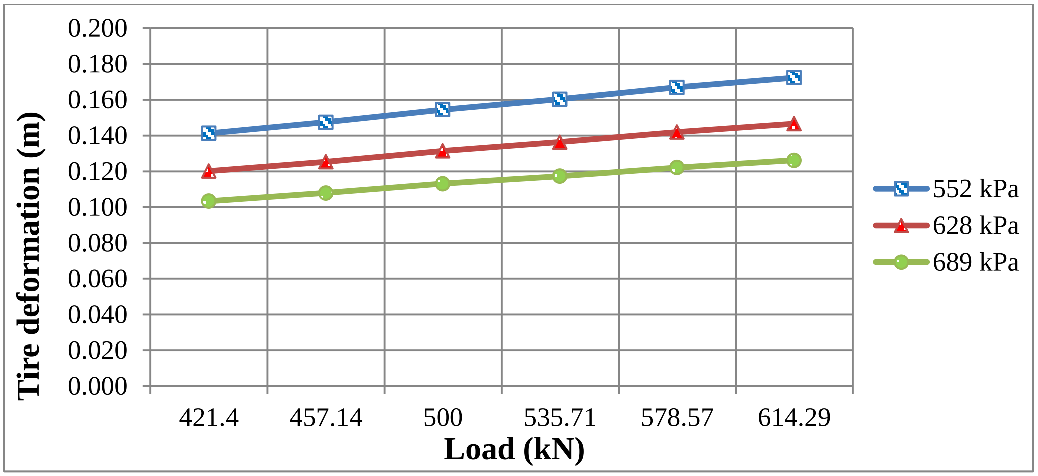

Figure.4.10. Tire deformation on oil sand with load for 2.85m diameter tire

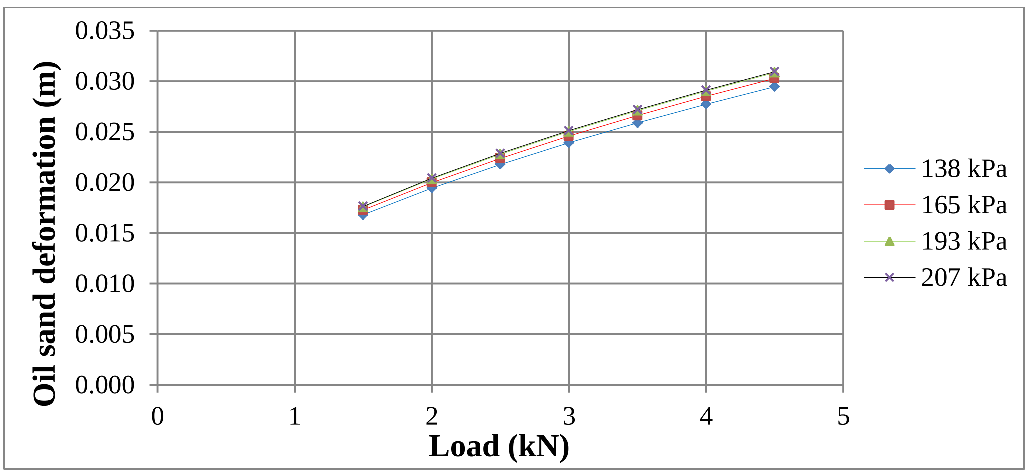

Figure.4.11. Oil sand deformation with load for 0.368m diameter tire

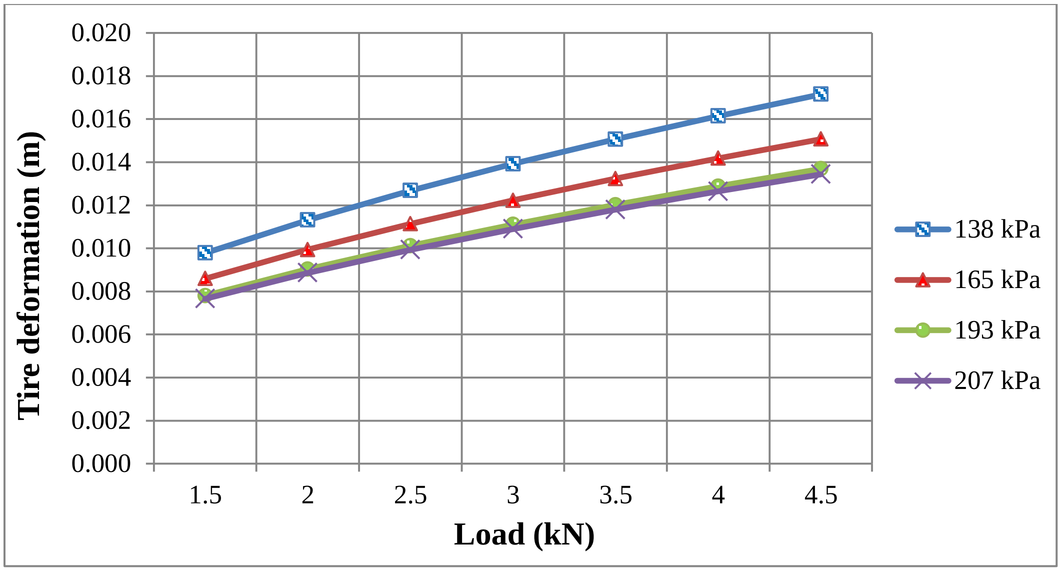

Figure.4.12. Tire deformation on oil sand with load for 0.368m diameter tire

Figures (4.11) and (4.12) illustrate the oil sand and tire deformation by varying load for a 0.368m diameter tire. The deformation behavior for this tire on oil sand was the same as for the 2.85m diameter tire.

CHAPTER 5

RHEOLOGICAL MODEL FOR PERFORMANCE PREDICTION OF TRUCK SUSPENSION AND TIRE ON A RIGID SURFACE

5.1. Introduction and Objective

Rheological models are similar to mathematical models but provide a different mode of approaching a problem in a more theoretical manner. The mathematics involved here is not difficult and as such makes the rheological model approach an easy tool to understand. The main aim of this model was to predict the performance of the truck components and the ground through simple viscoelastic models and to convey an alternative and mode of understanding the overall relationship.

Based on properties behavior, a model has been assigned to each of the components in the system like suspension, tire and ground. This chapter consists of only the model for suspension and tire since the ground is essentially considered rigid, with no deflection. Although the responses that can be predicted using these models are limited, the main advantage comes in predicting the deformation behavior with an acceptable approximation to actual behaviour. This field of study provides results close to field values maintaining the physics of the issue. Connecting the individual parts and obtaining the performance relationship between them is interesting since each part has separate functions and characteristics.

5.2. Basic assumptions

i) The deformation of the rigid surface is lower compared to a tire and suspension, hence no model has been assigned for a rigid surface
ii) The force throughout the system is same

5.3. Model layout and equations

Establishing the relationship between the stress and deformation is the key task in rheology. The models described in the literature review are used matched to the corresponding components of the truck based on behavior. Only a few elements are included in the overall model. This is because the mathematics become more complex with more elements, regardless with just few elements the prediction is good.

5.3.1. Rheological model for truck suspension and tire on a rigid surface

Both the suspension and tire model combined together give a rheological model for truck suspension and tire on a rigid surface (Figure.5.1). The suspension model is viscoelastic because of the presence of both viscous and elastic element. But the tire is merely an elastic element. The force applied on each model is used to predict the total and individual component strain values.

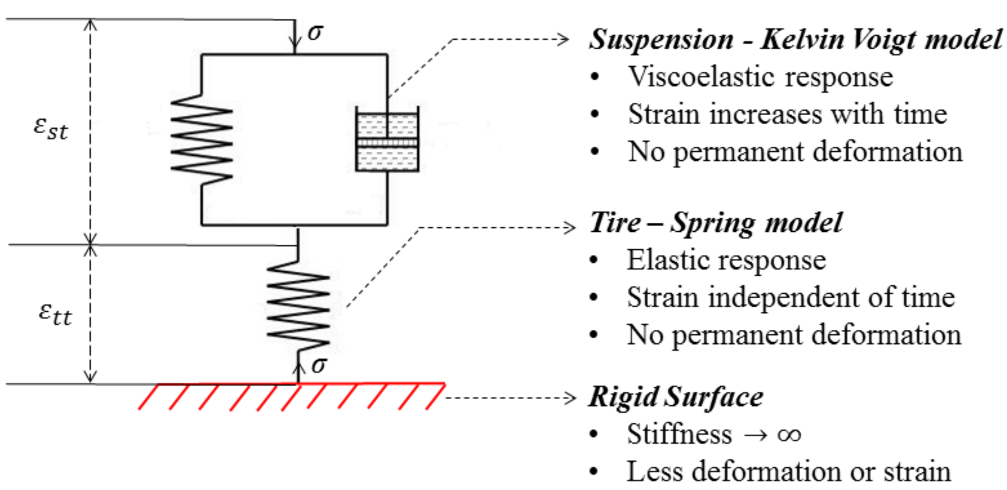

Figure.5.1. Rheological model for truck suspension and tire on a rigid surface

The suspension exhibits no permanent deformation as spring stiffness is higher than the stiffness of the damper (viscosity). Due to this the spring is able to pull the hydraulic oil back from the annulus in retraction mode into the damper with no permanent deformation. The total strain of the combined model is a combination of viscoelastic and elastic model strains (Equation.5.1). Even though the force is same on each model, the stress developed is not the same because of different contact areas. This model can be used to predict the total and individual strain for various loading conditions. Since the system is a continuous moving system the effect of creep and relaxation are not a major concern and as such are not considered for prediction here.

$$\varepsilon_{rt} = \varepsilon_{st} + \varepsilon_{tt} \quad [5.1]$$

Where, ε_{rt} is the total strain on a rigid surface, ε_{st} is total strain of the suspension, ε_{tt} is total strain of the tire

5.3.2. Truck Suspension model and related equations

For a rheological model, the two main truck suspension elements, the gas spring and the hydraulic oil damper are considered. The shape of the suspension is not important for the model. Based on the corresponding behavior, Kelvin – Voigt model has been used for the suspension (Figure.5.2).

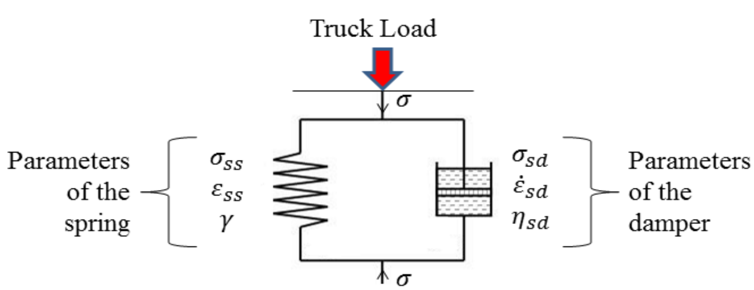

Figure.5.2. Rheological model for the truck suspension

The spring in the model acts for the gas in the suspension. Meanwhile the damper in the model acts for the hydraulic oil in the suspension. Both these constitute to the overall performance of the suspension.

In the suspension, the gas takes the initial load and total strain occurs (Equation.5.2) with respect to the time due to the damping force provided by the damper. The strain value increases gradually and when the maximum strain is reached, it remains as a constant for the remaining time until the stress on the suspension changes. The total stress is the sum of stress acting on the spring and the damper (Equation.5.3) [10].

$$\varepsilon_{st} = \varepsilon_{ss} = \varepsilon_{sd} \qquad [5.2]$$

$$\sigma_{st} = \sigma_{ss} + \sigma_{sd} \qquad [5.3]$$

Where, ε_{st} is the total strain of the suspension, ε_{ss} is the suspension spring strain, ε_{sd} is the suspension damper strain, σ_{st} is the total stress on the suspension (MPa), σ_{ss} is the suspension spring stress (MPa), σ_{sd} is the suspension damper stress (MPa)

An important point to be noted is that the strain of the suspension spring is directly proportional to the Elastic modulus (Equation.5.4) [58].

$$\varepsilon_{ss} = \frac{E_{ss}}{\sigma_{ss}} \qquad [5.4]$$

Where, E_{ss}, ε_{ss}, and σ_{ss} are the Young's modulus (MPa), strain, and stress of the suspension spring (MPa)

The gas shows a different behavior than the spring, hence the Elastic modulus property is not applicable for the gas in the suspension. Even considering the stiffness of the spring is not an appropriate method for rheological models.

The stiffness is not a constant and it varies with the available stroke length. The lesser the available stroke length, the more the stiffness and more the available stroke length, the lesser the stiffness. But this is not the case of spring used in the model, which usually has a constant stiffness and Elastic modulus. Hence it was decided to use the general isentropic gas law to predict the strain value of the suspension.

For an isentropic suspension with constant temperature, the product of volume and pressure at any given situation is a constant (Equation. 5.5) [57].

$$PV^{\gamma} = C \qquad [5.5]$$

Where, P , V , γ are the pressure (kPa), volume (m^3), and Isentropic constant of the gas

The process is continuous and there are n pressure variations in the suspension due to load changes (Equation.5.6). Also the area of the suspension cylinder is a constant, which gives the variation of pressure with respect to only the available stroke length of the suspension (Equation.5.7) [57].

$$P_u V_u^{\gamma} = P_s V_s^{\gamma} = P_n V_n^{\gamma} \qquad [5.6]$$

$$\left(\frac{P_u}{P_s}\right) = \left(\frac{V_s}{V_u}\right)^{\gamma} \text{ and } \left(\frac{P_u}{P_n}\right) = \left(\frac{V_n}{V_u}\right)^{\gamma} \qquad [5.7]$$

$$\left(\frac{P_u}{P_s}\right) = \left(\frac{A_C \cdot S_a}{A_C \cdot S_u}\right)^{\gamma} = \left(\frac{S_a}{S_u}\right)^{\gamma} \qquad [5.8]$$

Re- writing equation (5.6)

$$\left(\frac{S_a}{S_u}\right)=\left(\frac{P_u}{P_s}\right)^{\frac{1}{\gamma}} \qquad [5.9]$$

Where, P_u is the suspension pressure at unloaded condition (kPa), P_s is the instantaneous pressure (kPa), P_n is the pressure at nth cycle (kPa), V_u is the volume of gas at unloaded condition (m^3), V_s is the volume of gas at loaded condition (m^3), V_n is the volume of gas at nth cycle (m^3), A_c is the area of the suspension cylinder (m^2), S_a is the available stroke length (m), S_u is the available stroke length at unloaded condition (m), γ is the Isentropic constant

The pressure in the suspension at the unloaded condition is kept as the reference point to derive a ratio of available stroke length to initial stroke length (Equation.5.10) equivalent to Equation (5.9). The strain of the suspension is a function of the reference point pressure, isentropic constant, and the current pressure indicated by the VIMS (Figure.5.3).

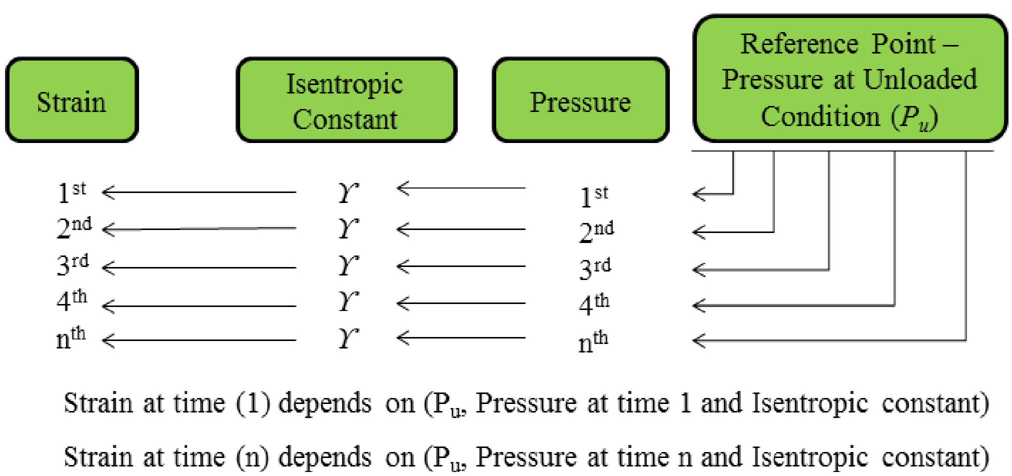

Figure.5.3. Relationship chart for strain value of the suspension

The focus of this model was to determine the strain value. Equation (5.9) provides the ratio value but the difference of the obtained value with unity gives the strain value; hence equation (5.10) is used to predict the strain value for varying load conditions.

$$\frac{S_a}{S_u} = \varepsilon_{ss} = f(\sigma, \gamma) = 1 - \left(\frac{\sigma_u}{\sigma_t}\right)^{\frac{1}{\gamma}} = 1 - \left(\frac{P_u}{P_s}\right)^{\frac{1}{\gamma}} \qquad [5.10]$$

Where, S_a is the available stroke length (m), S_u is the stroke length at unloaded condition (m), ε_{ss} is the effective suspension spring strain, σ_u is the stress at unloaded condition (MPa), σ_t is the stress at time t (MPa), P_u is the suspension pressure at unloaded condition (MPa), and P_s is the instantaneous suspension pressure (MPa)

The stress in equation (5.9) is replaced by pressure since the pressure and the stress on the suspension are the same. The instantaneous pressure and the pressure at the unloaded condition are used to evaluate the total strain value of the suspension.

$$\dot{\varepsilon}_{sd} = f(\sigma, \eta) = \frac{\sigma_{sd}}{\eta_{sd}} \qquad [5.11]$$

The strain rate of the damper is a function of both the stress and the viscosity of the hydraulic oil (Equation.5.11) [58]. To obtain the strain experienced by the damper, equation (5.11) was integrated. The truck suspension stress values vary with time and the variation is recorded per second. The applied stress per second is considered here for the prediction of damper strain (Equation.5.15).

$$\dot{\varepsilon}_{sd} = \frac{\mathrm{d}\varepsilon_{sd}}{\mathrm{d}t} = \frac{\sigma_{sd}}{\eta_{sd}} \qquad [5.12]$$

$$\mathrm{d}\varepsilon_{sd} = \left(\frac{\sigma_{sd}}{\eta_{sd}}\right)\mathrm{d}t \qquad [5.13]$$

Considering the initial strain as zero and time between zero and t, and integrating correspondingly, we obtain the final strain equation [46].

$$\int_0^{\varepsilon}\mathrm{d}\varepsilon_{sd} = \frac{\sigma_{sd}}{\eta_{sd}}\int_0^{t}\mathrm{d}t \qquad [5.14]$$

$$\varepsilon_{sd} = \left(\frac{\sigma_{sd}}{\eta_{sd}}\right)t \qquad [5.15]$$

Where, ε_{sd} , σ_{sd} , and η_{sd} are the strain, stress (MPa), and viscosity of the suspension damper (MPas), t is the time (sec)

Equation (5.15) clearly shows that the strain experienced by the damper increases with respect to time. For a given time period the stress is considered a constant (as the data acquisition is 1Hz) and based on the viscosity of the hydraulic oil, the strain increases with time until it reaches its maximum corresponding to a given stress. The stress in the suspension system varies per second and the strain value depends on the stress. Hence once a maximum strain is reached, there is no increase or decrease in strain unless the stress is changed. The viscosity of the hydraulic oil is always constant since there is no effective temperature change inside the suspension for any adjacent records within a period of time.

The total strain experienced by the Kelvin – Voigt model may be discerned using either the strain equation for the spring or the strain equation for the damper. Since the gas spring undergoes an immediate deformation resulting in strain increase or decrease, the equation yielding suspension gas spring strain is used to obtain a more appropriate value.

5.3.3. Truck tire model and related equations

A truck tire has a linear load - deformation relationship similar to that of a spring. Rubber acts as an elastic material and hence it was decided to use the concept of an elastic spring for the tire. There might be some minor permanent deformation in the tire but it is negligible, hence no damper is included in the model. The tire takes the load and deforms immediately. Also when the load is removed, the tire regains its original shape regardless of time delay (the recovery is immediate).

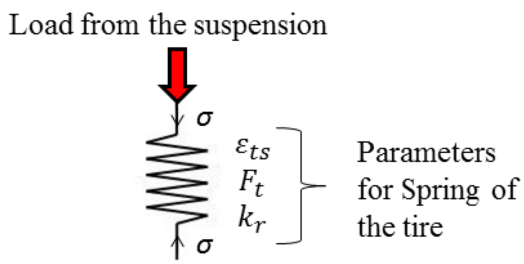

Figure.5.4 Truck tire element

The load from the suspension is directly transferred to the tire and the strain varies accordingly. The process is different from the suspension gas spring and hydraulic damper where the strain and recovery depends on time. But here, both the strain and recovery are immediate (Equation.5.19).

$$\delta_{tr} = \frac{F_t}{k_r} \qquad [5.16]$$

$$\varepsilon_{ts} = \frac{\delta_{tr}}{\phi_t} \qquad [5.17]$$

$$\delta_{tr} = \varepsilon_{ts} \cdot \phi_t \qquad [5.18]$$

$$\varepsilon_{ts} = f\left(F,k,\phi\right) = \frac{F_t}{k_r \cdot \phi_t} \qquad [5.19]$$

Where, F_t is the force on the tire (kN), k_r is the radial stiffness of the tire (kN/m), ϕ_t is the diameter of the tire (m)

5.4. Performance prediction

The pressure data from the VIMS system of a CAT 797B truck was used along with the rheological model equations to predict the performance for actual full size truck. Tire comparisons were made for the tires used by Sharma (2009) and Bolster (2007).

5.4.1. Prediction for CAT 797B truck components

Due to high loading for the rear suspension and tire sets as seen in the analysis from chapter 3 (See Figure.3.2), both the LR and RR of the truck are considered here for equation validation and comparison.

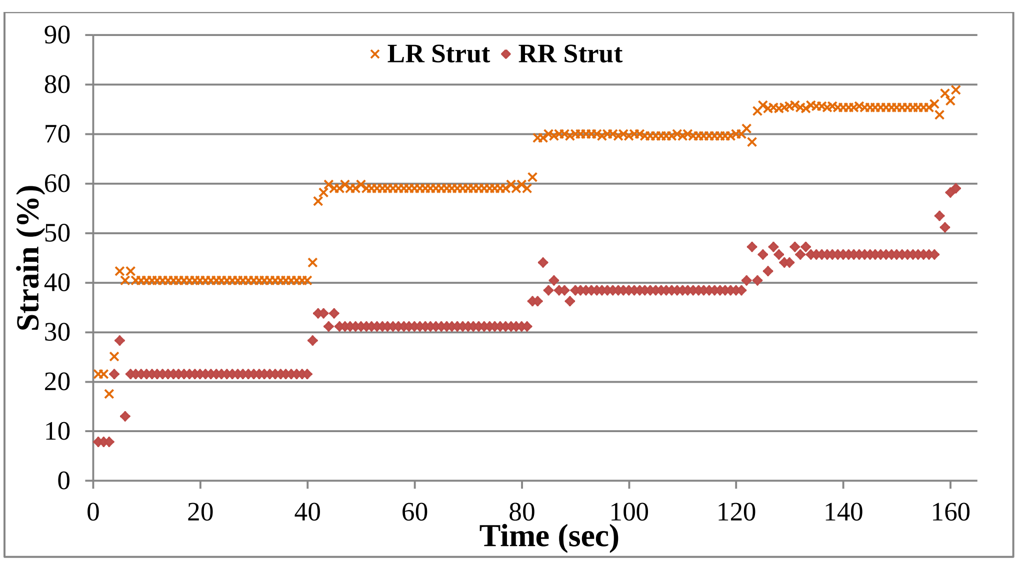

Figure.5.5. Suspension strain with time during loading cycle

The LR strut experienced a higher strain than the RR strut (Figure.5.5). The maximum strain on the LR strut was 20% greater than the maximum strain on the RR strut. As time increased the strain increased in a non-linear fashion.

As a general rule, the mining industry assumes an available stroke length of 0.025m for safe operation, at which status the maximum strain should be 83.4%. In Figure.5.5 it can be seen that the LR strut is close to the minimum safe operational strain value. The remaining strain percentage could be easily closed during an active cycle due to of bad road conditions.

An important aspect to be noted is that the force required for the suspension to reach an available stroke length of 0.025m from 0.152m happens quickly, but the amount of force required to move from 0.025m to 0.003m increases rapidly, with smaller increment of strain. This was clearly indicated by the behavior of the gas calculated using equation (5.9). The variation is provided in figure (5.6).

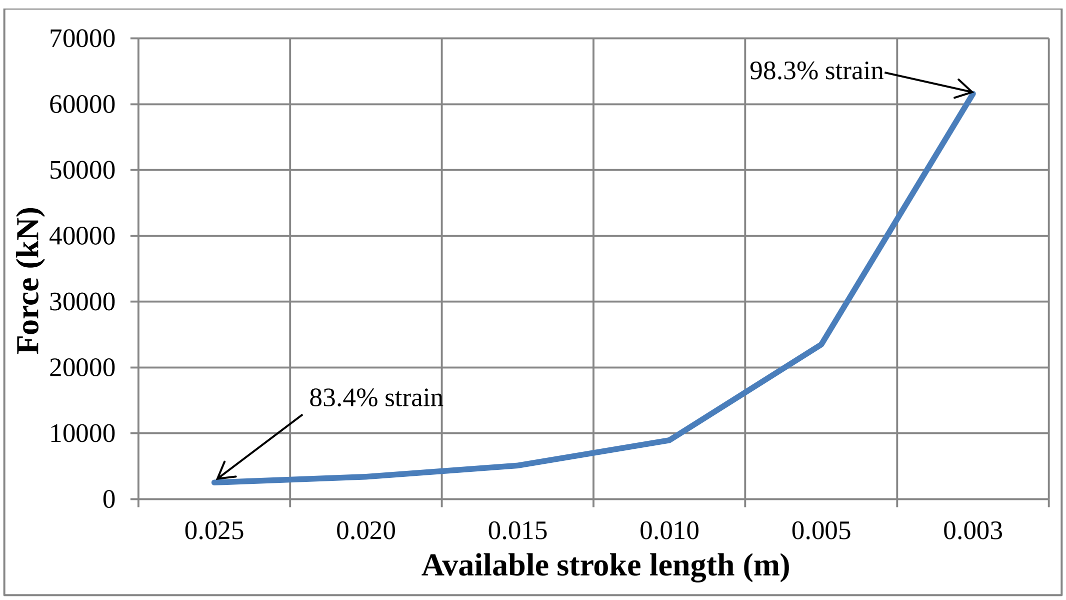

Figure.5.6. Variation of required force with available stroke length

Figures (5.7) and Figure (5.8) provide the strain variation for the suspension when the truck moved to a dumping area. The maximum strain of the LR strut is 83.11%, whereas for RR strut it is 78.71%. The variation in RR strut shows that the minimum and maximum strain values reached are 3% and 78.71%. A truck experienced this difference in strain levels during moving cycle clearly highlights the bad road conditions.

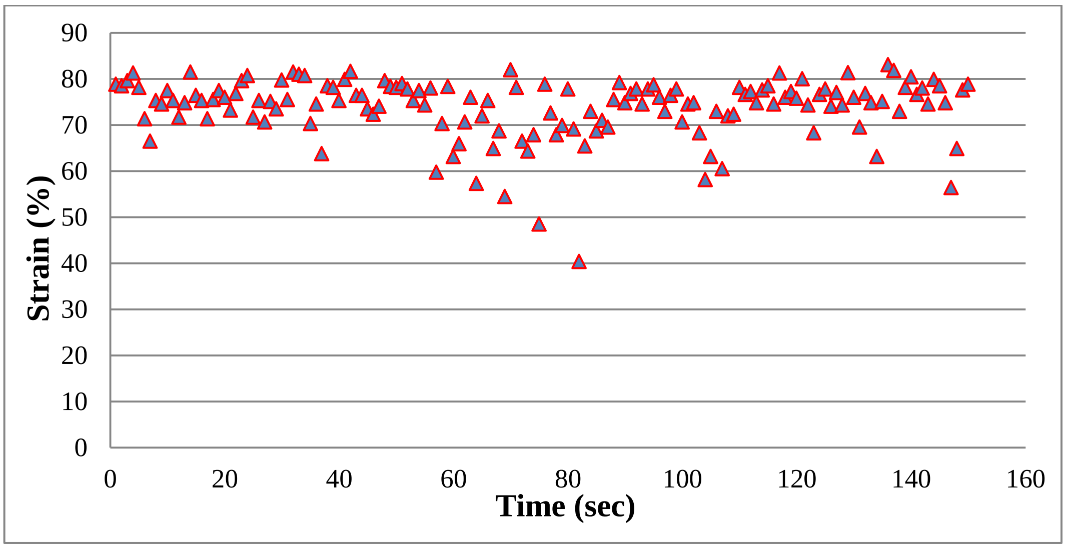

Figure.5.7. Suspension strain with time during moving cycle for LR Strut

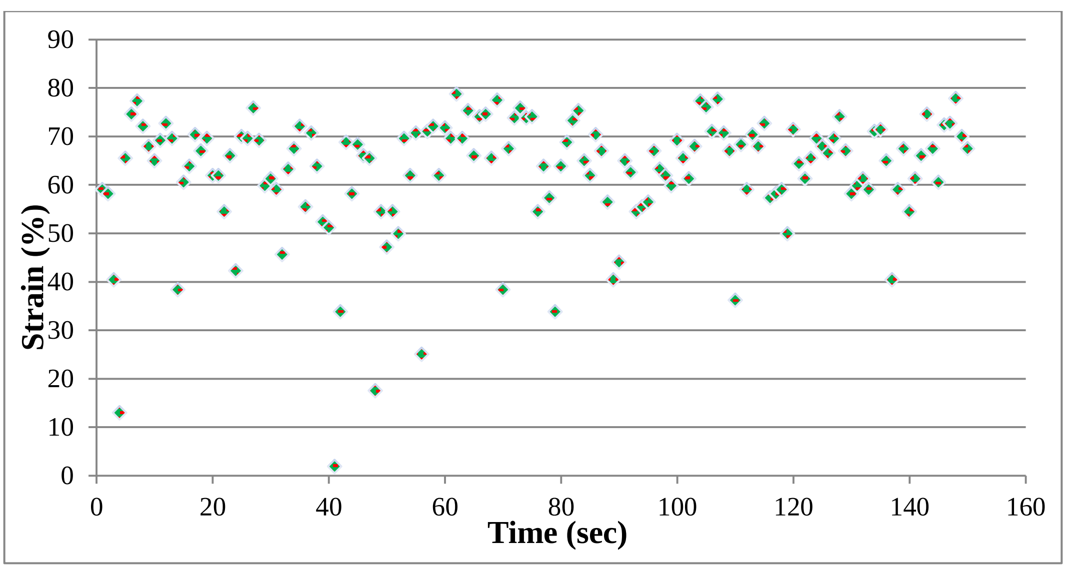

Figure.5.8. Suspension strain with time during moving cycle for RR Strut

Figures (5.9) and (5.10) show the strain of LR and RR tire for a CAT 797B truck. At 1-g load the strain for a tire is 7% which defines the correct applicable pressure for any OTR tire. It may be seen that the LR tire has its strain value above the 1-g load strain. This is just for one cycle which has around 150 seconds. When considering the number of cycles the truck has to go around per month, the number of larger strains experienced by the truck tire will be more.

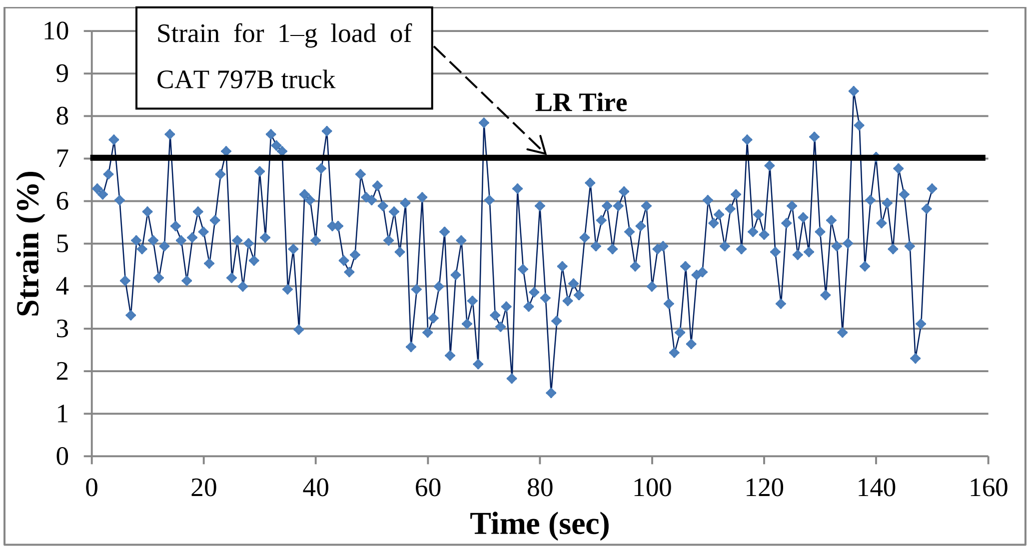

Figure.5.9. Tire strain with time during moving cycle for LR Tire

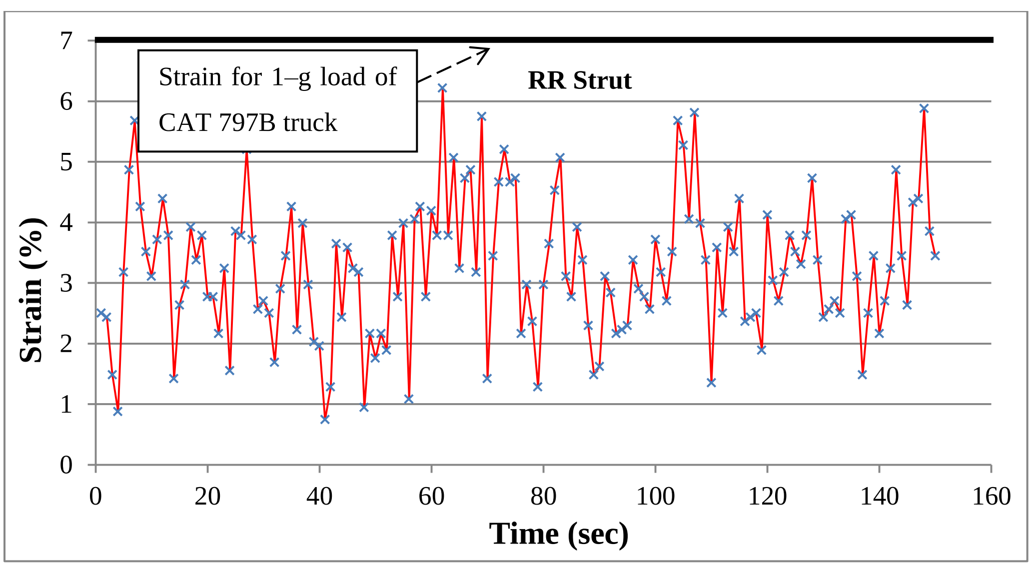

Figure.5.10. Tire strain with time during moving cycle for RR Tire

Since the truck experiences a huge amount of load in the field, the difference in strain for various inflation pressure and g-loads were studied (Figure.5.11). The strain increases linearly with the load. The lower inflated tire has the highest strain percentage because of less stiffness and the less ability to withstand load than the higher inflated tire

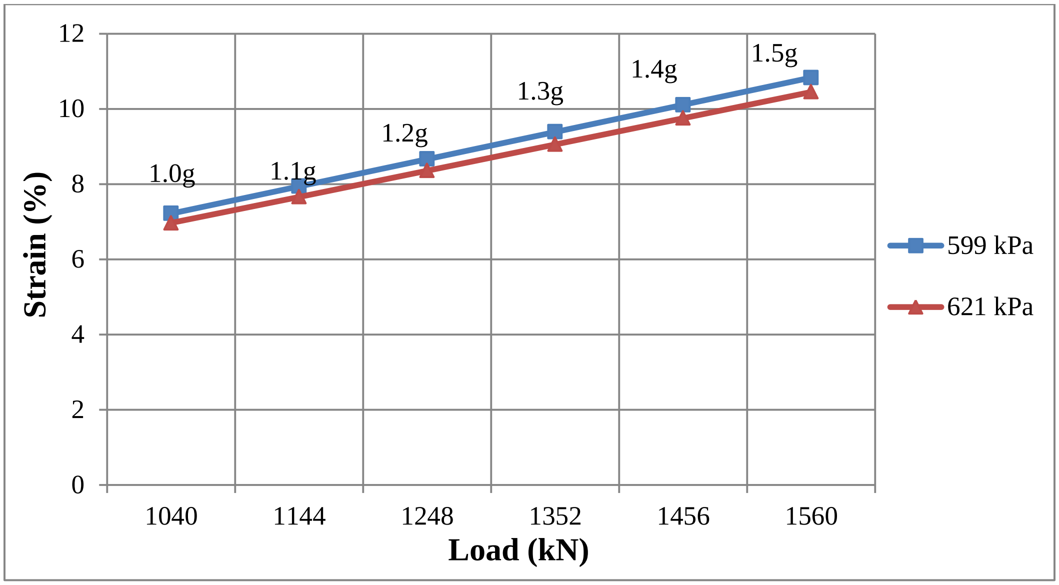

Figure.5.11. Strain for CAT 797B tire with g-loads

5.4.2. Prediction for the previous laboratory result tires

The strain - load relationship for 2.85m and 0.368m diameter tires is linear (Figure.5.12 and 5.13). Similar to all tires the strain is more for the lower inflated tire

At 1.5g load, the strain experienced by the 2.85m diameter tire is 9.4%. The load withstanding capability of this tire is good. Since there is no data available for comparison above 1.5g, the strain value above 1.5g was not predicted. More comparisons could be done in the future to predict the capability of the derived equations above 1.5g.

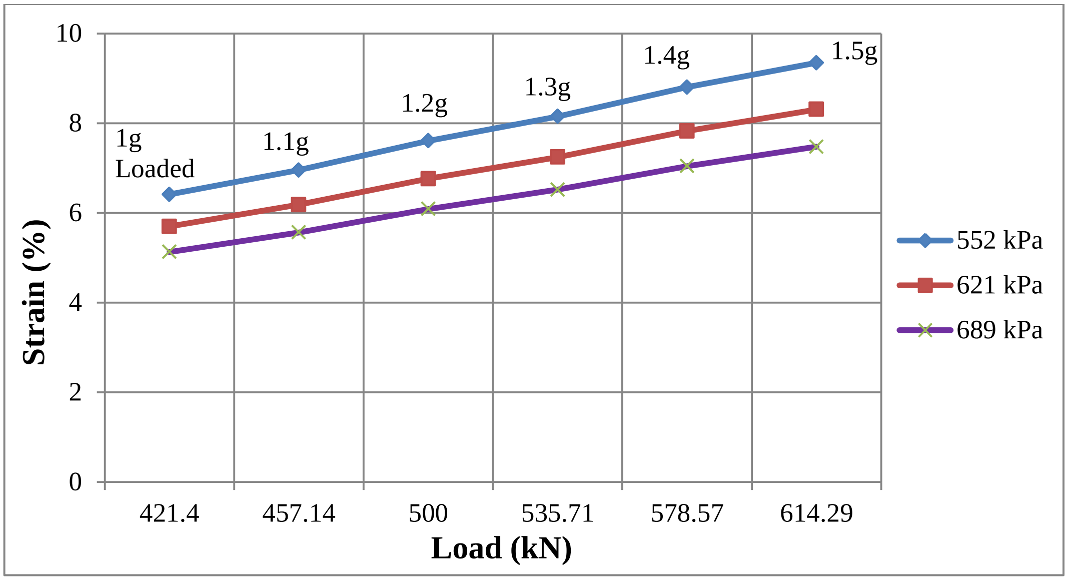

Figure.5.12. Strain for 2.85m diameter tire with g – loads

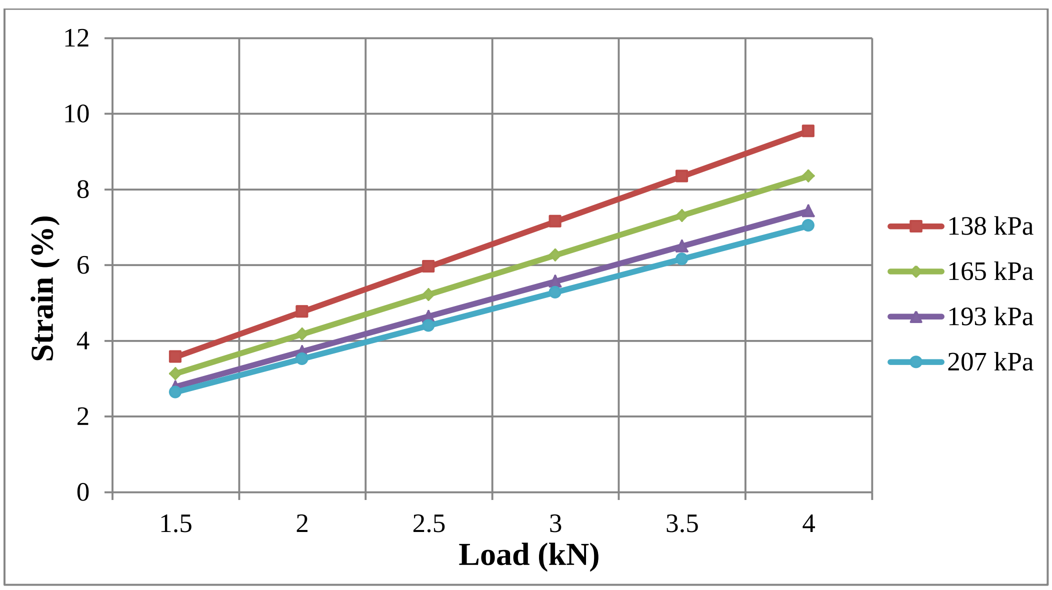

Figure.5.13. Strain for 0.368m diameter tire

Similarly for maximum load, the strain experienced by the 0.368m diameter tire is 9.6%. Both tires investigated show a good resistance to load and the prediction done here matches with the laboratory results and shows that the equations are valid. Even the comparison done for the full size truck (CAT 797B) tire provided results closer to the field value. More comparisons can be done to predict the accuracy of the equations for different types of truck.

5.5. Damping characteristics

Since the suspension model consists of spring and the dashpot, it is easy to predict the damping properties through the conventional spring damper method. The damping ratio decides the behavior of the suspension and provides an estimate of how the suspension provides the damping with various load condition. It gives a prediction of the damping level of the system corresponding to critical damping. Equations (5.20 to 5.24) provide an outline of the relationship of various parameters involved in finding out the damping properties [61].

$$\omega_0 = \sqrt{\frac{k_{ss}}{m_s}} \qquad [5.20]$$

Where, ω_0 is the undamped natural frequency (Hz), k_{ss} is the stiffness of the suspension spring (N/m), m_s is the mass on the spring (kg)

$$\omega_d = \omega_0 \sqrt{1-\zeta^2} \qquad [5.21]$$

$$\omega_d = 2\Pi f \qquad [5.22]$$

Where, ω_d is the damped natural frequency (Hz), ζ is the damping ratio, f is the frequency of vibration (Hz)

$$\zeta = \frac{c}{c_c} \qquad [5.23]$$

$$\zeta = \frac{c}{2\sqrt{m_s \cdot k_{ss}}} \qquad [5.24]$$

Where, c is the damping coefficient (Ns/m^2), c_c is the critical damping coefficient

The spring stiffness usually is a constant. But since the gas acts as a spring in the suspension, the stiffness here is not a constant. The frequency of vibration is considered as unity since the pressure data is recorded per second and assumption is made that there is only one vibration per second.

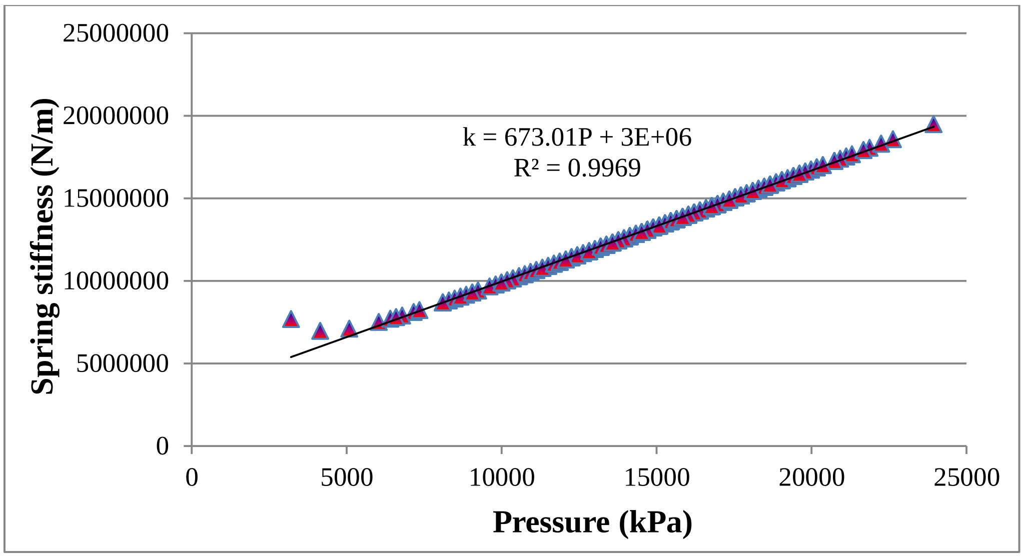

Figure.5.14. Variation of spring stiffness with pressure

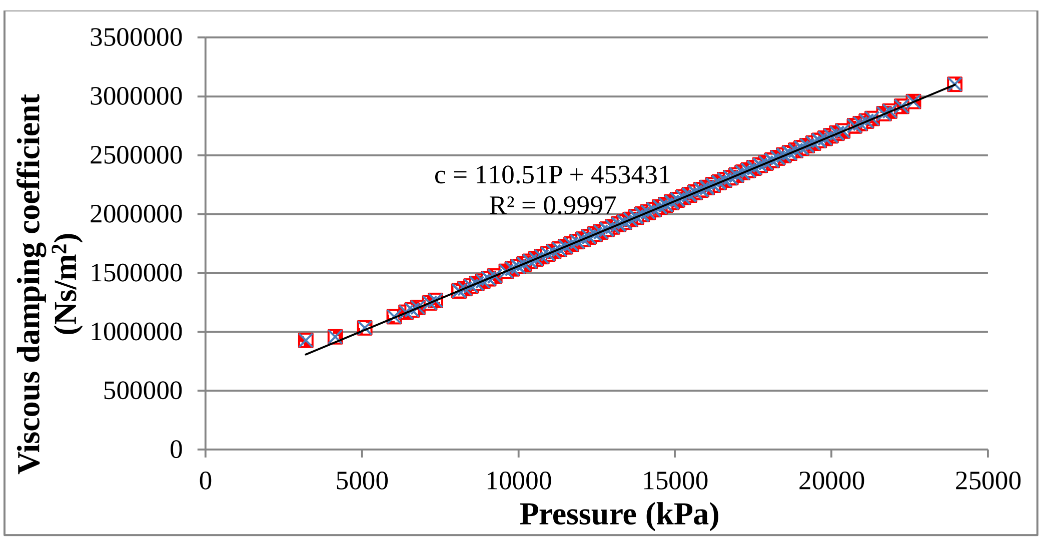

Figure.5.15. Variation of viscous damping coefficient with pressure

The stiffness of the spring increases linearly with pressure (Figure.5.14). This generally means that the spring force is more when the pressure is more. The property of the gas is the reason for this behavior. The viscous damping coefficient is a property of the damper and is responsible for providing the damping force. This also increases linearly with load (Figure.5.15). This property generally is also a constant but for this type of spring damping system, it becomes a variable since the stiffness and the mass on the spring varies with time.

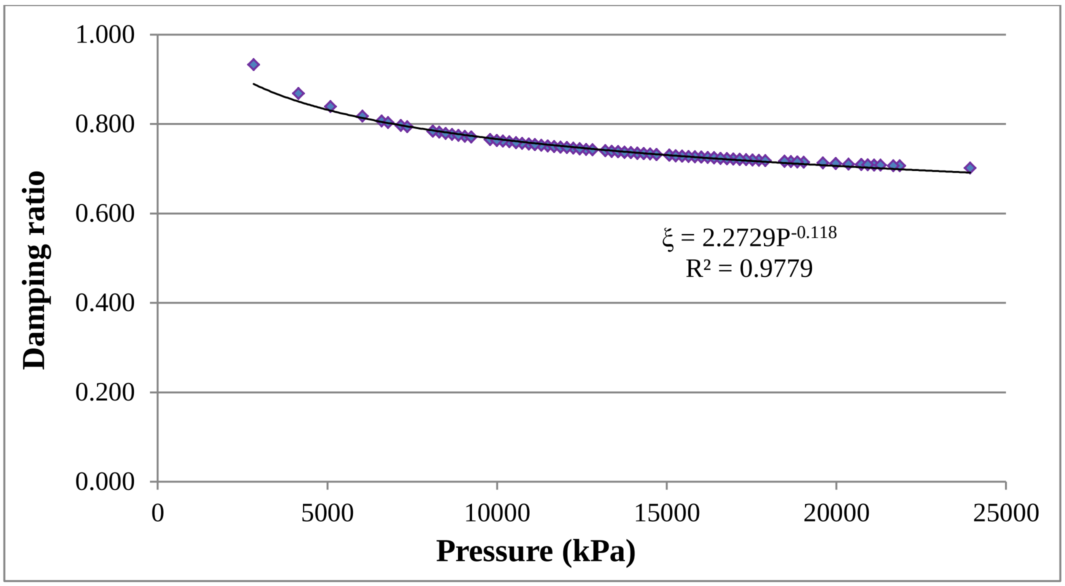

Figure.5.16. Variation of damping ratio with pressure

Figure.5.16 provides the damping ratio of the suspension. The maximum damping ratio is 0.93 and the minimum is 0.70. This type of damping is known as "Under damped condition", which means that if the damping ratio is in the range 0 to 1 then the system regains its original position with less vibration and within seconds. Also the systems velocity and amplitude with force decreases exponentially with time [31]. For the suspension of CAT 797B, the retraction time is within this range. The vibration is also less and attaining the state corresponding to a given pressure is not affected. All the characteristics predicted give a good approximation of the suspension behavior.

CHAPTER 6

RHEOLOGICAL MODEL FOR PERFORMANCE PREDICTION OF OIL SAND, TRUCK SUSPENSION AND TIRE ON OIL SAND

6.1. Introduction and objective

In chapter 5, the model for suspension and tire performance prediction relative to a rigid surface was considered. Here, the model is studied for a truck operating on oil sand. Oil sand has two main running surface characteristics relative to truck motion; sinkage and rutting. The method to predict sinkage in oil sand with a 11% bitumen content was provided in chapter 4. The main objective of this chapter is to provide a method to predict the rutting characteristics in oil sand under different loading conditions.

6.2. Rheological model for truck suspension and tire on oil sand

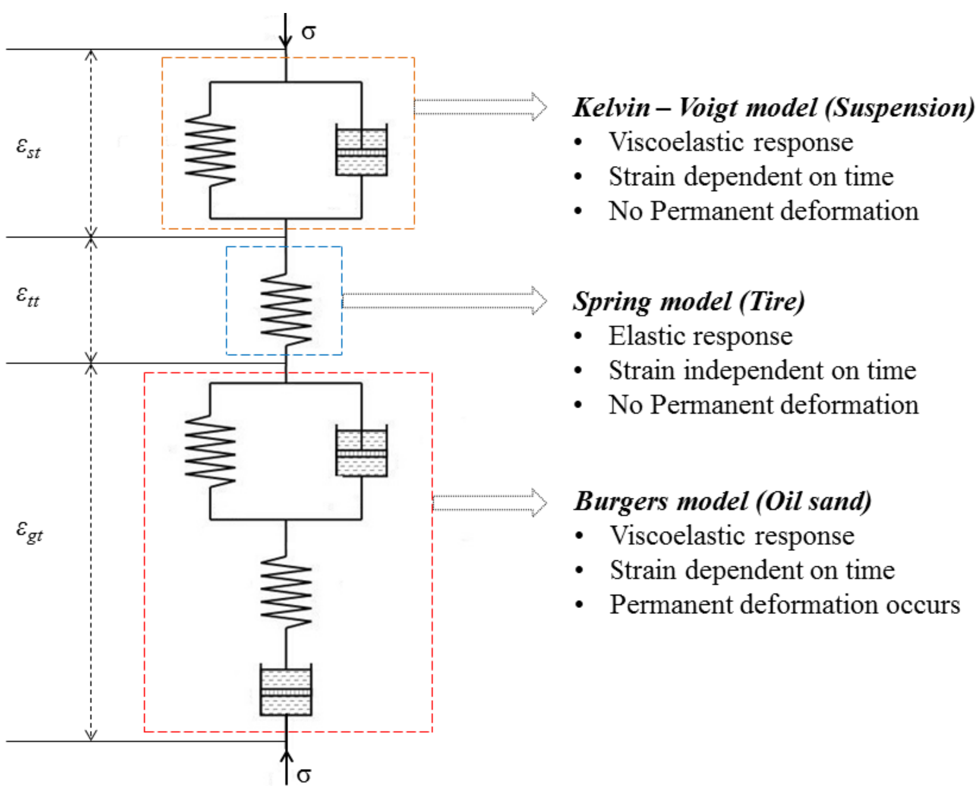

Figure.6.1. Rheological model for truck suspension, tire and oil sand

Similar to the models in chapter 5, only the spring and dashpot are assigned to represent the behavior of suspension, tire, and oil sand for predicting the overall behavior of a truck ground composite. The models of each component are connected and their corresponding equations are used to predict the strain characteristics. The only difference between the overall models in chapter 5 and chapter 6 is that the oil sand model is included here since it is far softer than a rigid surface, and strain will develop for varying load. The total strain of the model is the sum of strains of the individual models (Equation.6.1).

$$\varepsilon_{ost} = \varepsilon_{st} + \varepsilon_{tt} + \varepsilon_{gt} \qquad [6.1]$$

Where, ε_{ost} is the total strain of the rheological model, ε_{st} is the total strain of the suspension model, ε_{tt} is the total strain of the tire model, and ε_{gt} is the total strain of the oil sand ground model

6.2.1. Truck suspension and tire model parameters and equations

The model for the suspension is the same as that used in the chapter 5. This is because the suspension used for trucks on any ground surface is the same. The behavior of the suspension is thus similar to the Kelvin – Voigt model, with the only difference developing for varying ground conditions. The tire model is also the same because it is considered here to behave only elastically, even if it is operated on different surfaces. Hence the final strain equation for the suspension is the same. The same suspension parameters are considered and so the strain characteristics will not change from that investigated in chapter 5.

However, when a tire is loaded on flexible oil sand, it deflects under the action of load and that gives rise to a different strain behavior from that experienced on a rigid bearing surface. Also the footprint area of the tire on oil sand varies from that on the rigid surface, hence the general Hooke equation for a spring is used (Equation 6.2) [58].

$$\varepsilon_{st} = \frac{\sigma_{ts}}{E_{ts}} \qquad [6.2]$$

Where, ε_{st} and σ_{ts} are the total strain and stress on tire spring (MPa), E_{ts} is the Young's modulus of the effective tire spring (MPa)

6.2.2. Oil sand model parameters and equations

There are different rheological models like Kelvin – Voigt, Maxwell, and Burgers models. When a saturated viscoelastic medium such as oil sand is subjected to loading and unloading conditions, an appropriate rheological model should be able to predict the exact behavior. During loading, oil sand exhibits instantaneous strain followed by time dependant strain including permanent strain. Similarly during unloading, there will be elastic strain recovery followed by time dependant strain recovery. In this chapter the analysis accounts for the vehicle in motion.

Behavior under loading and unloading conditions illustrated in figure.6.2, gives an idea of the response of the models. In this work here, the response shown by a model was matched to actual oil sand response. However, these are the drawbacks to three models, which do not match the response of the material

- **Maxwell model** – When unloaded, there is an instantaneous recovery but there is no time dependant recovery
- **Kelvin – Voigt model** – During loading there is no time – independent strain and when unloading there is no permanent deformation
- **Standard linear solid model** –Fails to provide permanent deformation under loading conditions.

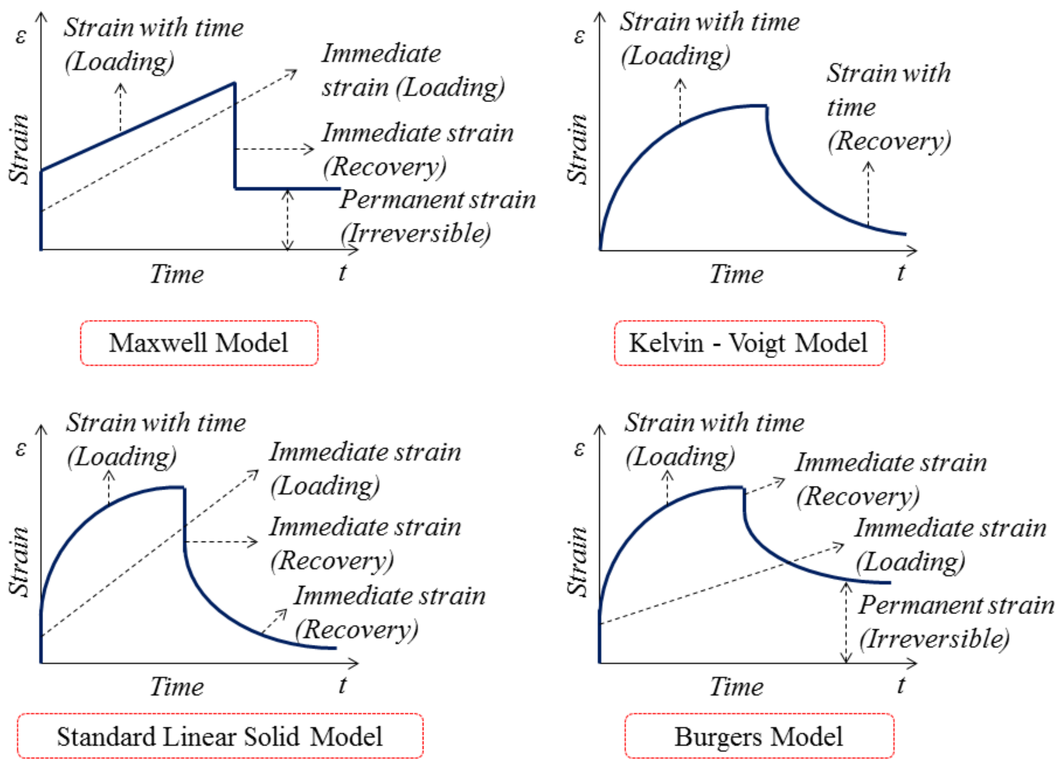

Figure.6.2. Response of different rheological model under loading and unloading conditions (after [25])

These differences are accounted for in the Burgers model (Figure.6.2 and 6.3). When a truck is moving, a load is applied on the ground which is accounted for immediately in the spring of model 2 (Figure.6.3). This is followed by an increase in strain with time in model 1. Finally there will be a permanent deformation that is recorded by the damper in model 2 and is irreversible (Figure.6.3).

Of the four models described above, the ability of the Burgers model to predict the behavior of the oil sand made it more appropriate option to use for oil sand. This model consists of both the Kelvin – Voigt (Ground model 1) and Maxwell model (Ground model 2) (Figure.6.3). The overall behavior of these two models was used to discern the strain characteristics of the oil sand.

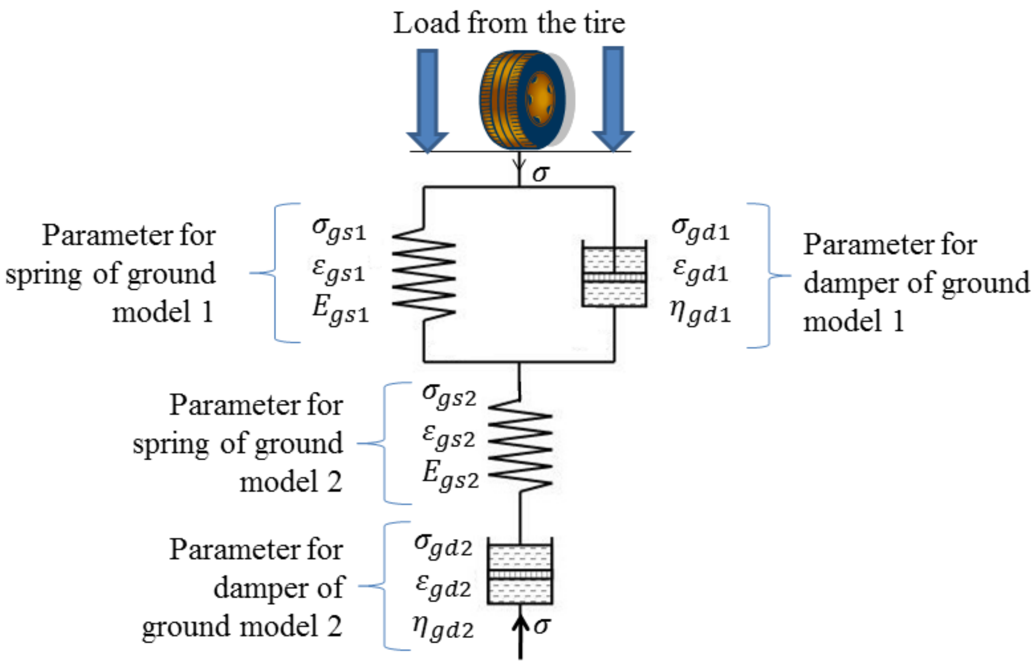

Figure.6.3. Rheological model for oil sand (Burgers model)

Equations (6.3) to (6.6) provide the equations relative to model 1 [10]. The total strain on both the spring and the damper are the same, but the stress is the sum of the stresses on the spring and the damper.

$$\varepsilon_{tg_1} = \varepsilon_{gs_1} = \varepsilon_{gd_1} \qquad [6.3]$$

$$\varepsilon_{gs_1} = \frac{\sigma_{gs_1}}{E_{gs_1}} \qquad [6.4]$$

$$\varepsilon_{gd_1} = \left(\frac{\sigma_{gd_1}}{\eta_{gd_1}}\right) \cdot t \qquad [6.5]$$

$$\sigma_{tg_1} = \sigma_{gs_1} + \sigma_{gd_1} \qquad [6.6]$$

Where, ε_{tg_1} is the total strain for oil sand model 1, ε_{gs_1} and ε_{gd_1} are the strains in the model 1 spring and damper, σ_{gs_1} and σ_{gd_1} are the stresses for model 1 spring and damper (MPa), E_{gs_1} is Young's modulus for model 1 spring (Mpa), η_{gd_1} is the viscosity of model 1 damper (MPas), and t is time (sec)

Equations (6.7) to (6.10) provide the equations for model 2 [10]. The total strain is the sum of the strains on both the spring and the damper. But the total stress in this case is the same as the stress for the spring and the damper.

$$\varepsilon_{tg_2} = \varepsilon_{gs_2} + \varepsilon_{gd_2} \quad [6.7]$$

$$\varepsilon_{gs_2} = \frac{\sigma_{gs_2}}{E_{gs_2}} \quad [6.8]$$

$$\varepsilon_{gd_2} = \left(\frac{\sigma_{gd_2}}{\eta_{gd_2}}\right) \cdot t \quad [6.9]$$

$$\sigma_{tg_2} = \sigma_{gs_2} = \sigma_{gd_2} \quad [6.10]$$

The total strain of the oil sand model (equation.6.12) is the sum of the strain of the ground model 1 (equation.6.3) and ground model 2 (equation.6.5). The stress experienced by each model throughout is the same because of the influence of same tire footprint area at any instantaneous time influence of the trucks motion (Equation.6.13).

$$\varepsilon_{tos} = \varepsilon_{tg_1} + \varepsilon_{tg_2} \quad [6.11]$$

$$\varepsilon_{tos} = \left(\frac{\sigma_{gs_1}}{E_{gs_1}}\right) + \left(\frac{\sigma_{gs_2}}{E_{gs_2}}\right) + \left(\frac{\sigma_{gd_2}}{\eta_{gd_2}}\right) \cdot t \quad [6.12]$$

$$\sigma_{osm} = \sigma_{gs_1} = \sigma_{gs_2} = \sigma_{gd_2} \quad [6.13]$$

Where, σ_{osm} is the overall stress on the model (Mpa), ε_{tos} is the total strain experienced by the model, ε_{tg_2} is the total strain of the model 2, ε_{gs_2} and ε_{gd_2} are the strains of the model 2 spring and damper, σ_{gs_2} and σ_{gd_2} are the stresses of the model 2 spring and damper (MPa), E_{gs_2} is Young's modulus of model 2 spring (MPa), η_{gd_2} is the viscosity of model 2 damper (MPas), and t is the time (sec)

The time taken to reach an equilibrium value for a particular load depends on the load applied. When a constant load is applied the total increase in strain follows the relationship (Equation.6.14) [25].

$$\varepsilon_{tos}(t) = \frac{\sigma_{osm}}{E_{gs_1}}\left(1 - e^{-\left(\frac{E_{gs_1}}{\eta_{gd_1}}\right)t}\right) + \left(\frac{\sigma_{osm}}{E_{gs_2}}\right) + \left(\frac{\sigma_{osm}}{\eta_{gd_2}}\right)t \qquad [6.14]$$

Similarly when the load is removed, the recovery strain follows the relationship (Equation.6.15) [25]

$$\varepsilon_{ros} = \frac{\sigma_{osm}}{E_{gs_1}}\left[\mathrm{e}^{\left(\frac{E_{gs_1}}{\eta_{gd_1}}\right)t} - 1\right]\left[\mathrm{e}^{-\left(\frac{E_{gs_1}}{\eta_{gd_1}}\right)t_u}\right] \qquad [6.15]$$

Where, ε_{ros} is the oil sand recovery strain, t_u is the time after unloading (sec), and t is the time at which stress is removed (sec)

6.3. Analytical output for the model

6.3.1. Analysis parameters

The response of the suspension is not described here as the same parameters are used as in chapter 5. Due to the varying oil sand ground conditions, only the response of a truck tire and the oil sand is predicted. Analysis was performed here based on the loading and footprint of a CAT 797B truck.

The important parameters for prediction using a spring damper system are Young's modulus and viscosity. For oil sand with 11% bitumen content, Sharma (2009) found these parameters (Table.6.1) which have been used here for prediction of the strain characteristics of oil sand.

Ground model	Element	Parameter	Value
1	Spring	Young's modulus (MPa)	7.3
	Damper	Viscosity (MPas)	200 – 400
2	Spring	Young's modulus (MPa)	7.6
	Damper	Viscosity (MPas)	4000 - 12000

Table.6.1. Parameters of oil sand rheological model elements [60]

For analysis purpose, an average viscosity is considered for both the models. Hence for model 1 and model 2 dampers, viscosities of 300MPas and 8000MPas are used.

6.3.2. Analytical output to a CAT 797B truck

VIMS data from a CAT 797B truck was used to predict the forces applied on the tire and oil sand. Although the speed of the truck varied, pressure data was available at 1Hz collection. Hence the assumption was made that for every second the truck will come into contact with a new ground surface. The tire footprint area was obtained using the equations in chapter 5, and then the stress was calculated based on the force and the footprint area.

Figure.6.4 shows the tire strain acting on oil sand with stress. A tire acting on oil sand creates a larger footprint area than acting on rigid surface. This permits the tire to deform less.

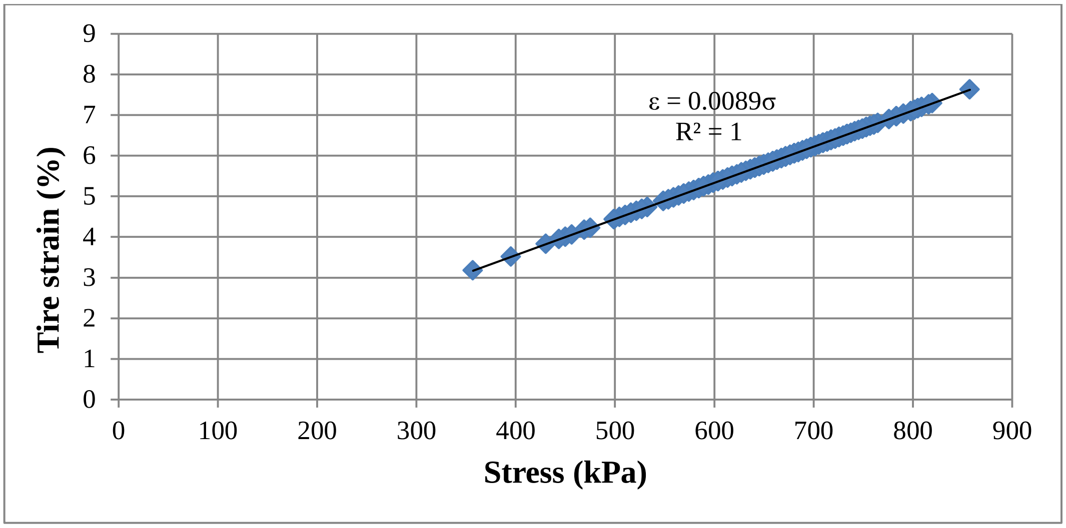

Figure.6.4. Tire strain with stress on Oil sand

To determine the strain characteristics of oil sand, two conditions were considered reflecting the actual field loading conditions. The first condition considered that the stress was applied on the ground for just one second, due to motion of the truck. Figure.6.5 illustrates the oil sand strain when loaded for 1sec. The maximum strain value reached during a moving cycle was 11.28%. This showed that even when the duration of loading is small, the oil sand deforms greatly creating an undulated surface.

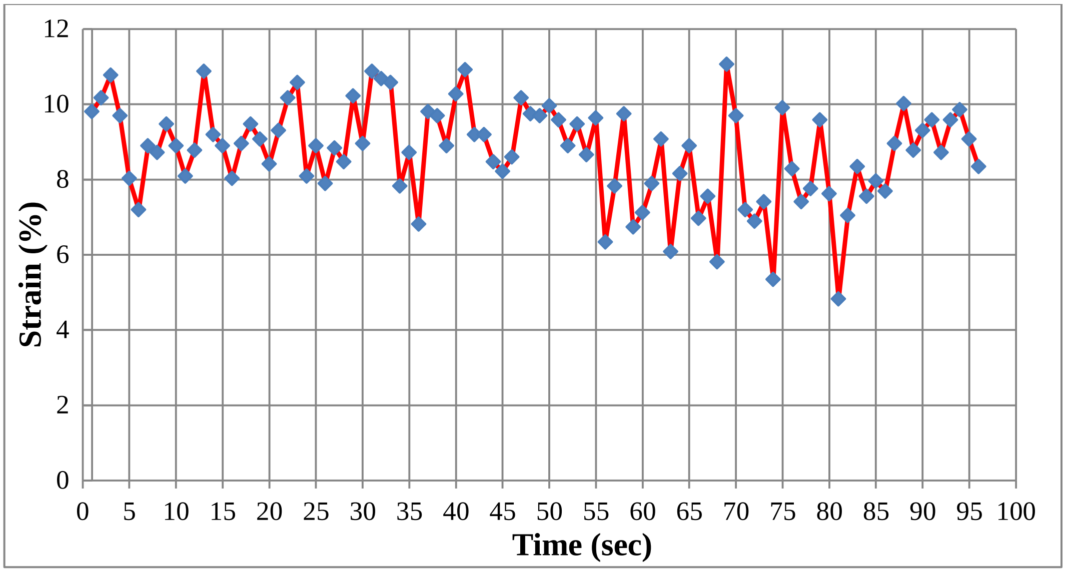

Figure.6.5. Oil sand strain for 1sec loading duration during truck motion

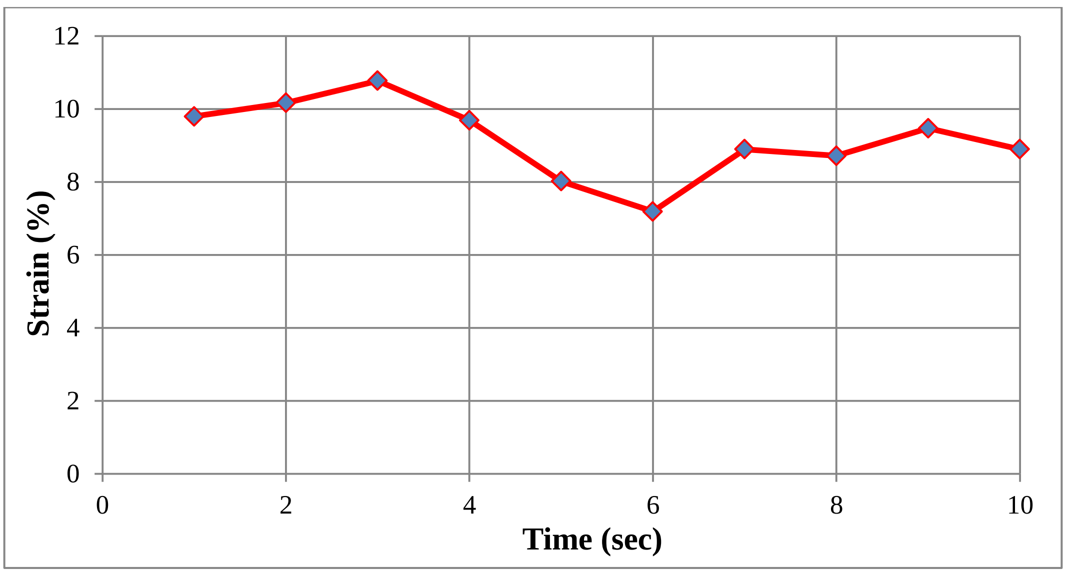

Figure.6.6. Strain for 1sec loading on oil sand during first 10sec of a truck in motion

The strain experienced by the oil sand during a 10 seconds period (Figure.6.6) clearly highlights the poor load carrying capability of the oil sand, where the strain varies highly.

The overall strain of the oil sand when loaded may be evaluated in three parts viscoelastic medium. Upon loading, an immediate elastic strain occurs which will be followed by a time dependant strain. There will be a permanent deformation which depends on the amount of time the load has been applied. Figure.6.7 shows the percentage strain experienced by oil sand for the different strain components when loaded for 1second. The strain value of the immediate elastic strain is greater since it is independent of time and the total strain due to it occurs immediately. Both the permanent strain and time dependant strain, since the time of loading is just 1 second, is very low. Another criterion was considered based on the available data. When a truck suddenly stops at a location during the hauling cycle, a constant load is applied to the ground for that amount of time. The durations considered in this analysis were 10, 20, and 30 seconds (Figure.6.8).

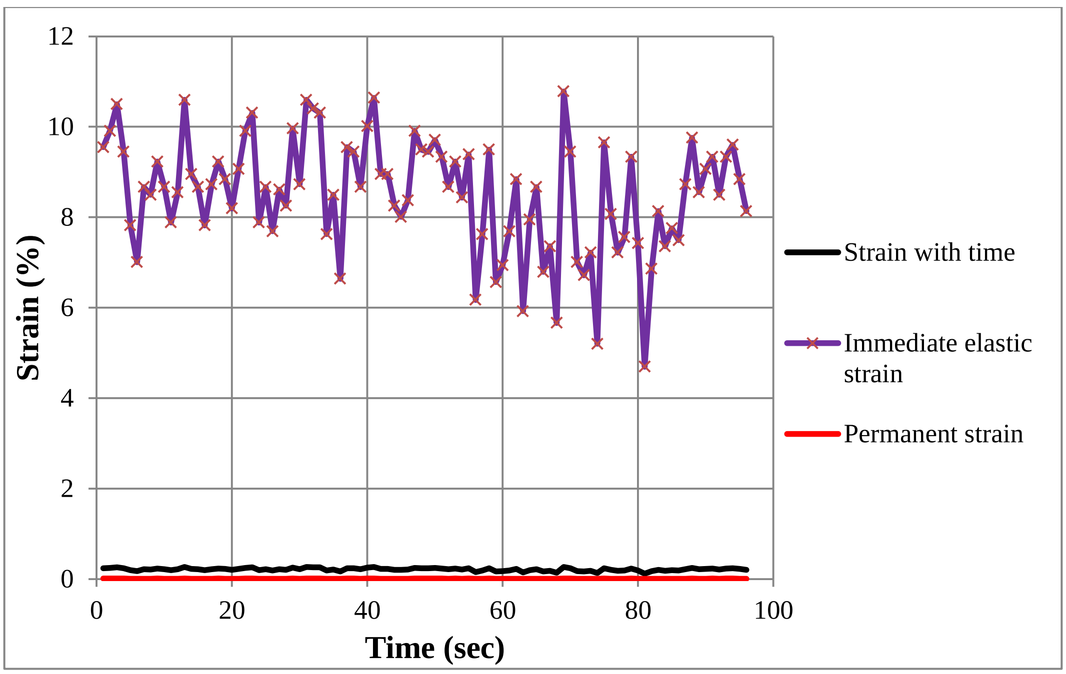

Figure.6.7. Oil sand strain for 1sec loading period

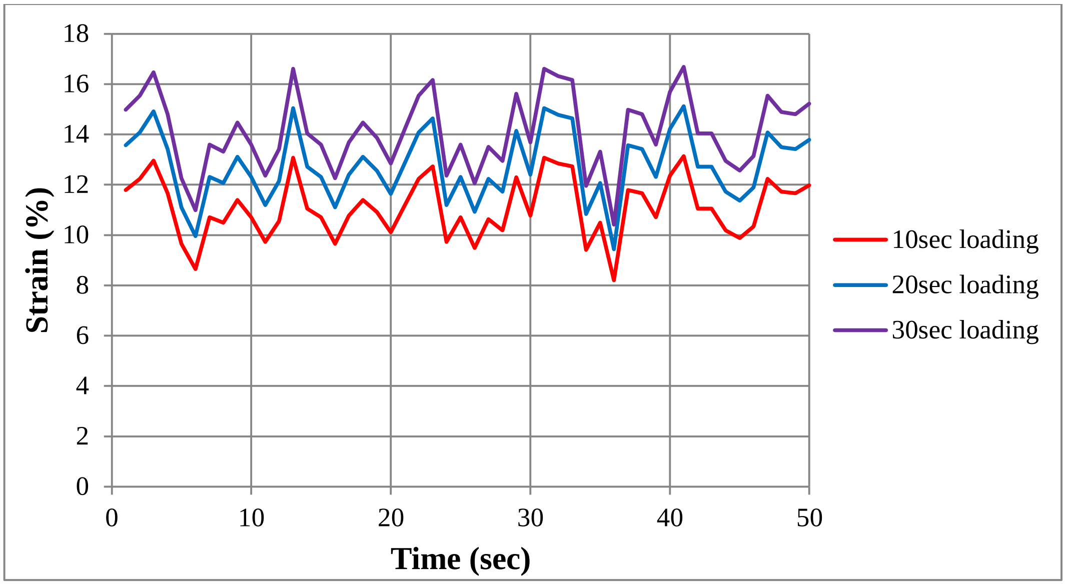

Figure.6.8. Oil sand total strain for different loading periods

The total strain of oil sand for 30 second duration of constant loading was as expected higher (Figure.6.8). Figure.6.9 provides the variation of strain with stress for various stationary truck – ground loading times, where clearly the stress for the higher duration creates the largest strain.

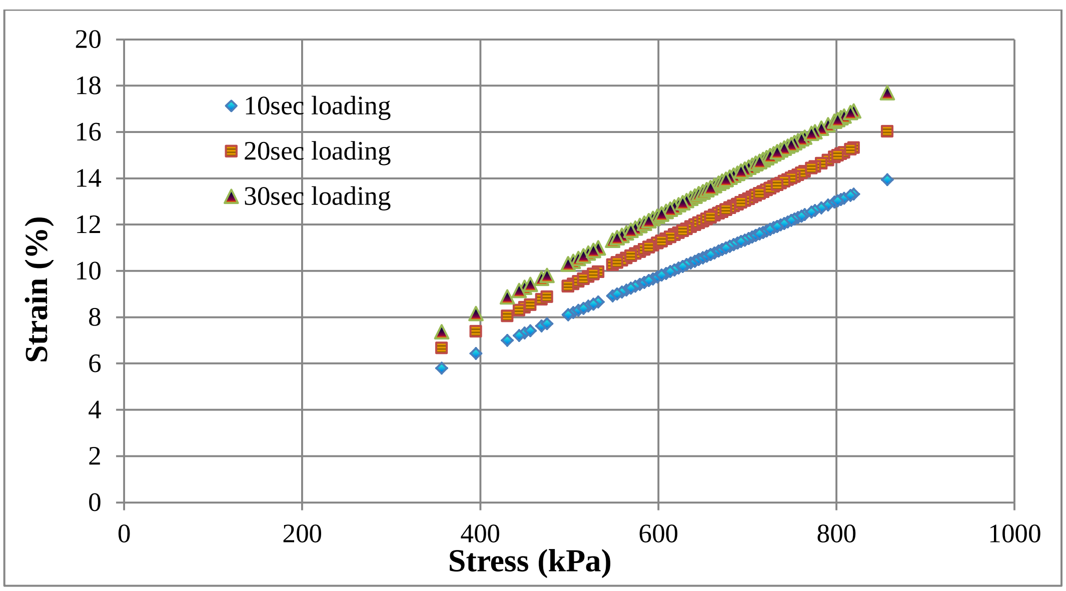

Figure.6.9. Oil sand stress versus strain for different loading periods

To evaluate the difference type of strains experienced by oil sand, study was carried out for different loading durations (10, 20, and 30 seconds). The ground model 1 (Kelvin – Voigt) in figure.6.3 provides the time dependant strain, whereas the damper in ground model 2 (Maxwell) provides the permanent strain (Figure.6.3). The variation in immediate elastic strain of spring in ground model 2 was not studied since the strain is independent of time.

Figures.6.10 and 6.11 illustrates the effect of loading duration on strain with time. Both time dependant (Figure.6.10) and permanent strains (Figure.6.11) are dependent on time and thus the loading duration clearly affects the total oil sand strain.

The strain increase which is dependent on loading duration causes the undulated ground conditions. As the number of truck passes increases along the same path, the permanent strain increases. Poor load carrying capability of oil sand is evident. Other road materials which withstand a constant stress for long durations do not deform like oil sand.

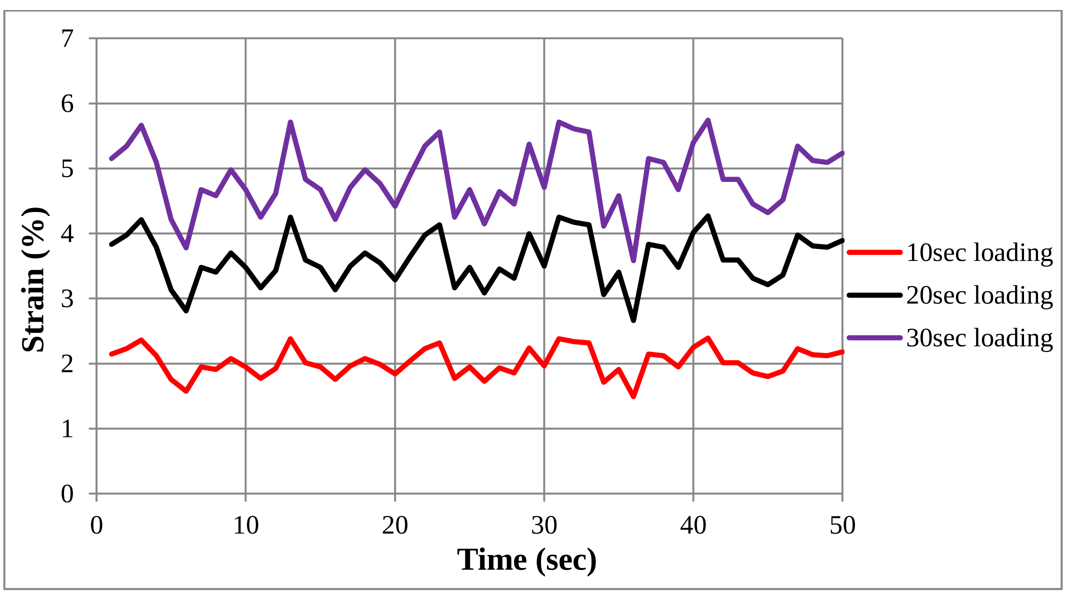

Figure.6.10. Oil sand time dependant strain for different loading periods

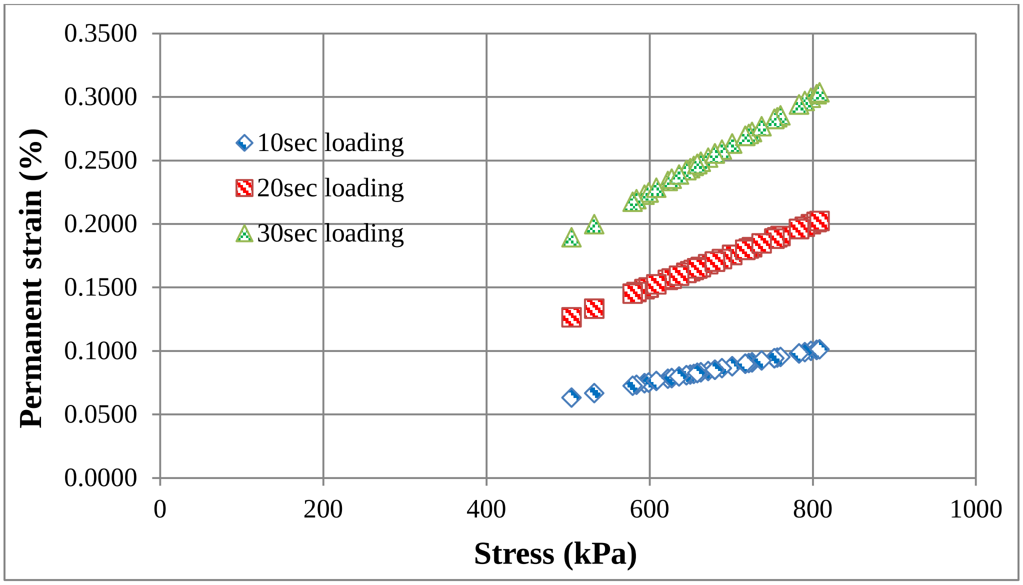

Figure.6.11. Oil sand permanent strain for different loading periods

The behavior of oil sand material for an applied stress of 857kPa commensurate with a 797B hauler for three loading durations was studied. Figure.6.12 provides the strain characteristics for a loading duration of 1second and figure.6.13 provides the strain characteristics for loading durations of 30 and 120 seconds.

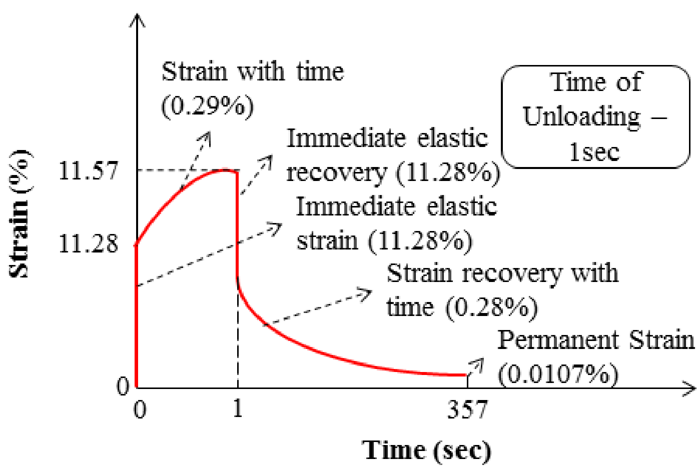

Figure.6.12. Oil sand permanent strain modeling for 1 sec loading period

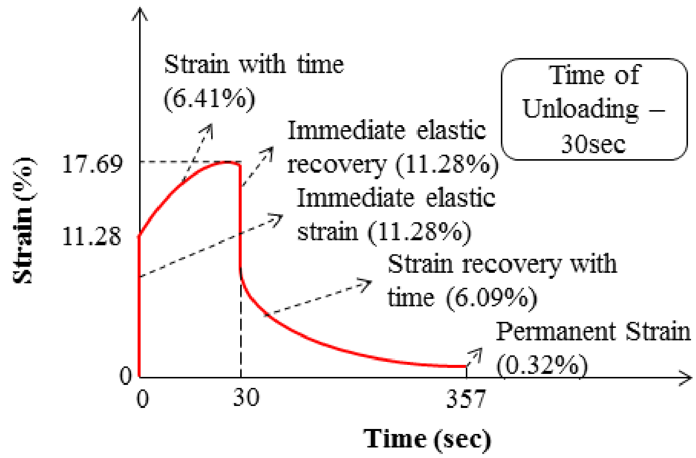

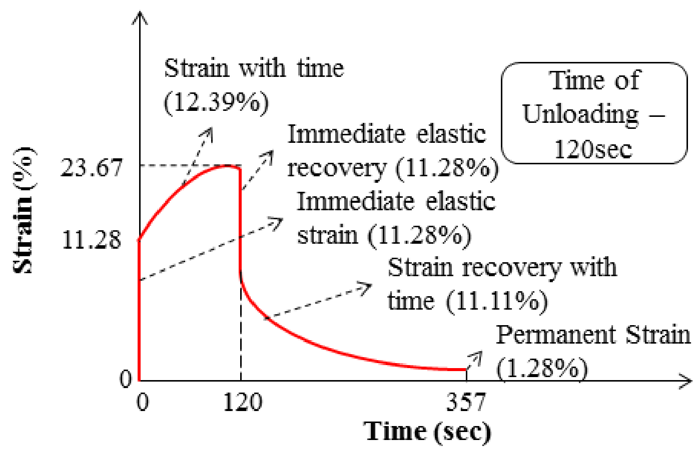

Figure.6.13. Oil sand permanent strain modeling for different loading periods

The immediate elastic strain in these three cases is the same since it is not dependant on time and the strain occurs immediately. The total strain is however affected by both the time dependant strain and the permanent strain. As the loading duration increases, the time dependant strain increases rapidly. For loadings durations from 30 to 120 second, the increase in strain with time is almost double. This is due to properties of oil sand, the smaller duration for the truck at rest on oil sand, and gives rise to better serving quality for the road surface. The duration of loading and the stress applied are important factors for the performance prediction of oil sand. As the number of cycles increases, the permanent strain of oil sand increases.

CHAPTER 7

COMPOSITE MODELING OF TRUCK SUSPENSION, TIRE, AND OIL SAND

A simulation study was performed in Matlab/Simulink to predict the deformation of the suspension and the tire. Variation in these parameters with ground deformation was also studied. Since only few ouputs were required using the simulation model, simulink was used because of its simplicity to model the combined suspension, tire and oil sand ground conditions.

Springs and dampers were the two main elements considered in this analysis. The gas in the suspension was considered as a spring and the hydraulic oil considered to be a liquid damper. The tire model was considered as an elastic spring (Figure.7.1).

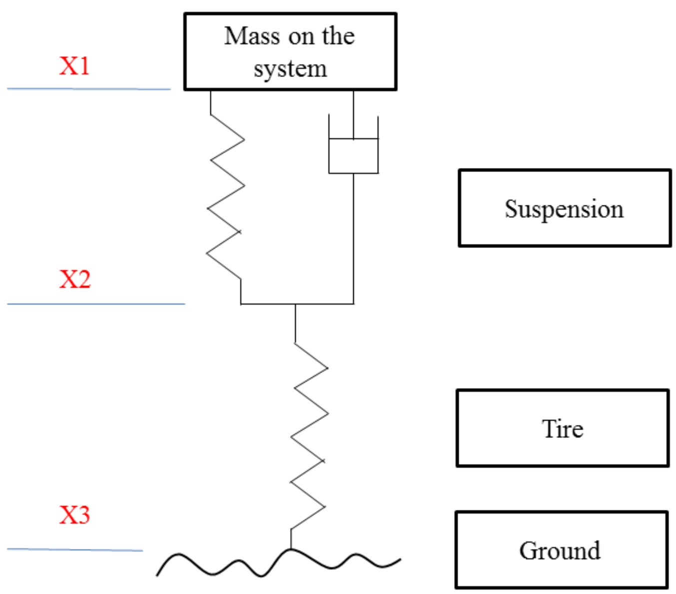

Figure.7.1. Spring – Damper system for a truck

X1, X2, and X3 are the relative datums of suspension, tire and the ground. For the suspension and tire systems, simulation using the spring and dashpots provided values that closely matched field values. Two models were created to analyze the response of the system. The first model was created for the suspension alone, where the deformation of the suspension and the time taken to achieve equilibrium was simulated (Figure.7.2). The parameters related to the suspension model were obtained for 1g from mathematical model used in chapter 5.

Parameters (at 1g load)	**Value**	**Unit**
Force (F)	2080	kN
Stiffness of spring (k1)	16855339	N/m
Viscous damping coefficient (b1)	2682194	Ns/m^2
Stiffness of the tire (k2)	3751237	N/m
Mass (m)	212023	kg

Table.7.1. Parameters for the Simulink model

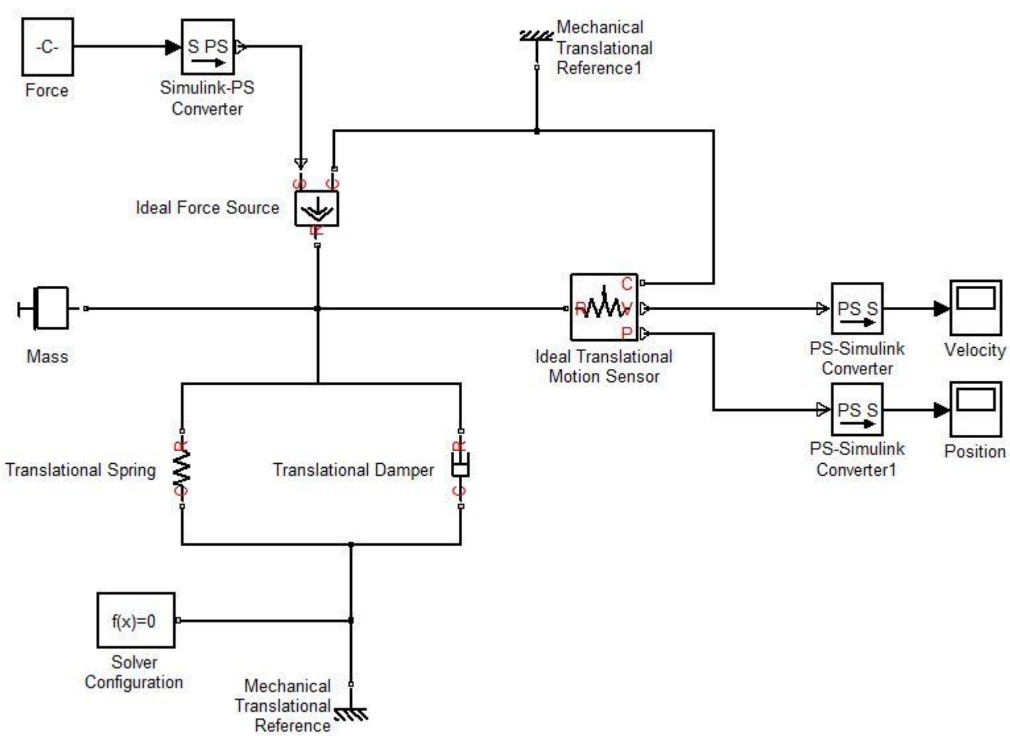

Figure.7.2. Simulink model for truck suspension

Figure.7.3 shows the output for a CAT 797B truck at 1g load obtained using the Simulink suspension model (Figure.7.2). The suspension deforms to a value of 0.123m and then stabilizes at that point within fraction of a second. This deformation remains the same until the force on the suspension is removed.

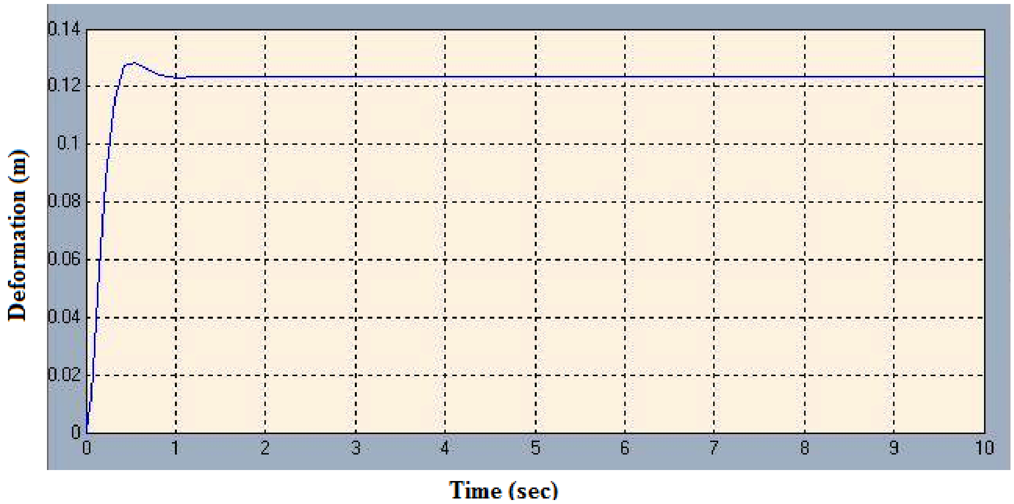

Figure.7.3. Output for CAT 797B rear suspension at 1g load

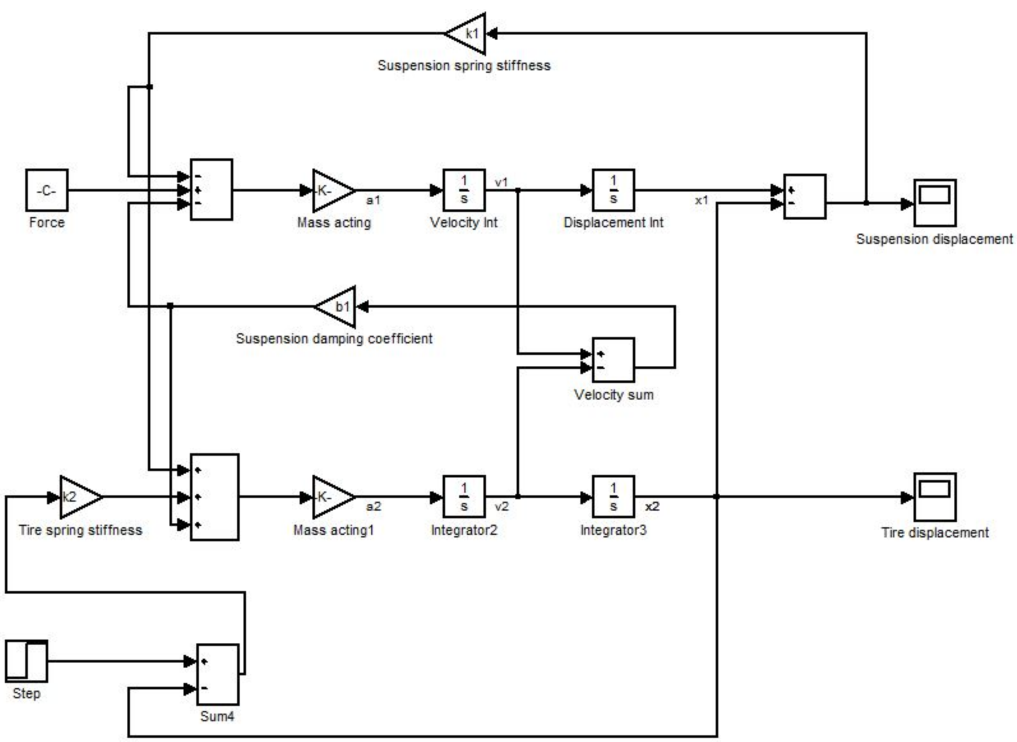

Figure.7.4. Simulink model for CAT 797B suspension and tire

To simulate results for a model that consists of both the suspension and a tire, a different approach was used (Figure.7.4). Newtons second law of motion was considered to be the basis to this model. Forces acting on the model were used and the deformation of both the suspension and a tire were obtained.

The Simulink model was analyzed using a force to create a displacement of tire and suspension. Since this is a system which attains equilibrium and also which is considered to return back to its initial position once the load is removed, the net force acting on it should be zero (equation.7.1). A step input models the oil sand ground and the deformation of it is modeled based on the mathematical model output for different loads from chapter 4. The basic equations used in this model are given below

$$\Sigma F = 0 \qquad [7.1]$$

$$m\frac{\mathrm{d}^2 x_1}{\mathrm{d}t^2} = F - k_1\left(x_1 - x_2\right) - b_1\left(\dot{x}_1 - \dot{x}_2\right) \qquad [7.2]$$

$$m\frac{\mathrm{d}^2 x_2}{\mathrm{d}t^2} = k_1\left(x_1 - x_2\right) + b_1\left(\dot{x}_1 - \dot{x}_2\right) + k_2\left(w - x_2\right) \qquad [7.3]$$

Where, F is the force (kN), x_1 and x_2 are the suspension and tire positions (m), k_1 and k_2 are the stiffness of suspension and the tire (kN/m), b_1 is the viscous damping coeffiecient (Ns/m^2), w is the step input parameter, m is the mass (kg)

When a force is acting on the system, the opposing force would be from the combined suspension spring and the damper and the tire spring. The force acting on the suspension and damper are given by the second and third terms ($k_1\left(x_1 - x_2\right)$ and $b_1\left(\dot{x}_1 - \dot{x}_2\right)$) in equation 7.2. Similarly the force due to the tire is given by the third term ($k_2\left(w - x_2\right)$) in equation 7.3. The step input here is modeled using a sinusoidal estimation with time limits based on an evaluation of the actual field data. The relationship used produces a road profile similar to a bump or potholes based on the input values (equation.7.4) [2].

$$w(t) = a(1 - \cos 8\pi t) / 2 \text{ for } 0 \cdot 5 \le t \le 0 \cdot 75 \qquad [7.4]$$

$$\text{and } w(t) = 0 \text{ otherwise} \qquad [7.5]$$

Where, $w(t)$ is the step input with respect to time, a is a constant parameter, t is the time (sec)

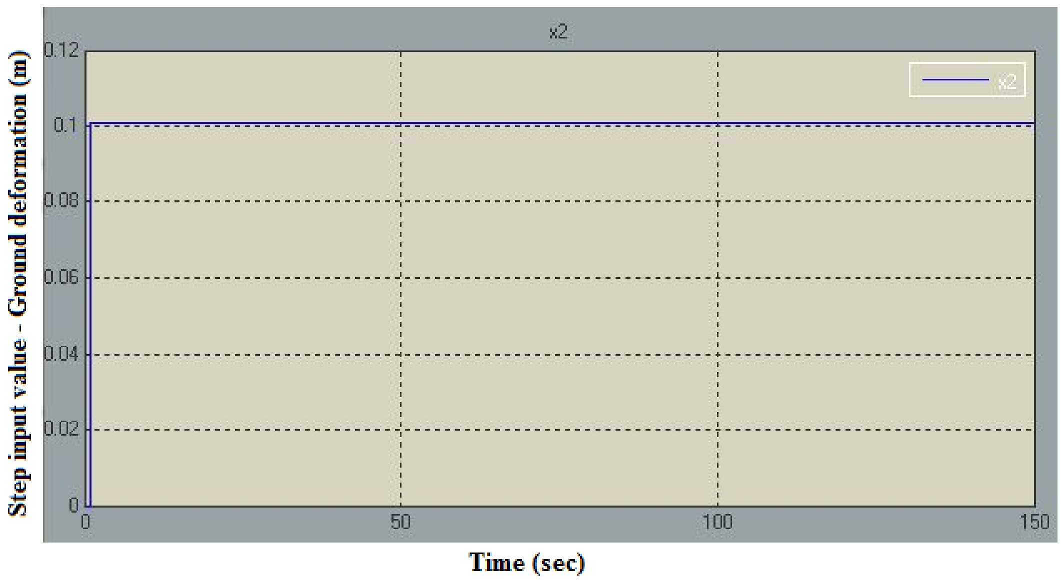

Figure.7.5. Step input value (ground deformation)

Figure.7.5 and provides a simplified ouput for the ground deformation model as a step input. Here the ground is modeled to be deformed by 0.1m, from which the deformation of a tire is obtained (Figure.7.7).

Figures.7.6 and 7.7 provide the deformation of a tire with no ground deformation (rigid surface) and with ground deformation. The deformation of the tire increases as the tire passes over a bump (Figure.7.7). It clearly shows that the deformation of tire varied with respect to a step input. If the step input is positive, the deformation of tire increases, whereas if it is negative, the deformation of the tire decreases.

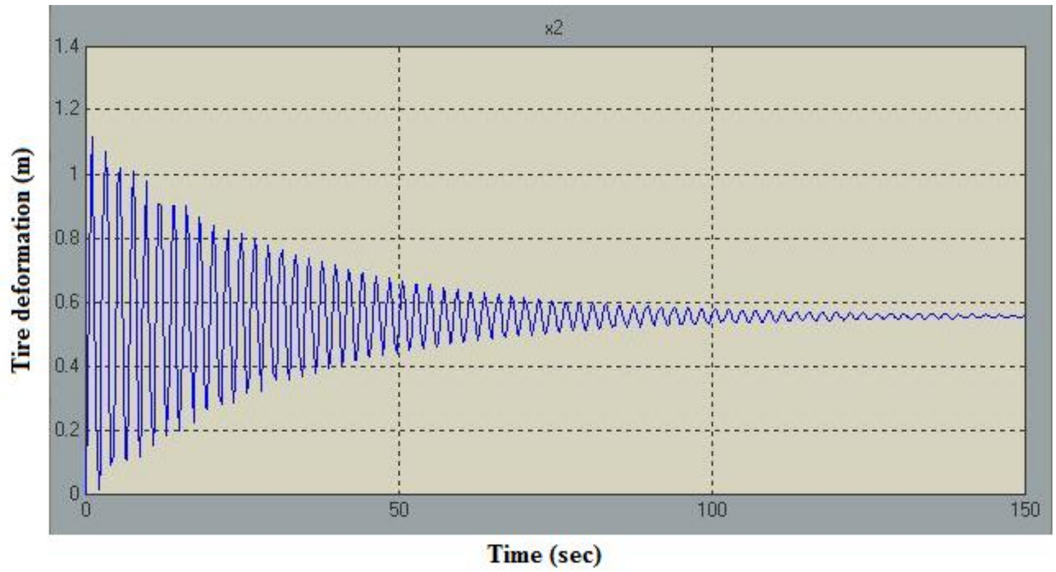

Figure.7.6. Tire deformation at 1g load without step input

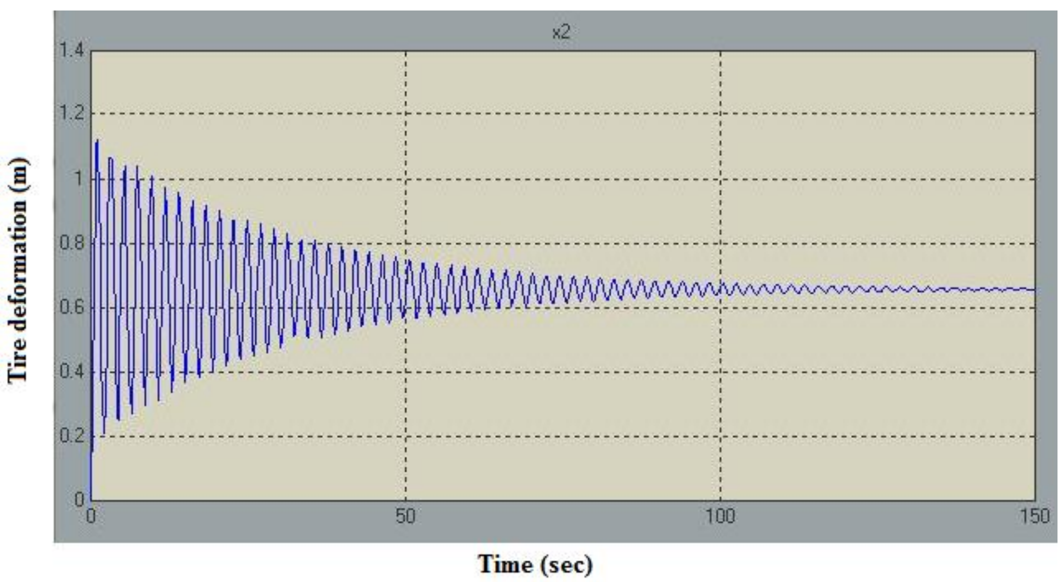

Figure.7.7. Tire deformation at 1g load with step input

The figures also show that the displacement after a particular period of time reaches equilibrium. The time taken by the tire to reach equilibrium is higher

(Figure.7.6 and 7.7). This is because in the system design, the tire does not have any damping property to attain equilibrium and the damping from suspension is considered as a overall damping coeffiecient value for the system (Figure.7.4). The damping is not sufficient to permit the tire to attain equilibrium within fraction of seconds. This is due to the total stiffness increase in the overall model (Figure.7.4) compared to a sole model for the suspension (Figure.7.2).

The ouput provides a tire deformation of 0.554m. But for a set of dual rear tires, there are two parameters (stiffness) that oppose the force, whereas in the model only one (stiffness) is considered. Hence the deformation of a single tire at the rear should be half of the total deformation (i.e. 0.277m). Ouputs were provided for various input parameters to validate the Simulink model (Table.7.2).

Force (N)	**Suspension deformation (m)**	**Tire deformation (m)**
290000	0.033	0.039
650000	0.085	0.087
1060000	0.105	0.140
1500000	0.110	0.198
2080000 (1g)	0.123	0.278

Table.7.2. Simulink model output for different loads

The model created in this chapter can be used for comparison of various truck models and sizes. Since the response of the gas in the suspension is different from a spring, the stiffness and viscous damping coeffiecients are different. Hence before running the Simulink model, these parameters are important to verify to obtain accurate results.

CHAPTER 8

SUMMARY OF THESIS OUTCOMES AND CONCLUSION

This thesis had two main focusses. The first was to predict a method that can determine the deformation and strain of the suspension and tire for a truck by varying inflation pressures and operating conditions. The second was a prediction of sinkage, rutting, and permanent deformation of oil sand. Other important parameter such as damping ratio for a suspension was also discussed during the course of the research.

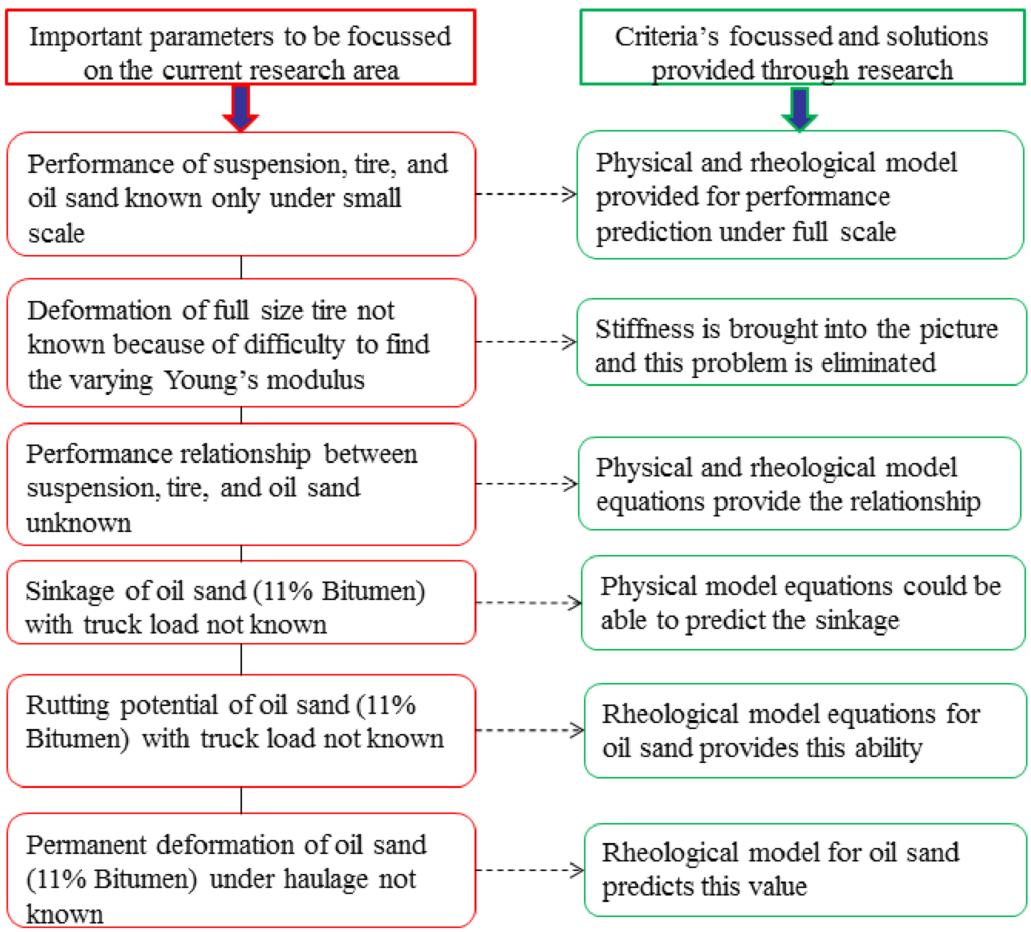

Figure.8.1. Research focus area and solutions

With the help of the mathematical and rheological models used here, some of the problems related to current research were eliminated. Figure.8.1 provides a summary of the problems and solutions provided through this research.

The mathematical equations and rheological models were created for performance prediction of oil sand, as well as suspension and tire on a rigid and oil sand ground surfaces. The thermodynamics of the suspension, and parameters related to the tire were used to predict the overall relationship between the deformation of a suspension and tire on a rigid surface (Equation.8.1 and 8.2). Inclusion of the radial stiffness of a tire was a key point here since performance of any size tire and for any inflation pressure can be discerned. Also difficulty in discerning Young's modulus for various tires is eliminated.

$$\delta_{tr,f} = \frac{P_u \cdot A_C}{\left(\frac{S_a}{S_u}\right)^{\gamma} \cdot \left(2.68 p_i \sqrt{w_t \cdot \phi_t} + 33 \cdot 1\right)} \qquad [8.1]$$

$$\delta_{tr,r} = \frac{P_u \cdot A_C}{2\left(\frac{S_a}{S_u}\right)^{\gamma} \cdot \left(2.68 p_i \sqrt{w_t \cdot \phi_t} + 33 \cdot 1\right)} \qquad [8.2]$$

Equation (8.1) is for front tires because there is only one tire per suspension and equation (8.2) is for rear tires since there are two tires configured to a single suspension. Comparisons done with previous field and laboratory results proved that the above two equations are valid. It showed that the deformation of the tire follows an exponential relationship with respect to the available stroke length of the suspension.

For performance of a truck on an oil sand surface, the criteria was different, where the deformation of oil sand also effects the overall relationship. Sharma (2009) provided the equation for deformation of a tire on oil sand. A pressure stiffness for the oil sand was included to be able to eliminate the problem due to varying performance oil sand, after the earlier work of Sharif – Abadi (2006).

Both the pressure stiffness and the deformation of a tire on oil sand were combined and the final equation for the deformation of oil sand was obtained (equation.8.3). The output using this equation showed that the response of oil sand depends on the amount of load, number of loading cycles, and the type of loading (increasing cyclic, varying, constant). The sinkage, ground deformation characteristics of the oil sand can be found out using this equation.

$$\delta_{os} = \sqrt{\frac{F_t \cdot E}{\left(k_p^2 \cdot C \cdot \phi_t^2\right) + \left(k_p \cdot C \cdot E \cdot \phi_t\right)}} \qquad [8.3]$$

In predicting the strain value for the suspension, tire, and oil sand, rheological models were used. Equations related to Kelvin – Voigt, Elastic spring, Maxwell, and Burgers model were used in the research. Equation (8.4) provides the total strain value for the truck on a rigid surface.

$$\varepsilon_{tr} = \left(\frac{\sigma_{ss}}{E_{s_b}}\right)\left(1 - \mathrm{e}^{-\left(\frac{E_{ss} t}{\eta_{sd}}\right)}\right) + \left(\frac{F_t}{k_r \cdot \phi_t}\right) \qquad [8.4]$$

Equation (8.5) provides the total strain value for the truck on oil sand. This equation can be used to find the rutting ground deformation characteristics of the oil sand. Oil sand experiences permanent strain because of its viscoelastic nature. The difficulty to find this parameter is now eliminated. Rheological model term 3 in equation (8.5) can be used to predict this value. From the output it showed that the permanent deformation depends on the load applied, duration of the load, and the loading cycle.

$$\varepsilon_{tos}(t) = \frac{\sigma_{osm}}{E_{gs_1}}\left(1 - e^{-\left(\frac{E_{gs_1}}{\eta_{gd_1}}\right)t}\right) + \left(\frac{\sigma_{osm}}{E_{gs_2}}\right) + \left(\frac{\sigma_{osm}}{\eta_{gd_2}}\right)t \qquad [8.5]$$

The recovery rate of oil sand was also found (equation.8.6) where the rate of recovery was more for smaller loads and durations, whereas for higher loads and durations, the rate of recovery and the amount of recovery was less.

$$\varepsilon_{ros} = \frac{\sigma_{osm}}{E_{gs_1}}\left[e^{\left(\frac{E_{gs_1}}{\eta_{gd_1}}\right)t} - 1\right]\left[e^{-\left(\frac{E_{gs_1}}{\eta_{gd_1}}\right)t_u}\right] \qquad [8.6]$$

Finally simulation was done using Matlab Simulink software. Two models were created in the simulation. The first model was only for the suspension, which was used to predict the time taken by the suspension to attain a steady state.

The second model was used to simulate the entire model consisting of suspension, tire, and the ground. The ouput from the first model showed that the suspension attained steady state within seconds. The output from the second model gave the tire deformation value for various loads.

A step input and a sinusoidal wave were provided for the road profile. To validate each of the models used in this research, comparisons were made for various loads (Table.8.1). The most important factor in this research is the comparison of outputs of all the three models used (Mathematical, Rheological, and Simulink). The comparison was made for a CAT 797B truck suspension, and tires considering an inflation pressure of 600kPa and diameter of 3.84m (Table.8.1).

Force (kN)	Suspension Deformation (m)			Tire deformation (m)		
	Mathematical model	**Rheological model**	**Simulink**	**Mathematical model**	**Rheological model**	**Simulink**
290	0.033	0.033	0.033	0.039	0.039	0.039
450	0.064	0.065	0.064	0.062	0.062	0.060
650	0.085	0.086	0.084	0.087	0.088	0.087
850	0.096	0.097	0.096	0.113	0.114	0.113
1060	0.105	0.105	0.105	0.141	0.142	0.141
1400	0.114	0.114	0.114	0.186	0.187	0.185
1500	0.116	0.116	0.115	0.198	0.200	0.198
1700	0.118	0.119	0.118	0.228	0.231	0.228
2080 (1g)	0.123	0.123	0.123	0.277	0.277	0.277
2450	0.125	0.126	0.126	0.325	0.330	0.325

Table.8.1. Comparison between mathematical, rheological, and Simulink model outputs for CAT 797B

The comparisons show that all the models provide values close to each other and even matching with the field values at 1g load. The ability of these models can now be visualized and the equations and the simulation models used here may now be utilized for various truck sizes under different operating conditions, such that performance can be predicted. Another important factor is the ability of these models and equations to eliminate the drawbacks in the current research area, providing a simple method to predict the various performance characteristics of suspension, tire, and oil sand.

CHAPTER 9

FUTURE RECOMMENDATIONS

The mathematical equations for the relationship between deformation of tire and suspension available stroke length were calculated for a CAT 797B truck. However comparisons with field data and various other trucks operated on rigid surfaces need further validation. Hence field studies should be done for various trucks and comparisons made.

Oil sand surfaces with deformation characteristics were considered in this research. But some of the mines are now employing limestone as the surface material for the haul roads. This material behaves plastically and there could be some deformation which might effect the performance of the truck. Hence studies could be done on this material and the overall relationship between suspension, tire, and the ground be predicted.

Room temperature condition were considered for the oil sand in the model and with a bitumen content of 11%. But in field the bitumen content varies from 8% - 15% and temperature varies between -30°C to +30°C. Hence suitable laboratory set up could be done to predict the deformation and footprint area equations for these varying operating conditions.

The wear rate of the tire is another important factor. If the road condition is very bad it might create more wear on the tire. This results in reduction of the overall diameter of the tire and in turn reduces the stiffness. Hence the effect of this parameter could be included to predict the stiffness of the tire as the operating hours increases. This will definitely help to find out the change in strength of the tire with time providing a better relationship between truck components and the ground.

A truck encountering a haul road corner will create the forces acting on the tire deviate from the central axis due to slip resulting in transfer of force on a footprint area. In this case the deformation at that area will be more than the expected. Slip angle and the cornering stiffness are the parameters behind this behavior. This analysis could also be done through dynamic analysis on a truck.

The value of Young's modulus and viscosity of oil sand with 11% bitumen content was used in the rheological model to predict the deformation characteristics. This value was obtained from Sharma (2009) by performing laboratory tests and with the help of a Burgers model. A similar method could be performed for oil sand with various bitumen content and using the value obtained and the equations from this research, deformation characteristics could be predicted for different operating conditions.

The effect of rolling resistance was not included in determining the rutting potential of oil sand. After finding out the Youngs modulus and viscosity of various oil sand materials, these values could be used in a rheological model along with the effect of rolling resistance to predict the rutting potential.

REFERENCES

[1] *About Rheology*. (n.d.). Retrieved July 10, 2013, from http://www.iq.usp.br/mralcant/About_Rheo.html

[2] Agharkakli, A., Chavan, U., & Phrithran, S. (2012). Simulation and analysis of passive and active suspension system using quarter car model for non - uniform road profile. *International Journal of Engineering Research and Applications, 2*(5), pp 900 - 906.

[3] Anochie - Boateng, J. K. (2007). Advanced testing and characterization of transportation soils and bituminous sands. *PhD Thesis*. University of Illinois, Illinois.

[4] Anochie - Boateng, J. K., Tutumluer, E., & Carpenter, S. H. (2010). Case study: Dynamic modulus characterization of naturally occuring bituminous sands for sustainable pavement applications. *International Journal of Pavement research and technology, 3*(6), pp 286-294.

[5] Appleyard, M., & Wellstead, P. E. (1995). Active suspensions : some background. *IEE Proc-Control theory Appl, 142*(2), pp 123-128.

[6] Attila, C., Zoltan, D., & Laszlo, D. (2004). Changing the rheological features of AG-BAG type packaging foil tubes depending on temperature.

[7] Balhoff, M. (2005). Modeling the flow of Non - Newtonian fluids in packed beds at the pore scale. *PhD Thesis*. Louisiana State University, Louisiana.

[8] Banfill, P. F. (2006). Rheology of fresh cement and concrete. pp 61-130.

[9] Barksdale, R. D. (1972). Laboratory evaluation of rutting in base course

materials. *3rd International conference on structural design of asphalt pavements*, (pp. 161-174).

[10] Barnes, H. A., Hutton, J. F., & Walters, K. (1999). *Introduction to Rheology* (2nd ed.). Elsevier Science Publications Ltd.

[11] Berezan, J. J., Joseph, T. G., & del Valle, V. D. (2004). Monitoring whole body vibration effects on ultra-class haulers. *CIM Bulletin, 97, 1082*, pp 1-4.

[12] Blanchard, E. D. (2003). On the control aspects of semiactive suspensions for automobile applications. *MSc. Thesis*. Virginia Polytechnic Institute and State University, Virginia.

[13] Bolster, M. J. (2007). Tire rim interactions for ultra-class truck performance. *MSc Thesis*. University of Alberta, Edmonton.

[14] Bridgestone, F. (2008). Earthmover tire catalogue and base price list, Off-The Road tires. pp 16-18.

[15] Cameron, R., Mahood, R., Lewko, R., & Skitmore, J. (1996a. 1995). *Haul road investigation of problem areas for 240 - Ton heavy haulers driving on 170 - Ton haul road design at Syncrude Canada Limited.* Internal report , Syncrude Canada Limited.

[16] Cameron, R., Mahood, R., Lewko, R., & Skitmore, J. (1996b. 1996). *Haul road design, construction and monitoring procedures for 240 - Ton heavy haulers at Syncrude canada Limited.* Internal report, Syncrude Canada Limited .

[17] Cao, J., Liu, H., Li, P., & Brown, D. J. (2008). State of the art in vehicle active suspension adaptive control systems based on intelligent

methodologies. *IEEE Transactions on intelligent transportation systems, 9*(3), pp 392-405.

[18] Caterpillar. (2002). *Caterpillar service manual for 793C truck, manual form SENR 1540, specifications, SENR 1455-04.*

[19] Caterpillar Inc. (2004). Caterpillar performance handbook.(35th Edition),5-9.

[20] Choudhury, S. F., & Sarkar, M. R. (2012). An approach on performance comparison between automotive passive suspension and active suspension system (PID Controller) using Matlab/Simulink. *Journal of Theoretical and Applied Information Technology, 43*(2), pp 295 - 300.

[21] Creed, B., Kahawatte, N., & Varnhagen, S. (2010). Development of a full car vehicle dynamics model for use in the design of an active suspension control systems.

[22] Cunagin, W. D., & Grubbs, A. B. (1984). *Automated acquisition of trucl tire pressure data.* Transportation research record 1123, Transporation research board, pp 112 - 121.

[23] De Haan, Y. M., & Sluimer, G. M. (2001). Standard linear solid model for dynamic and time dependant behavior of building materials. *46*(1), pp 49-76.

[24] Dekker, M. (1999). Nonlinear and variable stiffness systems.

[25] Dey, A., & Basudhar, P. K. (2010). Applicability of Burger model in predicting the response of Viscoelastic soil beds.

[26] Doraisamy, D. (2001). *The origins of rheology : A short historical excursion.*

[27] Doucet, R. (2001). 21st Century maintenance management. *CIM Bulletin*, (p. 93).

[28] El-Sayed, M. (2003). Suspension Systems in Large Mining Trucks. *MEng Dissertation*. University of Alberta, Edmonton.

[29] Findley, W. N., Lai, J. S., & Onaran, K. (1989). Creep and relaxation of nonlinear viscoelastic materials.

[30] Gao, W., Zhang, N., & Du, H. (2007). A half - car model for dynamic analysis of vehicles with random parameters. *5th Australian congress on applied mechanics.* Brisbane.

[31] Gavin, H. P. (2010). Vibrations of single degree of freedom systems.

[32] Goodman, R. E. (1989). *Introduction to rock mechanics* (2nd ed.). New York: John Wiley and Sons.

[33] Grozic, J. H. (1999). The behavior of loose gassy sand and its susceptibility to liquefaction. *PhD Thesis*. University of Alberta, Edmonton.

[34] Guglielmino, E., Sireteann, T., Stammers, C. W., Ghita, G., & Giuclea, M. (2008). Semi active suspension control. Springer - Verlag London Limited.

[35] Hackley, V. A., & Ferraris, C. F. (2001). Guide to Rheological nomenclature : Measurements in ceramic particulate systems.

[36] Hadekel, R. (1940). A method of estimating the performance of Oleo-Pneumatic struts. *The Aircraft Engineer, 7*(174).

[37] *Haul roads.* (n.d.). Retrieved August 15, 2013, from Hammerstone

corporation:
http://www.hammerstonecorp.com/files/37.HammerStoneHaulRoadsWeb.pdf

[38] Hou, C.-Y., Hsu, D.-S., Lee, Y.-F., Chen, H.-Y., & Lee, J.-D. (2007). Shear - thinning effects in annular - orifice viscous fluid dampers. *Journal of Chinese Institute of Engineers, 30*(2), pp 275-287.

[39] Joseph, D. D. (1986). Historical perspectives on the elasticity of liquids. *Journal of Non - Newtonian fluid mechanics, 19*, pp 237 - 249.

[40] Joseph, T. G. (2002). OsEIP: the oil sands - equipment interactions program. *CIM Bulletin, 95*(1064), pp 58-61.

[41] Joseph, T. G. (2003). Large mobile equipment operating on soft ground. *18th International Mining Conference and Exhibition of Turkey*, (pp. 143-147).

[42] Joseph, T. G. (2005). *Mathematical, static and inferred dynamic loaded properties of oil sand.* Progress report, Phases II and III (Final report), CAT/0405.

[43] Joseph, T. G., & Hansen, G. (2002). Oil sand reaction to cable shovel motion. *CIM Bulletin, 95*(1064), pp 62-64.

[44] Joseph, T. G., Sharif - Abadi, A. D., & Shi, N. (2003). A broken material approach to modeling oil sand under dynamic load. *In Proceedings of CAMI Conference.* Calgary.

[45] Kasprzak, E. M., Lewis, K. E., & Milliken, D. L. (2006). Inflation pressure effects in the Nondimensional tire model.

[46] Kelly. (n.d.). *Solid Mechanics Part 1*. Lecture.

[47] Kizhakkethara, I. (1995). Non - linear static analysis of aircraft tire subjected to inflation pressure and ground contact loads using finite element analysis. *MSc Thesis* . University of New Orleans, New Orleans.

[48] Larson, R. G. (1999). *The structure and rheology of complex fluids.* NewYork: Oxford University Press.

[49] Lekarp, F., Isacsson, U., & Dawson, A. (2000). Permanent strain response of unbound aggregates. *Journal of Transportation Engineering, 126*(1), pp 76-83.

[50] Li, P., & Chalaturnyk, R. J. (2005). Geomechanical model of oil sands. *SPE International thermal operations and heavy oil symposium*, (pp. B453 - B457). Calgary.

[51] Lin, Z. (2007). Geometry and mechanics of pneumatic tires.

[52] Nguyen, Q.-H., & Nguyen, N.-D. (2012). Incompressible Non-Newtonian fluid flows. In Y. Gan (Ed.), *Continuum Mechanics - Progress in fundamentals and Engineering applications* (pp. 47 - 72). Intech Publication.

[53] Provenzano, P. P., Lakes, R. S., Corr, D. T., & Vanderby Jr, R. (2002). Application of nonlinear Viscoelastic models to describe ligament behavior. pp 45-57.

[54] Robert, W., Funnell, J., Maftoon, N., & Decreamer, W. F. (2012). Mechanics and modeling for the middle ear.

[55] Roylance, D. (2001). Engineering Viscoelasticity.

[56] Saarilahti, M. (2002). *Soil Interaction Model : Manual 1*. Seltra - Documentation of the computer programme for calculating of the trafficability of terrain and mobility of forest tractors, University of Helsinki.

[57] Santos, R. F. (2007). A Rapid Dampening Suspension for Ultra-Class Haulers. *MSc Thesis*. University of Alberta, Edmonton.

[58] Schiessel, H., Metzler, R., Blumen, A., & Nonnen, T. M. (1995). Generalized viscoelastic models : Their fractional equations with solutions. IOP Publishing Limited.

[59] Sharif-Abadi, A. D. (2006). Cyclic performance of soft ground. *PhD Thesis*. University of Alberta, Edmonton.

[60] Sharma, A. (2009). Scale tire - oil sand interactions. *MSc Thesis*. University of Alberta, Edmonton.

[61] Soni, R. K. (2009). Scaled rapid dampening suspension evaluations. *MSc Thesis*. University of Alberta, Edmonton.

[62] Stroshine, R. (1998). *Mathematical properties of agricultural materials and food products.* Purdue University, West Lafayette.

[63] *TA Instruments : Rheology application note*. (n.d.). Retrieved July 29, 2013, from http://www.tainstruments.com/library_download.aspx?File=RN9.pdf

[64] Tannant, D. D., & Regensburg, B. (2001). *Guidelines for Mine haul road design.*

[65] Tanner, R. I., & Walters, K. (1998). *Rheology:An historical perspective* (Vol. 7). Elsevier Publication Ltd.

[66] Tielking, J. T. (1994). Force transmissibility of heavy truck tires. *Tire Science and Technology: 22, 1*, pp 60-74.

[67] Tielking, J. T., & Abraham, M. A. (1990). *Measurement of truck tire footprint pressures.* Transportation research record : 1435, Transportation research board, pp 92-99, Washington, DC.

[68] Tomkins, E. (1981). The history of the pneumatic tyre. London: Eastland Press.

[69] Van der Steen, R. (2007). *Tyre/road friction modeling.* Literature survey, Eindhoren University of Technology, Eindhoren.

[70] Vermant, J. (n.d.). *Rheology and structure of complex fluids.* Retrieved July 10, 2013, from http://www.eu-softcomp.net/FILES/IFFFS_REO-1.pdf

[71] Walters, K. (n.d.). *History of Rheology.* Retrieved July 10, 2013, from http://www.eolss.net/Sample-Chapters/C06/E6-197-01.pdf

[72] Williams, R. A. (1994). Electronically controlled automotive suspensions. *Computing and control Engineering Journal, 5*(3), pp 143-148.

[73] Wills, D. S. (1989). *Guidelines for monitoring mine haul road construction at Syncrude canada limited.* Internal report, Syncrude Canada Limited.

[74] Xue, X. D., Cheng, K. E., Zhang, Z., Lin, J. K., Wang, D. H., Bao, Y. J., et al. (2011). Study of art of automotive active suspensions. *4th International conference on Power electronics systems and applications*, (pp. 360 - 366).

[75] Ziegenmeyer, J. D. (2007). Estimation of disturbance inputs to a tire coupled quarter - car suspension test rig. *MSc. Thesis*. Virginia Polytechnic Institute and State University, Virginia.

APPENDIX

Appendix – A

A.1. Dimensions of CAT 797B rear suspension

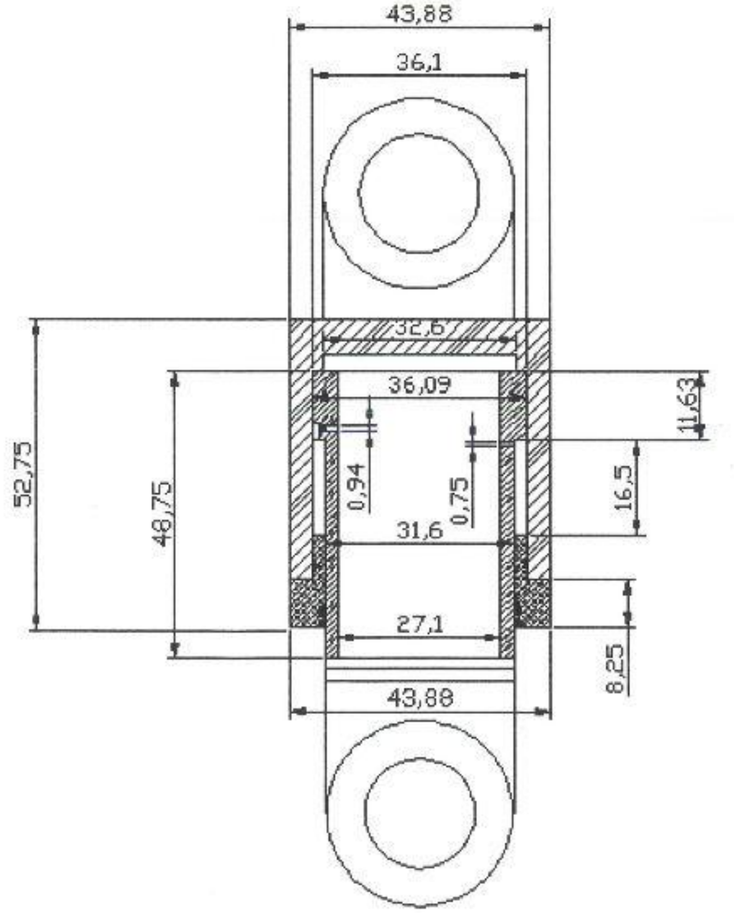

Appendix – B

B.1. Mathematical model output for ϕ 2.85m tire on a rigid surface

B.1.1. Result for various inflation pressures

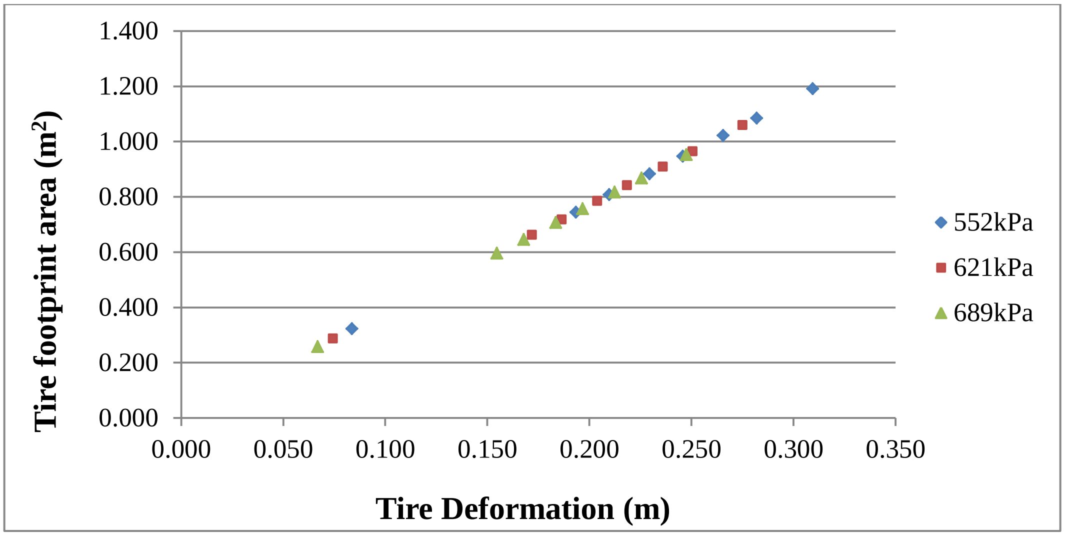

B.2. Mathematical model output for ϕ 0.368m tire on a rigid surface

B.2.1. Result for various inflation pressures

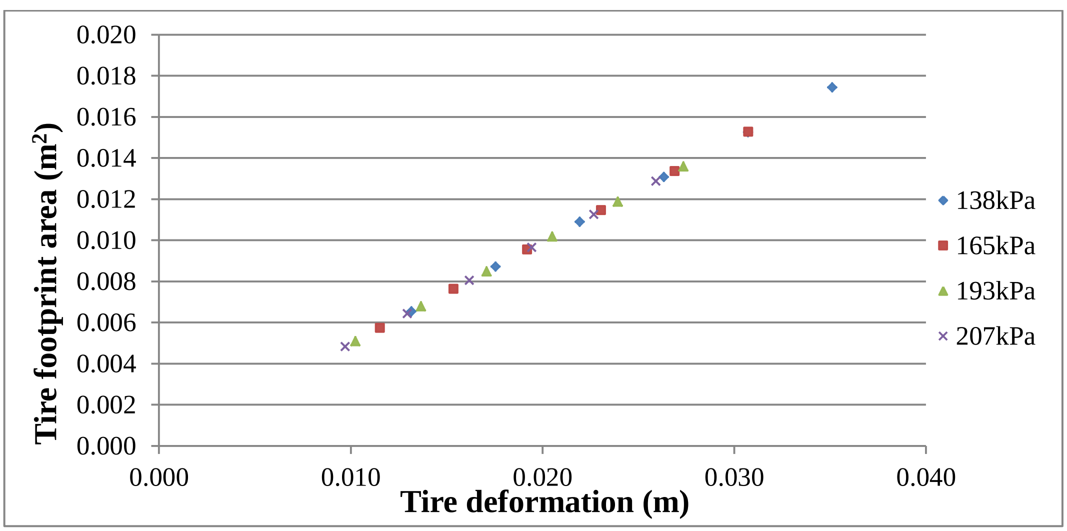

B.3. Mathematical model output for ϕ 3.84m tire on a rigid surface

B.3.1. Result at inflation pressure of 599 kPa

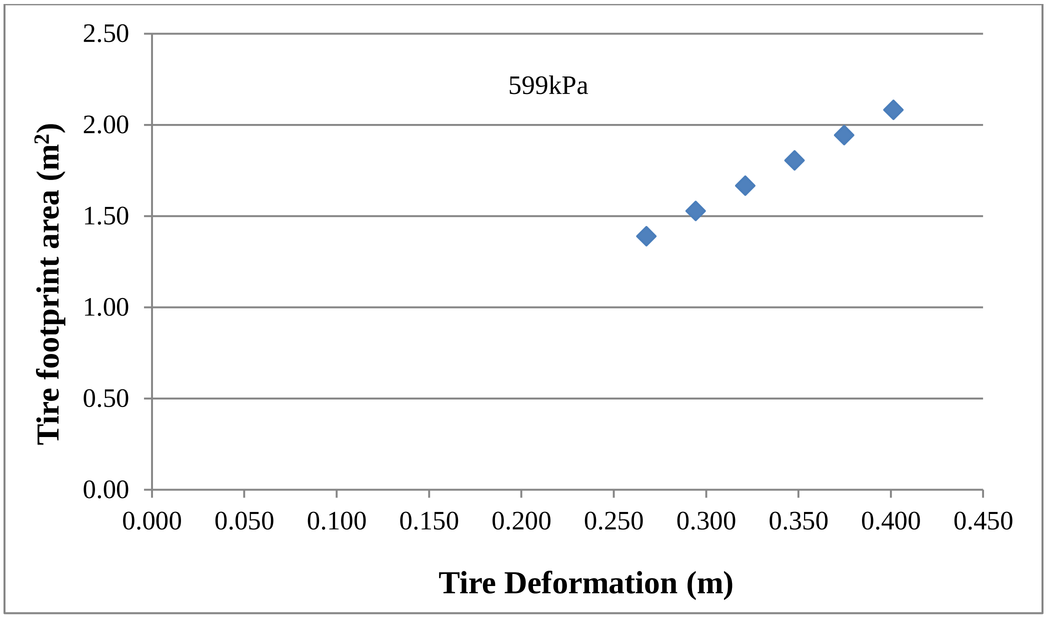

B.3.2. Result at inflation pressure of 620 kPa

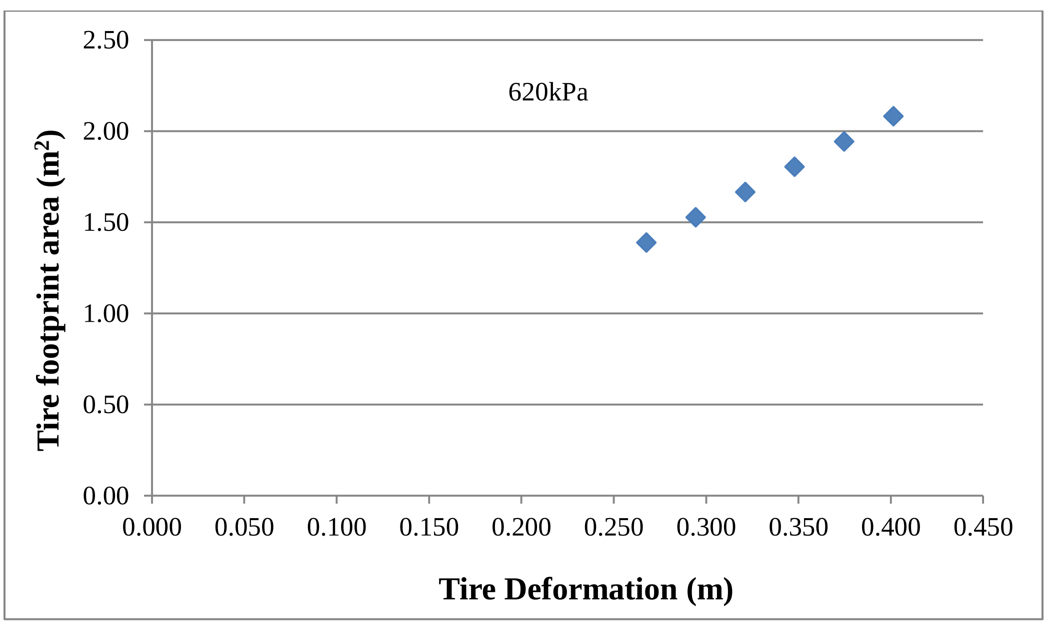

B.4. Mathematical model output for ϕ 3.84m tire on oil sand

B.4.1. Deformation of tire and oil sand with suspension pressure